ANTI CANCER EFFECTS OF COMBINED GAMMA-TOCOTRIENOL AND 13-CIS RETINOIC ACID AGAINST NEUROBLASTOMA CELLS AND XENOGRAFTS

CH'NG QIN TING, MPharm.

Thesis submitted to The University of Nottingham
for the degree of Doctor of Philosophy

MAY 2021

ABSTRACT

High-risk neuroblastoma mainly affects young children and is known to be resistant to treatment (surgery and chemotherapy) which is often attributed to amplified *MYCN*. Overexpressed Bcl-2 protein is also frequently a feature of neuroblastoma tumours. 13-cis retinoic acid (13cRA) is used as a differentiation agent in the final, maintenance stage of therapy to reduce recurrence of malignant tumours. However, response to this treatment is still not optimal due to side effects and treatment failure. Gamma-tocotrienol (γT3) has been found to induce apoptosis in neuroblastoma cells by binding to the BH3 groove of the Bcl-2 protein. It has also been investigated for its synergistic effects when used in combination with other drugs. This study had several aims. First, to explore the potential for a synergistic effect of γT3 and 13cRA used in combination for neuroblastoma, *in vitro* and *in vivo*. The mechanism of action by which γT3 acts in neuroblastoma will also be investigated. We investigated the effect of γT3 and/or 13cRA treatment on SH-SY5Y and SK-N-BE(2) cell lines and found that while individual treatments produced significant reduction in cell viability and increase in cell death, the addition of γT3 reduced the IC_{50} of 13cRA by more than half in both cell lines. Combination index values of <1 indicate that the combination of γT3 and 13cRA is synergistic. In the *in vivo* work, we found that the combination of γT3 and 13cRA significantly reduced tumour volume compared to other treatments ($p \leq 0.05$), including the specific Bcl-2 inhibitor, ABT-263. Annexin-FITC/PI flow cytometry showed increased population of apoptotic cells in the γT3 combination group in both cell lines, although it was not statistically significant compared to other treatment groups. Finally, protein expression studies were conducted using Bcl-2, Bcl-xL, MYCN, caspases-3 and -9 and p53. No conclusive changes were found when compared to other treatment groups from both *in vitro* and *in vivo* samples. In conclusion, the combination of γT3 and 13cRA showed significant anti-tumour effects on neuroblastoma, *in vitro* and *in vivo*. So, γT3 could potentially be used in combination with 13cRA, in a clinical setting. Further work is needed to confirm the mechanism of action.

ACKNOWLEDGEMENTS

First, I would like to thank God for continued grace, protection and provision.

I would like to express my deepest gratitude to my principle supervisor, Dr Then Sue-Mian for her endless patience, constant guidance and support throughout my PhD study. Her encouragement, constructive criticism and advice, both practical and theoretical, was invaluable.

I would also like to thank my co-supervisor Prof. Ting Kang-Nee for her support and advice, particularly when navigating numerous administrative hurdles.

My sincere thanks is also extended to all our collaborators. From The University of Nottingham Malaysia (UNM): Prof. Sandy Loh Hwei-San for her generous donation of tocotrienol isomers and Dr Suresh K Mohankumar for advice on the *in vivo* study. From Universiti Kebangsaan Malaysia (UKM): Prof. Wan Zurinah Wan Ngah for allowing us to use the animal lab and PET imaging system and her advice on the *in vivo* study plan and her successor, Dr Hanafi Damanhuri who continued to give valuable advice and help troubleshoot for the *in vivo* study. Ms Fathiah, head technician and Mr Fais, PET imaging lab technician, for all their support throughout the *in vivo* study. Dr Tan Jen Kit for his comments on his previous work, of which this study was a continuation of. And overall, thanks to staff and students at the Biochemistry Department, UKM for their welcome and support.

I would like to thank Dr Fang Chee Mun and Dr Ho Wan Yong, for their constructive criticism as my internal assessors, as well as Dr Fang's advice on flow cytometry. I would also like to thank Dr Le Cheng Foh, who helped with my cell culture training. My thanks also to the Graduate School of UNM for the programmes organised for both training and information, which were very useful during my study.

My heartfelt thanks goes to all the lab technicians from the Faculty of Science, UNM, for their support and patience, in particular Ms Siti Norazlin, Ms Asma and Mr Wong Siak Chung. Further thanks is extended to academic and administrative staff of the Division of Biomedical Sciences and the School of Pharmacy, for their contributions to my study and research. I would also like to

extend sincere thanks to the Fundamental Research Grant Scheme (FRGS), Ministry of Education Malaysia, for funding this study, and the University of Nottingham Malaysia for their generous PhD scholarship.

I would like to extend my thanks to my colleagues from the Division of Biomedical Sciences, with a special mention to Anusha Nawoor, Dr Lee Mei Kee and Dr Chan Won Ting, for all their advice and encouragement, as well as thanks to all my friends who continued to encourage and support me throughout my study.

Thank you to my wonderful family, for all their encouragement, prayers and love. Many thanks to my dearest Tushar Sinha for all his support and care.

This thesis is dedicated to my wonderful, darling mother, who has loved and supported me unconditionally in everything I do.

LIST OF TABLES

LIST OF FIGURES

LIST OF ABBREVIATIONS

13cRA	13-cis retinoic acid
18-FDG	18-flurodeoxyglucose
6G	6-gingerol
A1	BCL-2-related protein 1
Akt	protein kinase B
ALK	anaplastic lymphoma receptor tyrosine kinase
ALL	acute lymphoblastic leukaemia
alpha/αT	alpha tocopherol
alpha/α-TTP	alpha-tocopherol transfer protein
ANC	absolute neutrophil count
ANGPTL4	angiopoietin-like 4
APAF-1	apoptotic protease-activating factor 1
APS	ammonium persulfate
APS	ammonium persulfate
ATRA	all-trans retinoic acid
Bad	BCL-2-associated death promotor
Bak	BCL-2 antagonist or killer
Bax	BCL-2-associated X protein
Bcl-2	B-cell lymphoma 2
Bcl-B	BCL-2-like protein 10

Bcl-W	BCL-2-like protein 2
Bcl-X_L/Bcl-xL	B-cell lymphoma extra large
BH3	Bcl-2 homology domain 3
Bid	BH3-interacting domain death agonist
Bik	BCL-2-interacting killer
Bim	BCL-2-interacting mediator of cell death/BCL-2-like protein 11
BMF	BCL-2-modifying factor
Bok	BCL-2-related ovarian killer protein
BSA	bovine serum albumin
CDK	cyclin-dependent kinase
cDNA	complementary DNA
CI	combination index
cIAP	cellular inhibitor of apoptosis
c-Myc	v-myc avian myelocytomatosis viral oncogene cellular-derived homolog
CNS	central nervous system
CNS	central nervous system
COX2	cyclooxygenase 2
c-PARP	cleaved poly-ADP ribose polymerase
CT	computed tomography
CVD	cardiovascular disease

dATP	2’-deoxyadenosine 5’-triphosphate
DNA	deoxyribonucleic acid
DS	Down’s syndrome
ECL	enhanced chemiluminescence
EDTA	ethylenediaminetetraacetic acid
EFS	event free survival
EGF-R	epidermal growth factor receptor
ELISA	enzyme-linked immunosorbent assay
ER	endoplasmic reticulum
ERK1/2	extracellular signal-regulated kinases 1/2
Fas	FS-7-associated surface antigen
FBS	fetal bovine serum
FITC	fluorescein isothiocyanate
gamma/γT3	gamma-tocotrienol
G-CSF	granulocyte-colony stimulating factor
HILDPA	hypoxia-inducible lipid droplet-associated
HMGR	HMG-CoA reductase
HPLC	high performance liquid chromatography
HRK	hara-kiri, BCL-2 interacting protein
HRP	horseradish peroxidase
IAP	inhibitor of apoptosis protein

Id	inhibitors of DNA binding and cell differentiation
IFITM1	interferon-inducible transmembrane protein-1
IGFBPA	insulin-like growth factor binding protein A
IgG	immunoglobulin G
IL-8	interleukin-8
INRG	International Neuroblastoma Risk Group
INSS	International Neuroblastoma Staging System
JNK	Jun amino-terminal kinases
MAPK	mitogen-activated protein kinase
Mcl-1	myeloid cell leukaemia sequence 1
MDM2	mouse double minute 2 homolog
MEK/MAP2K	mitogen-activated protein kinase kinase
MLEM	Maximum Likelihood Estimation Method
MOMP	mitochondrial outer membrane permeabilization
MRI	magnetic resonance imaging
mTOR	mechanistic target of rapamycin
MYCN/N-myc	v-myc avian myelocytomatosis viral oncogene, neuroblastoma derived
NADH	nicotinamide adenine dinucleotide
NADPH	nicotinamide adenine dinucleotide phosphate
NF-κB	nuclear factor kappa-light-chain-enhancer of activated B cells

NMR	nuclear magnetic resonance
Noxa	phorbol-12-myristate-13-acetate-induced protein
PARP	poly (ADP-ribose) polymerase
PBS	phosphate buffered saline
PET	positron emission tomography
PHOX2B	paired-like homeobox 2b
PI	propidium iodide
PI3K	phosphatidylinositol-4,5-bisphosphate 3-kinase
PS	phosphatidylserine
Puma	p53 upregulated modulator of apoptosis
RA	retinoic acid
RAR	retinoic acid receptor
RCT	randomised controlled trial
RIPA	radioimmunoprecipitation assay
RNA	ribonucleic acid
ROI	region of interest
RXR	retinoid X receptor
SAR	structure-activity relationship
SCLC	small cell lung cancer
SD	standard deviation
SDS	sodium dodecyl sulfate

SEER	Surveillance, Epidemiology, and End Results programme
SELECT	Selenium and Vitamin E Cancer Prevention Trial
SMAC	second mitochondria-derived activator of caspase
Sp-1	specificity protein 1
TA	tolfenamic acid
tBID	truncated BID
TEMED	tetramethylethylenediamine
TGF-β	transforming growth factor beta
TRF	tocotrienol rich fraction
TTP	tocopherol transportation protein
WBC	white blood cell
WHS	Women's Health Study
WML	white matter lesion
Wnt	wingless-type MMTV integration site family
XIAP	X-linked inhibitor of apoptosis

CONTENTS

CHAPTER 1 INTRODUCTION

1.1 BACKGROUND

Neuroblastoma is a paediatric solid tumour that originates from the neural crest and is divided into categories ranging from low to high risk (Cheung & Dyer, 2013). While low-risk neuroblastoma tumours may spontaneously regress, high-risk neuroblastoma is resistant to first line treatments (Pinto *et al.*, 2015; Cheung & Dyer, 2013). Survival outcome worsens with increasing age. For example, stage 2 and 3 patients below 18 months of age had a statistically higher event free survival (EFS) than those aged 18 months or older (88% ± 1% vs. 69% ± 3%) Another main risk factor of high-risk neuroblastoma is an increased expression of the *MYCN* gene, which is linked to treatment resistance (Cohn *et al.*, 2009).

In an attempt to reduce relapse rate in high-risk neuroblastoma treatment, clinicians have introduced the use of 13-cis retinoic acid (13cRA) or isotretinoin as a differentiation agent (Matthay *et al.*, 2009). Initial studies showed a 3.7 year event-free survival rate of 29 ± 7% in high risk neuroblastoma patients receiving 13cRA after chemotherapy compared to 11 ± 4% in patients receiving chemotherapy alone, $p = 0.019$ (Matthay *et al.*, 1999). However, in a follow-up study, the 5-year event free survival rate was 42 ± 5% vs for patients who were given 13cRA compared to 31 ± 5% in those that were not. This difference was not significant (Matthay *et al.*, 2009). Therefore, further improvements to 13cRA therapy in high risk neuroblastoma need to be made.

Another possible mechanism in the resistance of neuroblastoma tumours to treatment is an overexpression of *Bcl-2*. The *Bcl-2* gene is increased in neuroblastoma compared to normal tissues and other cancers (Lamers *et al.*, 2012; Goldsmith *et al.*, 2010). It has been suggested that the combination treatment of a Bcl-2 inhibitor with retinoic acid may show improvement compared to retinoic acid alone as a differentiation treatment (Niizuma *et al.*, 2006). There are currently several synthetic Bcl-2 inhibitors available: ABT-737, ABT-263 and ABT-199 (Oltersdorf *et al.*, 2005; Tse *et al.*, 2008; Souers *et al.*, 2013). They have been extensively studied and shown to have high affinity to Bcl-2 protein, although to different degrees.

Gamma-tocotrienol (γT3) is one of eight natural isomers of vitamin E, divided equally between tocotrienols and tocopherols (Aggarwal *et al.*, 2010). Tocotrienols have demonstrated effects treating and preventing numerous disease states, including cardiovascular disease, diabetes, neurodegenerative diseases, bone metabolism and exposure to ionising radiation (Wong *et al.*, 2012b; Kulkarni *et al.*, 2012; Singh, Beattie & Seed, 2013). While tocotrienol has shown effects against cancer, a precise mechanism of action has still not yet been confirmed for neuroblastoma, and furthermore, central nervous system (CNS) cancers such as neuroblastoma are vastly under-represented in literature concerning the anti-tumour effects of tocotrienols (Sailo *et al.*, 2018).

Additionally, tocotrienols have been shown to work synergistically with other drug treatments. Tocotrienol rich fraction and tamoxifen in MCF7 and MDA-MB-435 breast cancer cells showed anti-proliferative and synergistic effects (Nesaretnam *et al.*, 2012) and more recently, a paper published results of the synergistic actions of γT3 and hydroxyl-chavicol, a plant extract, on 3 different

grades of glioma cell lines (Abdul Rahman *et al.*, 2014). When combined with jerantinine A, γT3 also demonstrated synergistic effects in the treatment of U87MG glioblastoma cells (Abubakar *et al.*, 2017). The combination of γT3 and 6-gingerol (6G) also showed a synergistic effect on HT-29 and SW837 colorectal cancer cell lines (CI = 0.89 ± 0.02 and CI = 0.79 ± 0.10) (Yusof *et al.*, 2015).

While there is still little research on the effects of tocotrienols on CNS cancers, a recent study has shown a novel mechanism of action of γT3 in neuroblastoma as a BH3 mimetic targeting the BH3 hydrophobic groove in the Bcl-2 protein (Tan *et al.*, 2016). The researchers found that γT3 reduced cell viability and induced cell death in SH-SY5Y neuroblastoma cells. Treatment with γT3 also depolarised the mitochondrial membrane potential, enabling release of cytochrome c to the cytosol and increasing the activities of caspases-9 and -3, but not caspase-8. Treatment with Bax and caspase-9 inhibitors also blocked the effects of γT3. Finally, they showed that γT3 binds at the hydrophobic groove (BH3 domain) of Bcl-2 using *in silico* docking, while in a binding assay a shift in fluorescence readings showed that γT3 competed with a fluorescent probe to bind at the hydrophobic groove.

There is still room for improvement in the treatment for high risk neuroblastoma (Peinemann *et al.*, 2015). As suggested by Niizuma *et al.* (2006), an adjunct to the post-consolidation stage to overcome treatment resistance in high risk neuroblastoma that targeted Bcl-2 pro-survival proteins may enhance the action of the current retinoic acid used in clinical therapy, 13cRA. Furthermore, γT3 has demonstrated synergy with other compounds, and has shown significant anti-proliferative effects on SH-SY5Y neuroblastoma cells as a single agent (Tan *et al.*, 2016).

Therefore, using the study by Tan *et al.*, (2016) as a foundation, we would like to further study the effects of γT3 on neuroblastoma, and it will be important to do so with a model that better represents high risk neuroblastoma with *MYCN* overexpression. Additionally, a known Bcl-2 inhibitor could be used to compare effects of γT3 both as single treatments and in combination. Finally, in order to best understand the effect of γT3 in a complex system, an *in vivo* model will be required. While *in vitro* studies give good indications of drug activity, an *in vivo* model will represent the interactions within a human body better than cell lines.

1.2 HYPOTHESIS

Based on the current, available literature, we hypothesise that γT3 has significant anti-tumour effects on neuroblastoma. We hypothesise that it binds to the hydrophobic groove of the Bcl-2 protein, initiating the intrinsic apoptosis cascade. Additionally, we predict that combination drug treatment will show a synergistic effect and show similar, although less significant anti-tumour effects compared to the Bcl-2 inhibitor ABT-263.

1.3 AIMS & OBJECTIVES

1.3.1 General aims

To confirm that γT3 binds to the BH3 domain of the Bcl-2 protein, and whether that binding is able to trigger the apoptosis signalling cascade, consequently reducing the tumour size of a neuroblastoma ectopic xenograft in a nu/nu Nude

Mouse Crl/NU-Foxnlnu (albino) model. We also want to confirm if the combination of γT3 and 13cRA is synergistic.

1.3.2 Specific objectives

1. To determine the exact effect of γT3 on cell viability and cell death, as a single agent, in combination with 13cRA, and in comparison to the Bcl-2 inhibitor, ABT-263 in normal *MYCN* expressing SH-SY5Y cell line and *MYCN* overexpressing SK-N-BE(2) cell line.
2. To confirm, using flow cytometry and FITC Annexin/PI staining, if cell death post-treatment with γT3 is caused by apoptosis. Also to compare level of apoptosis (if any) between single γT3, 13cRA and ABT-262, and 13cRA combinations with either γT3 or ABT-263.
3. To investigate anti-tumour effects of 13cRA and γT3 as single agents or of 13cRA combinations with either γT3 or ABT-263 in a nude mouse model, and monitor tumour volume manually (callipers) and PET scan.
4. To confirm that action of γT3 is caused by apoptosis by measuring protein levels of Bcl-2, Bcl-X_L, caspase-3, caspase-9, and p53 in *in vitro* and *in vivo* samples, post-treatment.
5. To investigate if MYCN protein expression in *in vitro* and *in vivo* samples is affected by treatments.

CHAPTER 2 LITERATURE REVIEW

2.1 NEUROBLASTOMA

2.1.1 General overview

Neuroblastoma is the most common cancer diagnosed before the age of one (Teitz *et al.*, 2011). In Malaysia, the disease is the fourth most common childhood cancer, with a rate of 4.9 per million of childhood cancer cases (Lim, 2002) and in Singapore, a neighbouring country, the disease was fifth most common of childhood cancers and recorded to have an incidence of 8.8 per million (Tan & Ha, 2005). In the United States, neuroblastoma is the third most common childhood cancer (7%) (Ward *et al.*, 2014) and it accounts for 8% of paediatric cancers in Japan (Nakagawara *et al.*, 2018) and 7.7% of cases in Europe (Gatta *et al.*, 2014). It is extremely rare in adults, with only ~4% of cases occurring ≥ 20 years of age (Esiashvili *et al.*, 2007).

Neuroblastoma tumours develop during embryogenesis and are thought to arise from a precursor cell in the neural crest committed to the sympatho-adrenal lineage. The neural crest is a structure that is only present in embryos, and cells that develop there go on to develop into multiple cell types and tissues, including, but not limited to, melanocytes, adrenal medulla and neurons of the peripheral nervous system. Primary tumours are commonly found in the paraspinal sympathetic ganglia (~60%) and adrenal medulla (~30%), while the remainder

arise from the sympathetic ganglia in the head/neck, chest and pelvis (Cheung & Dyer, 2013; Louis & Shohet, 2015; Maguire, Thomas & Goldstein, 2015).

Common presenting signs and symptoms of neuroblastoma include an enlarging abdominal mass, pallor, fever, weight loss and bone/joint pain. Some patients also present with paraneoplastic syndromes such as opsoclonus-myoclonus and severe, chronic watery diarrhoea (Ng *et al.*, 1999; Maguire, Thomas & Goldstein, 2015).

The median age of diagnosis is approximately 18 months (Brodeur, 2003) and survival outcome was found to worsen with increasing age. For example, stage 2 and 3 patients below 18 months of age had a statistically higher event free survival (EFS) than those aged 18 months or older (88% ± 1% vs. 69% ± 3%) (Cohn *et al.*, 2009). Additionally, relative survival statistics (net survival measure representing cancer survival in absence of other causes of death) in a 5 year follow up after diagnosis from the US National Cancer Institute's Surveillance, Epidemiology, and End Results (SEER) programme covering the years between 1973 and 2002, showed 85.6% relative survival in infants (<1 year old) compared to only 38.4% in adults (≥20 years) (Esiashvili *et al.*, 2007).

Unlike many cancers, neuroblastoma is rarely familial, affecting less than 1% of all cases (Schleiermacher, Janoueix-Lerosey & Delattre, 2014). In those rare cases, two genes, anaplastic lymphoma receptor tyrosine kinase (*ALK*) and paired-like homeobox 2b (*PHOX2B*) are associated with ~80% of cases of familial neuroblastoma, with the majority (~75%) of these attributed to *ALK* (Brodeur & Bagatell, 2014; Schleiermacher, Janoueix-Lerosey & Delattre, 2014). *ALK* is involved in the regulation of proliferation and differentiation of

the neural crest, while *PHOX2B* is also associated with differentiation and development of the autonomic neurons that arise from the neural crest (Cheung & Dyer, 2013). Neuroblastoma tumour formation is more likely attributed to somatic genetic alterations, as shown by the limited familial genetic predispositions. One of the most relevant genetic alterations, *MYCN* amplification, will be further discussed in *Section 2.1.2*.

Like many other cancers, there are different risk stages in neuroblastoma. Some cases of neuroblastoma regress spontaneously with no treatment needed and survival rates of up to 90% in low risk neuroblastoma cases have been reported (Yalçin *et al.*, 2013). However, this feature of neuroblastoma may in fact contribute to some under-reporting of cases in developing countries where extensive scanning of young children is not common (Shuangshoti *et al.*, 2012; Ng *et al.*, 1999). The majority of studies on neuroblastoma prevalence, treatment and outcomes have mostly been conducted in North America, Europe, Japan and Australia (Cohn *et al.*, 2009).

Unfortunately, far lower survival rates are reported in high risk neuroblastoma cases, with a less than 50% 5-year event-free survival rate (Cohn *et al.*, 2009) and 5-year overall survival of only up to 59%, and this with the most intensive treatment protocol (Yalçin *et al.*, 2013). For the purpose of this literature review, event-free survival can be defined as the time to the occurrence of a particular event, such as tumour progression, secondary tumour development, or death from any cause, while overall survival is the time until a patient dies from any cause, not only related to the cancer and treatments (Yalçin *et al.*, 2013).

The following section will explore neuroblastoma stage classification in further detail, including the different requirements for each risk stage and a discussion on specific risk factors such as *MYCN* expression.

2.1.2 Neuroblastoma classification

According to the International Neuroblastoma Risk Group (INRG) classification, there are four stages of neuroblastoma; with some cases on the lowest end of the scale able to spontaneously regress and on the other end of the scale, the most aggressive form of neuroblastoma considered "high-risk", where very intensive treatment is necessary (Cohn *et al.*, 2009; National Cancer Institute, 2014). These four groups can be further divided into sixteen subgroups, determined according to a variety of diagnostic factors, such as age, histopathology and biology of tumour and whether or not it has metastasised. There are a total of six specific prognostic risk factors, with four outlined in Table 2.1. The other two risk factors are: histologic category and ploidy (with diploid increasing risk group vs hyperdiploid) (Cohn *et al.*, 2009; Pinto *et al.*, 2015). Table 2.1 is a modified version of the original INRG Consensus Pre-treatment Classification schema, which was constructed based on analyses of 8800 children diagnosed with neuroblastoma between 1990 and 2002 from North America, Australia, Europe and Japan (Cohn *et al.*, 2009).

One current issue with reporting the stages of neuroblastoma advancement is that there are classification variations due to slightly different definitions depending on the clinician's risk group parameters. This can change depending on region (Cohn *et al.*, 2009; Yalçin *et al.*, 2013) as well as when the diagnosis

occurred, as many revisions have been made over the decades since the development of the Evans staging system in 1971 (Sokol & Desai, 2019).

The INRG Staging System is the most recently defined and has slowly been adopted globally as the common staging system, over the International Neuroblastoma Staging System (INSS). However, due to the currently evolving nature of staging classification, and therefore changing criteria for trial inclusion, it is difficult to evaluate all neuroblastoma studies equally. (Park *et al.*, 2013; Peinemann *et al.*, 2015). One specific factor that has caused some issues with reporting is a change in cut off age from 12 months to 18 months, for inclusion in the high risk neuroblastoma group. So, there was possible inclusion of patients from what is now considered intermediate risk included in the high risk cohort, which distorts the data and makes it difficult for future researchers to compare and utilise those reports (Yalçin *et al.*, 2013).

However, all the different risk group parameters do agree on several risk factors. One of which is *MYCN* gene amplification being not only an indicator of high risk neuroblastoma, but also a general predictor of poor disease prognosis at all stages and a high chance of recurrence (Park *et al.*, 2013; Cohn *et al.*, 2009; International Society of Paediatric Oncology Europe Neuroblastoma, 2014). Anything from a quarter to a third of neuroblastoma tumours found in human patients are known to possess *MYCN* amplification (Teitz *et al.*, 2011; Tang *et al.*, 2006). As seen in INRG Stage L1 in Table 2.1, presence of *MYCN* amplification alone is sufficient to upgrade the pre-treatment risk group from "very low" to "high" risk.

Table 2.1 International Neuroblastoma Risk Group (INRG) Consensus Pre-treatment Classification Schema, adapted from original version published by the INRG Task Force. Abbreviations: L1, localised tumour confined to one body compartment and with absence of image-defined risk factors (IDRF); L2, locoregional tumour with presence of one or more IDRFs; M, distant metastatic disease (except stage MS); MS, metastatic disease confined to skin, liver and/or bone marrow in children <18 months of age; NB, neuroblastoma; NA, not amplified; Amp, amplified; VL, very low; L, low; I, intermediate; H, high. (Cohn *et al.*, 2009).

INRG stage	Age (months)	Grade of tumour differentiation	MYCN	11q Aberration	Pre-treatment Risk Group
L1/L2					VL
L1			NA		VL
			Amp		H
L2	< 18		NA	No	L
				Yes	I
	≥ 18	Differentiating	NA	No	L
				Yes	I
		Poorly differentiated or undifferentiated	NA		I
			Amp		H
M	< 18		NA		L
	< 12		NA		I
	12 to < 18		NA		I
	< 18		Amp		H
	≥ 18				H
MS	< 18		NA	No	VL
				Yes	H
			Amp		H

One of the first reports regarding the significance *MYCN* gene amplification was a study of 89 patients with untreated neuroblastoma tumours (Seeger *et al.*, 1985). The researchers showed tumours classified as INSS Stage 4 progressed most quickly and overall, the results gave a strong indication that aggressiveness of neuroblastoma tumour progression is connected to the amplification of *MYCN*. In addition, they identified the absence of gene amplification at the 4S stage in the INSS classification, now a commonly known feature of INSS Stage 4S.

Unfortunately, directly focusing on *MYCN* as a treatment target has proven problematic due to several reasons. One reason is that Myc protein does not have intrinsic enzymatic activity, thus cannot be directly targeted by small molecule inhibitors like many other oncoproteins. Additionally, the same form of Myc is expressed in both normal and cancer cells (as well as other kinases associated with its activities), albeit in different quantities, so excessive toxicity is another problem with any Myc inhibitors (Fletcher & Prochownik, 2015).

The status of 11q chromosome is another known, unfavourable biological factor that is taken into account when assessing the risk group of neuroblastoma at diagnosis (Cohn *et al.*, 2009). Also known as 11q loss of heterozygosity (LOH), 11q aberration has a significant correlation with advanced stage disease, where $p = 0.042$ (Guo *et al.*, 1999). As observed in Table 2.1, the presence of an 11q aberration reduces the favourability of the diagnosis, such as at Stage L2, where presence of 11q aberration in a child <18 months elevates the risk group from low to intermediate, however, not to the same extent of just the presence of *MYCN* amplification elevating the risk group from very low to high at Stage L1.

2.1.3 Current treatments

Treatment for neuroblastoma is generally dependent on risk category where in the lowest risk cases, patients can simply be monitored because the tumour may regress without treatment. High risk neuroblastoma, which is the focus of this research project, has a more complex treatment plan which can include some, if not all, of the following: surgery, high dose chemotherapy, stem cell rescue, radiotherapy, immunotherapy and finally, differentiation therapy, using cis-retinoic acid (International Society of Paediatric Oncology Europe Neuroblastoma, 2014; National Cancer Institute, 2014). Figure 2.1 shows a summary of high risk neuroblastoma treatment.

13-*cis*-retinoic acid (13cRA) is administered at a high dose, with a pulsed frequency (160 mg/m^2/day in 2 divided doses for 14 out of every 28 days) for post-consolidation (maintenance) therapy in high risk neuroblastoma (Matthay *et al.*, 1999). This dosing schedule was based on *in vitro* studies that showed that drug action was reliant on optimal 13cRA plasma levels, which could be achieved this way, while limiting dose-dependent side effects (Matthay, 2013; Reynolds *et al.*, 2003).

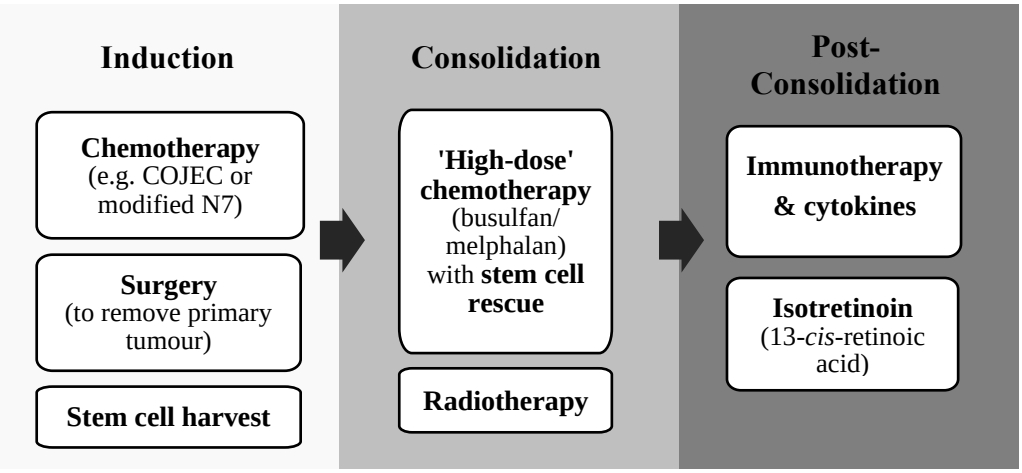

Figure 2.1 Summary of high-risk neuroblastoma treatment. COJEC-cisplatin, vincristine, carboplatin, etoposide, cyclophosphamide; N7-cyclophosphamide, doxorubicin & vincristine/cisplatin & etoposide. (International Society of Paediatric Oncology Europe Neuroblastoma, 2014; Pinto *et al.*, 2015)

However, treatment for high-risk cases is still far from optimal, in part due to the intensity and multiple stages of treatment. There are numerous side effects and complications associated with treatment for high risk neuroblastoma, some of which are briefly described here – general nausea and vomiting, dose-limiting myelosuppression from etoposide (Paediatric Formulary Committee, 2014); in addition to mucositis and longer hospitalisation, busulfan/melphalan treatment needs close monitoring for pulmonary damage and hepatotoxicity (Park *et al.*, 2013); dose-limiting pain associated with anti-GD2 monoclonal antibody therapy (Cheung & Dyer, 2013) and dose related mucotaneous toxicity, skin dryness and cheilitis from 13-cis retinoic acid (Reynolds *et al.*, 2003).

Furthermore, many neuroblastoma patients still encounter treatment resistance. While improvements have been made to high risk neuroblastoma treatment over the last few decades, there is still a portion of patients who have a poor survival rate. In a non-randomised trial carried out in Europe, 30% of study candidates

either experienced disease progression or did not respond to induction chemotherapy. Candidates recruited for this trial were infants below one year of age with *MYCN* amplification (Canete *et al.*, 2009).

Clinical trials have been conducted in order to optimise high-risk neuroblastoma treatments. A Cochrane Review on treatment for high-risk neuroblastoma in children evaluated three randomised controlled trials (RCT) that focused on high-dose chemotherapy, also known as myeloablative therapy, and stem cell transplantation (Yalçin *et al.*, 2013). In total, 739 children were studied in this evaluation. Unfortunately, the investigators were unable to make recommendations on an optimal treatment programme due to incomplete or statistically insignificant data. They found that while there was a statistically significant difference in overall survival when comparing myeloablative therapy to conventional chemotherapy or no treatment, there was no more statistically significant difference once additional follow up data was added to the analyses. Only the difference in event-free survival remained statistically different. The researchers attributed the statistical insignificance largely due to methodological limitations, such as the lack of standardised staging systems (i.e. parameters for the categorisation of risk group varied from study to study), a change in cut off age for high risk disease, and insufficient data.

A similar problem emerged when Cochrane evaluated another set of high-risk neuroblastoma studies, this time evaluating efficacy and adverse events of 13cRA post-consolidation therapy with high-dose chemotherapy followed by bone marrow transplantation, compared to placebo or no therapy for high risk neuroblastoma patients (Peinemann *et al.*, 2015). The details of this review will

be discussed in further detail in the following *Section 2.1.3.1*, but in concluding the review, Peinemann *et al.* (2015) theorised that the many changes in treatments and risk classifications contributed to their inability to properly assess the significance of the treatments in trials.

2.1.3.1 Retinoic acid and neuroblastoma

Retinoic acid (RA) is a known, potent differentiation inducer for human cancer cells, including neuroblastoma, and *in vitro*, has been shown to significantly reduce *MYCN* RNA expression during active treatment and more than 60 days after treatment removal. There are two families of retinoic acid receptor: RA receptor (RAR) and retinoid X receptor (RXR), and each can be further divided into α, β and γ. RA binds to these receptors, and they have been found to be expressed in most neuroblastoma lines and primary tumours (Reynolds *et al.*, 2003).

All-trans-retinoic acid (ATRA) and 13-cis-retinoic acid (13cRA) are two common clinically used RA isomers, although 13cRA is the isomer that is used in neuroblastoma post-consolidation treatment. 13cRA was found to produce higher drug levels than ATRA in a phase I trial, and additionally, a self-induced increase in rate of ATRA metabolism was found (Reynolds *et al.*, 2003).

Drawing on earlier work that presented the ability of retinoids, including 13cRA (shown in Figure 2.2), to induce differentiation in neuroblastoma cells, researchers demonstrated in a trial that the addition of 13cRA was beneficial to patients following chemotherapy or bone marrow transplantation. Of the patients who received 13cRA, 46 ± 6 percent had an event free survival rate 3 years post

randomisation versus 29 ± 5 percent of patients who did not receive 13cRA (p = 0.027) (Matthay *et al.*, 1999). However, in a follow-up study by the same research group, the 5-year event free survival rate was 42 ± 5% vs for patients who were given 13cRA compared to 31 ± 5% in those that were not. This difference was not significant (p = 0.1219) (Matthay *et al.*, 2009). Matthay *et al.* (2009) also found an increase in 5-year overall survival when comparing 13cRA post-consolidation treatment to no further treatment: 50 ± 5% vs 39 ± 5%. Unfortunately, this was not significant (p = 0.1946).

As mentioned in *Section 2.1.3*, a Cochrane Review evaluating efficacy and adverse events of 13cRA post-consolidation therapy with high-dose chemotherapy followed by bone marrow transplantation, compared to placebo or no therapy for high risk neuroblastoma patients, searched several electronic databases covering a period of nearly 70 years, trial registries, conference proceedings and references from recent reviews with no limit on publication year and language. Only one randomised controlled trial (RCT) that met all the parameters in the Cochrane methodology was identified: the previously mentioned study by Matthay *et al.* (2009) (Peinemann *et al.*, 2015). The analysis found no statistical difference in overall survival and event-free survival between the groups in the RCT. While the retinoic acid group showed a higher five-year overall survival rate than the no further treatment group (59% vs 41%), this difference was also not statistically significant. The lack of statistical difference was attributed to a low power, and further issues such as changes in risk assessment and treatments since the original RCT was performed in the late 1990s.

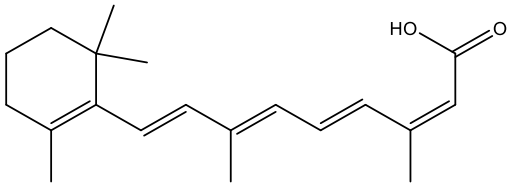

Figure 2.2 Chemical structure of 13-*cis*-retinoic acid (PerkinElmer Informatics, 2019; Hadjidaniel & Reynolds, 2010).

2.1.3.2 13-*cis*-retinoic acid and other drugs

It is interesting to note that while 13cRA has shown some benefit when given as post-consolidation therapy to eliminate residual disease, an *in vitro* study demonstrated its antagonism of cytotoxic agents commonly used in induction and consolidation stages of high risk neuroblastoma therapy. The study showed that overlapping treatment of 13cRA and cytotoxic agents used in induction chemotherapy for high-risk neuroblastoma treatment, such as cisplatin and doxorubicin, increased the expression of anti-apoptotic Bcl-2 family proteins, which was detrimental to the action of the cytotoxic agent. However this antagonistic action was considered consistent with the action of retinoic acid to differentiate tumour cells into mature cells, which naturally have a higher threshold for apoptotic death (Pinto *et al.*, 2015; Hadjidaniel & Reynolds, 2010).

Reassuringly, while 13cRA may have antagonistic properties when combined with cytotoxic agents such as cisplatin and doxorubicin, there are other agents that have shown synergy when used together with 13cRA in the treatment of cancer.

Milanovic *et al.* (2015) concluded that 13cRA was synergistic when used with thalidomide *in vitro* on glioblastoma cell lines (U251 and U343) and when used

in vivo in subcutaneous xenografts in nude mice, caused significant tumour growth inhibition. Additionally, they found that the addition of thalidomide suppressed genes associated with treatment resistance in glioblastoma that were usually induced by treatment with 13cRA (*IL-8*, *HILDPA*, *IGFBPA*, and *ANGPTL4*). It should be noted however, that the paper did not publish quantitative results of synergy.

Tolfenamic acid (TA), a small molecule non-steroidal anti-inflammatory drug, was found to significantly inhibit cell viability ($p<0.0001$) when used in combination with 13cRA when compared to individual treatments in an *in vitro* study using neuroblastoma cell lines (LA1-55n and SH-SY5Y), although synergy was only quantitatively demonstrated in SH-SY5Y cell lines (Shelake *et al.*, 2015). They also found a decrease in Sp1 and survivin expression and an increase in apoptotic markers, Annexin-V positive cells, caspase-3 and -7 activity, and c-PARP levels and a downregulation of Akt and ERK1/2 when combination treatment was used.

The use of 13cRA in the treatment of neuroblastoma still appears to be limited. The same Cochrane Review researchers performed an update search two years after their original paper, but did not find any additional studies that met their criteria (Peinemann *et al.*, 2017). Additionally, resistance to RA treatment has now been observed and linked to lower 5-year overall survival rates (Waetzig *et al.*, 2019).

Nevertheless, there are some potential routes to overcome the treatment drawbacks. As demonstrated by Shelake *et al.* (2015), it could be feasible to add

an adjunct drug to the 13cRA post-consolidation treatment to overcome treatment resistance, thus enhancing treatment effectiveness.

And although not directly studying 13cRA, Niizuma *et al.* (2006) found that treatment with the retinoic acid isomer, ATRA, slightly induced accumulation of anti-apoptotic Bcl-2 in a neuroblastoma cell line (NB-39-nu), which normally has low expression of Bcl-2. They also examined the effect of enforced expression of Bcl-2 in another naturally low Bcl-2-expressing neuroblastoma cell line (CHP134), and found that caspase-3 activated apoptosis was inhibited when the cells were treated with ATRA, thus rendering the treatment ineffective. A possible adjunct to counteract the anti-apoptotic actions of Bcl-2 may improve the actions of retinoic acid differentiation on cancer cells.

We hypothesise, based on previous work completed by Tan *et al.* (2016), that a vitamin E isomer, γ-tocotrienol (γT3), might be a potential candidate for this adjunct treatment. Their work showed that γT3 was able to induce apoptosis in human neuroblastoma cells (SH-SY5Y). The study showed that apoptosis was induced via the intrinsic pathway due to increased caspase-9 activity in γT3-treated cells, as well as increased cell viability when a Bax inhibitor was added. Furthermore, molecular docking analysis suggested that γT3 binds to the hydrophobic groove of Bcl-2, while a binding assay showed that γT3 competed with a fluorescent probe to bind at the same groove.

The following section will discuss γ-tocotrienol and evaluate available literature on its background, possible mechanisms, and advantages and disadvantages.

2.2 VITAMIN E

Vitamin E is the name given to a large group of natural and synthetic hydrophobic substances, which were first identified as “factor X”, an essential dietary factor for fertility in rats (Evans & Bishop, 1922). Shortly after that, the chemical structure and antioxidant activity of vitamin E was discovered, leading to research into this particular property of vitamin E which continues on till the present day (Zingg, 2007).

The two naturally-occurring members of the vitamin E family are tocopherol and tocotrienol. They each have four isomers– α, β, γ and δ. Tocopherol and tocotrienol are structurally very similar and only differ in terms of saturation, with tocotrienols having an unsaturated isoprenoid side chain in place of the saturated phytyl tail on tocopherol. Additionally, tocopherols possess 3 chiral centres, as indicated in Figure 2.3 (Kannappan *et al.*, 2012; Cardenas & Ghosh, 2013). Figure 2.3 shows structural representations of all eight isomers.

Tocopherol is far more easily and widely available than tocotrienol. It is present in common components of the human diet, such as vegetable oils including soybean, corn and sesame, as well as in nuts (Ju *et al.*, 2010). One of the best sources of γT3 is the *Elaeis guineensis* tree, where crude palm oil is extracted from its fruit. Up to 800mg/kg of tocotrienols, mostly composed of γ- and α-tocotrienol, can be extracted from this source (Sen, Khanna & Roy, 2006). Other good sources of tocotrienols include rice bran oil, with about 450mg/kg (Ahsan *et al.*, 2014) and cereal grains, such as oats, barley and rye, but in trace amounts (Theriault *et al.*, 1999; Ju *et al.*, 2010). Compared to tocopherol sources, tocotrienol sources are not widely consumed.

With regards to vitamin E pharmacokinetics, alpha-tocopherol transfer protein (α-TTP) facilitates the transport of α-tocopherol (αT) in the liver, which is then secreted into the blood. Mice that were α-TTP$^{-/-}$ consistently recorded lower levels of αT in organs and blood plasma than wild-type mice, both on a normal diet and even when fed αT supplements (Lim & Traber, 2010). In a small study of 10 healthy men and women, detectable concentrations of tocotrienols, including γT3, were found in blood plasma after supplementation with tocotrienol rich fraction (TRF) containing 70% tocotrienols. However, levels of αT were still significantly higher than that of tocotrienols (30.13 ± 2.91 μM to 22.95 ± 1.26) (Fairus *et al.*, 2012).

Tocopherol

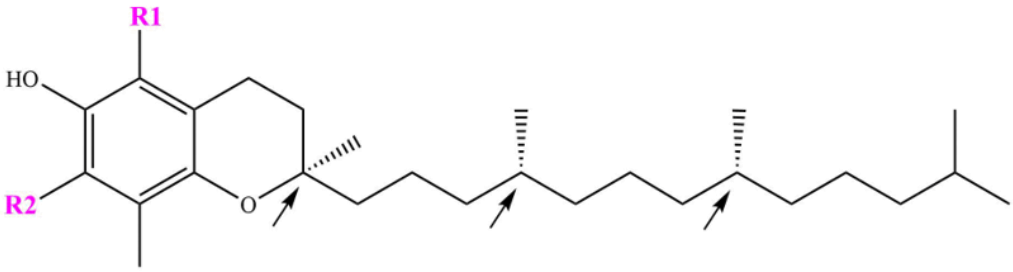

Tocotrienol

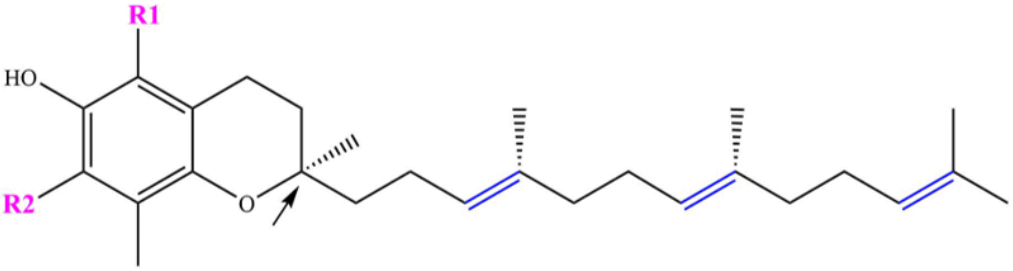

	α	β	γ	δ
R1	CH_3	CH_3	H	H
R2	CH_3	H	CH_3	H

Figure 2.3 Vitamin E isoforms. Structural differences between tocopherol and tocotrienol; chiral centres are indicated by small arrows, and methyl groups on the chromonal head that determine α, β, γ and δ isoforms are indicated in the key as either R1 or R2. Also shown are the saturated tocopherol (farnesyl) and unsaturated tocotrienol (phytyl) tails and unsaturated bonds on phytyl tails are shown in blue. (PerkinElmer Informatics, 2019; Cardenas & Ghosh, 2013)

2.2.1 Tocopherol

Tocopherols are known to have a higher bioavailability, with higher detected plasma concentrations, than tocotrienols. When administered orally, tocopherols have both a longer circulation time and better distribution (Fu *et al.*, 2014). Much of vitamin E research has focused on α-tocopherol (Cardenas & Ghosh, 2013; Kannappan *et al.*, 2012); one possible reason being that α-tocopherol was the first vitamin E isomer recognised (Ahsan *et al.*, 2014) and another being that it is more readily available than tocotrienols in common components of the human diet, such as vegetable oils (Ju *et al.*, 2010).

Unfortunately, large clinical trials in the last decade demonstrated a lack of significant clinical improvement influenced by tocopherol. These results have been compiled and reviewed in recent years (Cardenas & Ghosh, 2013; Ling *et al.*, 2012).

The SELECT (Selenium and Vitamin E Cancer Prevention Trial) clinical trial showed the possibility of a higher risk of prostate cancer with α-tocopherol instead of a reduction, as was originally hypothesised (Klein *et al.*, 2011). The SELECT trial investigated the long term effects of selenium and vitamin E on 35533 relatively healthy men in over 400 centres in the USA, Canada and Puerto Rico. The men were randomly assigned to control, selenium only, vitamin E (α-tocopherol) only, both, or control groups. The trial was run over almost three years and the main outcome measure was prostate cancer incidence. The unfortunate conclusion of the SELECT trial was that dietary supplementation with vitamin E (α-tocopherol) significantly increased the risk of prostate cancer among healthy men.

The Women's Health Study (WHS) showed that taking 600IU of natural source vitamin E (α-tocopherol) on alternate days did not give an overall benefit for cardiovascular disease (CVD) or cancer (Lee *et al.*, 2005). The blinded study looked at nearly 40000 healthy American women aged at least 45 years old. The women were sorted into a vitamin E or a placebo group and the study took place between 1992 and 2004. Endpoints were the occurrence of a cardiovascular event, e.g. myocardial infarction, or the occurrence of one of the following cancers: breast, lung and colon. The WHS researchers concluded by cautioning against vitamin E supplementation for CVD or cancer prevention.

2.2.2 Tocotrienol

Contrary to tocopherol, tocotrienol has recently been found to possess more promising therapeutic abilities than expected, leading researchers to shift their focus to tocotrienol. This is despite the superior bioavailability and easy dietary availability of tocopherols (Theriault *et al.*, 1999; Sen, Khanna & Roy, 2006; Wong & Radhakrishnan, 2012). Some studies have used tocotrienol rich fractions (TRFs), others used pure tocotrienol homologues, while some used both (Theriault *et al.*, 1999; Sen, Khanna & Roy, 2006; Kannappan *et al.*, 2012).

An important consideration is that the proportions of tocotrienol homologues in a TRF vary depending on the batch (Fu *et al.*, 2014) and despite their structural similarities, individual tocotrienol homologues may have very different targets and actions from each other (Nesaretnam, 2008; Kannappan *et al.*, 2012).

Similar to the clinical effects, pharmacokinetics of tocotrienols are lesser studied than tocopherols. Both tocopherols and tocotrienols are known to be transported in plasma and to tissues using a tocopherol transportation protein (TTP) (Fu *et al.*, 2014). However, when administered together, levels of tocopherols are found to be higher, due to tocopherols more successfully competing with tocotrienols for uptake by TTPs. An *in vivo* study comparing uptake of α-tocopherol and α-tocotrienol showed decreased levels of tocotrienol when co-administered with tocopherol compared to administration alone (Khanna *et al.*, 2005). The study noted that tocotrienols have an 8.5-fold less affinity to TTP than tocopherols. However, the same study also found that in TTP knockout mice, tocotrienols were found to be significantly higher in some tissues than tocopherols. These results lead to researchers to hypothesise a possible TTP-independent pathway.

Despite over two decades of increased interest in vitamin E, there has not yet been a clinical trial using tocotrienol on the same large scale as the SELECT or the WHS trials. However, there are many preclinical studies currently ongoing and promising data has been published, some of which may eventually lead to large-scale human studies.

For example, Ghosh *et al.*, (2009) found that γT3 acted as a radioprotector in CD2F1 mice, preventing radiation-induced neutropenia and thrombocytopenia. The mice were given subcutaneous injections of γT3 at different doses and at different intervals prior to irradiation. They found that 200 mg/kg, 24 hours prior to irradiation gave the optimum results. During the course of that investigation, total white blood cell (WBC) and absolute neutrophil counts (ANC) were seen

to increase after subcutaneous γT3 injection into mice. A further investigation into the effects of γT3 on the hematopoietic system showed that many cytokines and chemokines, such as the haematopoietic growth factors granulocyte-colony stimulating factor (G-CSF) and numerous interleukins, were significantly elevated 12 to 24 hours post γT3 dose (Kulkarni *et al.*, 2012). These levels were elevated with and without radiation. The investigators concluded that the induction of G-CSF by γT3 might play a role in preventing radiation-induced neutropenia and thrombocytopenia and that there is potential for future studies in humans.

Other small trials have proven promising, such as a recent Phase 2, double-blind randomised study investigating protective effects of palm oil vitamin E tocotrienols on brain white matter, that studied a cohort of 121 volunteers in Malaysia (Gopalan *et al.*, 2014). The primary outcome measure was the regression of white matter lesion (WML) load in the brain (numbers and size) as WMLs can be considered indicative of increased risk of or even a subclinical infarct. The study concluded that mixed tocotrienols were found to reduce the progression of WMLs; this was based on 2 years of MRI scans and blood samples.

With regards to cardioprotection, some human studies were reported in a review, although all were small, with most having less than 50 participants and the largest reported with 81 participants (Meganathan & Fu, 2016). Results were mixed, sometimes even contradictory and some of the major drawbacks include failure to report exact composition and purity of tocotrienol fractions (as most studies used TRFs). However, the many cardioprotective effects of tocotrienols

in vivo were discussed in a review (Aggarwal *et al.*, 2010). This review evaluated numerous investigations and found that tocotrienols mainly work by affecting lipid metabolism, in particular cholesterol biosynthesis. They also demonstrate positive effects on blood pressure, as well as antioxidant and anti-inflammatory activity, which included protective effects in diabetes mellitus.

Tocotrienols have been shown to work synergistically with other drug treatments. A review paper mentioned that treatment with tocotrienol rich fraction and tamoxifen in MCF7 and MDA-MB-435 breast cancer cells showed anti-proliferative and synergistic effects (Nesaretnam *et al.*, 2012) and more recently, a paper published results of the synergistic actions of γT3 and hydroxyl-chavicol, a plant extract, on glioma cell lines (Abdul Rahman *et al.*, 2014). The study treated 1321N1 (Grade II), SW1783 (Grade III) and LN18 cell lines with single or combination treatments and found that sub-lethal combination doses demonstrated moderate to strong synergistic interactions in all 3 cell lines. Annexin FITC staining showed increased apoptosis after 24 hours combined treatments. Abubakar *et al.* (2017) also published findings regarding the synergistic effect of γT3, this time when combined with a natural plant product, jerantinine A. Treatment of U87MG glioblastoma cells at low concentrations showed potent antiproliferative effects and led to a reduction on the new half maximal inhibitory concentration of γT3. The mechanisms of γT3 in this study are discussed in *Section 2.2.1.1*. Another study, this time on colorectal cancer, using the combination of γT3 and 6-gingerol (6G) showed a synergistic effect on HT-29 and SW837 cell lines (CI = 0.89 ± 0.02 and CI = 0.79 ± 0.10) (Yusof *et al.*, 2015).

2.2.1.1 Tocotrienol targets in cancer

As mentioned earlier, tocotrienol has been found to act on numerous molecular targets. As shown in Figure 2.4, there are some drugs already on the market that target the same targets as tocotrienols. However, while these drugs have single targets, tocotrienols have multiple targets. In some cases, a single target approach is desirable in order to reduce side effects, but at the same time, a multi-target drug approach may be useful to overcome resistance to drug treatments (Ramsay *et al.*, 2018).

It should be noted that much of current research publications regarding effects of tocotrienols on cancer has focused on the most common cancers: breast cancer, followed by colorectal, liver, pancreatic and prostate cancer (Sailo *et al.*, 2018; Aggarwal *et al.*, 2019). However, much less research has investigated the action of tocotrienols on other cancers. In a recent review paper discussing the potential of tocotrienols as cancer therapeutics, only 3 out of 133 papers referenced in the paper discussed cancers originating from the central nervous system (CNS), and of those, two were written by the same authors (Sailo *et al.*, 2018).

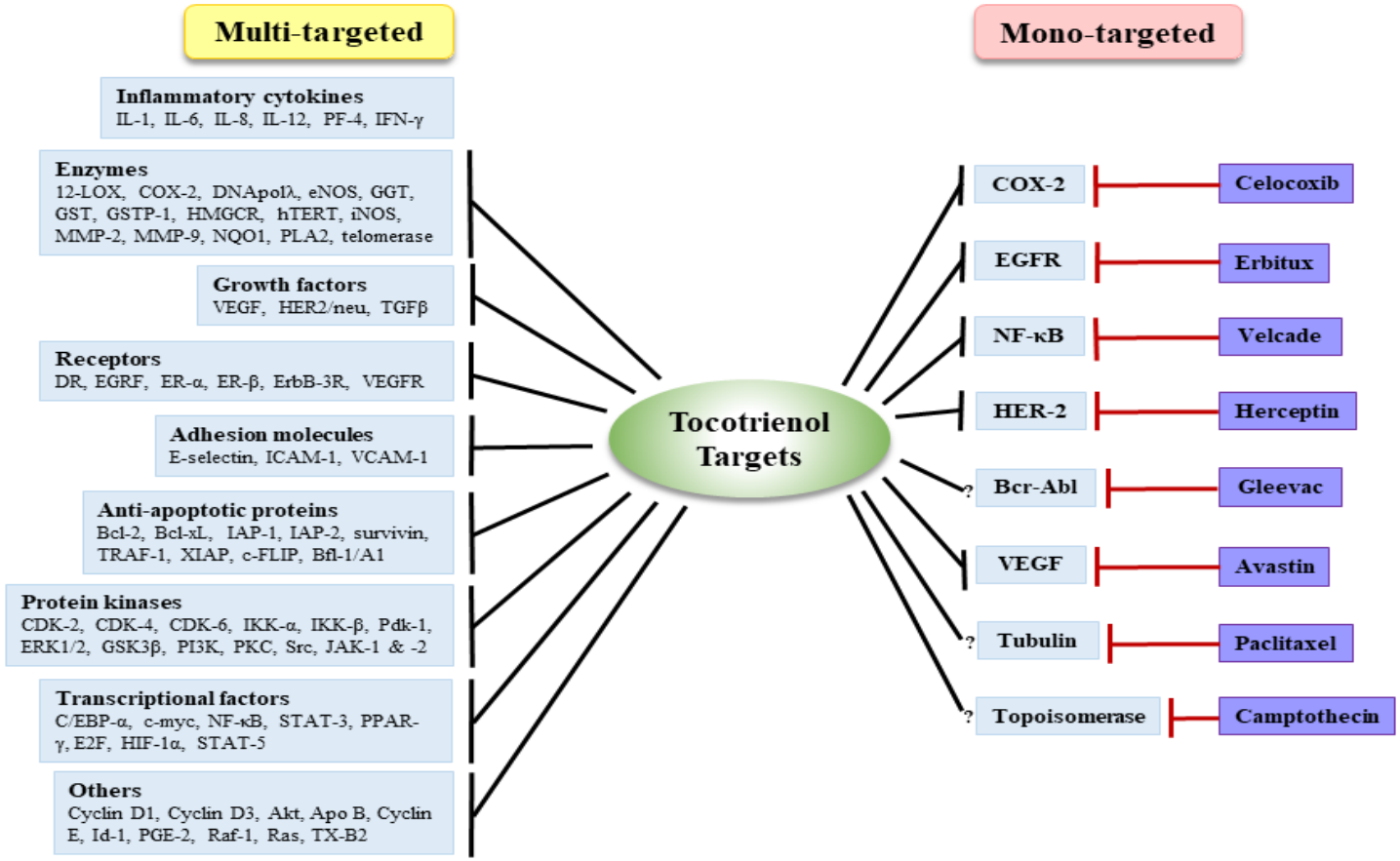

Figure 2.4 Multiple cell signalling pathways targeted by γT3 in cancer (Kannappan *et al.*, 2012).

A study to investigate cytotoxicity and apoptotic activity of tocotrienol isomers found that α-, γ- and λ-tocotrienol inhibited growth of grade IV glioblastoma (U87MG) cell lines in a concentration- and time-dependent manner. The cells were also shown to have apoptotic morphological changes such as condensation of chromatin and cellular blebbing; flow cytometry later confirmed apoptosis by showing cell accumulation at the pre-G_1 stage. Furthermore, ELISA showed that cytochrome c release was significantly higher in the tocotrienol-treated groups than untreated groups ($p<0.05$) and western blotting demonstrated visibly lower levels of Bax protein expression in treated cells than untreated cells (Lim *et al.*, 2014).

A few years later, the same research group investigated the effects of combining lower concentrations of γ-tocotrienol with a natural plant extract (Jerantinine A) on the same U87MG cell line, in order to minimise toxicity of Jerantinine A. They concluded that the combination with Jerantinine A increased the potency of γ-tocotrienol to induce apoptosis and this was via the death receptor and mitochondrial pathways (Abubakar *et al.*, 2017).

In contrast, there are numerous studies regarding the effects of tocotrienols on breast cancer. Sailo *et al.* (2018) compiled evidence of tocotrienol effects on breast cancer, and amongst the proposed mechanisms of action are suppression of HMGR, ER, PI3K/Akt/mTOR, NF-κB, PARP, c-myc, COX2, cyclin D1 and CDK-2, -4, -6; while elevating Bcl-xL, TGF-β, Fas, and JNK. Some investigations showed multiple molecular targets while others only investigated one target.

Nesaretnam *et al.* (2004) injected athymic nude mice with MCF-7 breast cancer cells and then fed mice orally with TRF for 20 weeks. After 20 weeks, there was a significant delay in onset, incidence and size of tumours in TRF-fed mice compared to controls. Additionally, a cDNA array analysis found that interferon-inducible transmembrane protein-1 (*IFITM1*) gene and CD59 glycoprotein precursor gene, both involved in the immune system, were significantly up-regulated, while the c-myc gene, from the family of *MYC* proto-oncogenes, was significantly downregulated in tumours from TRF-fed mice. The expression of c-myc is often overexpressed or aberrant in many breast cancers and this was the focus of an *in vitro* study on two breast cancer cell lines (Parajuli, Tiwari & Sylvester, 2015). Mouse mammary +SA epithelial cell line and human MCF-7 mammary cancer cell lines showed anti-proliferative effects after treatment with γT3. The investigators also carried out western blot and qPCR and found rather than directly targeting c-myc, γT3 acted on targets involved in the stabilisation and degradation of c-myc, such as reduction in phosphorylated-c-myc-serine 62, increase in phosphorylated-c-myc-threonine 58 levels, reduced PI3K/Akt/mTOR and Ras/ MEK/Erk mitogenic signalling, cyclin D1 and cyclin-dependent kinase 4 levels, and increased p27 levels.

In another *in vitro* study, Ahmed, Alawin & Sylvester, (2016) investigated the suppression of the canonical Wnt/β-catenin signalling pathway, involved in cell proliferation and stem cell maintenance, in breast cancer cells. They found evidence that γT3 caused a dose-responsive inhibition of MDA-MB-231 and T-47D cell proliferation, as well as a dose- responsive decrease in the levels of Wnt ligands Wnt3a and Wnt5a/b, which are usually very low in normal cells but are high in breast cancer cells. High levels of Wnt can ultimately lead to

overexpression of Wnt target genes such as *c-myc*, which are involved in survival and proliferation of cancer cells (Laezza *et al.*, 2012).

The effect of TRF and tamoxifen was also investigated in humans. A 5-year double-blinded, placebo-controlled pilot trial recruited 240 women with stage I or II breast cancer and gave them a daily dose of either TRF and tamoxifen or in the control group, placebo and tamoxifen. At the end, although there was a 60% reduction in risk of mortality due to breast cancer in the intervention group, this was not statistically significant ($p = 0.27$) (Nesaretnam *et al.*, 2010).

The action of tocotrienols on prostate cancer has also been heavily investigated. Yap *et al.* (2008) found that γT3 had the most potent anti-proliferative effect on prostate cancer (PCa) cells. After observing activation of pro-caspases and the presence of sub-G^1 cell population, they found that cell death was caused by suppression of NF-kB, EGF-R and Id family proteins (Id1 and Id3), all pro-survival genes. The study also indicated that γT3 was induced by the JNK-signalling pathway, as the effects of γT3 were partially blocked by a JNK specific inhibitor (SP600125).

Another study on prostate cancer also showed that γT3 suppressed the NF-κB–mediated inflammatory pathways linked to tumorigenesis (Kunnumakkara *et al.*, 2010). The investigators showed that γT3 alone and in combination with gemcitabine had an anti-proliferative and pro-apoptotic effect on prostate cancer cell lines *in vitro* and *in vivo*. Treatment with γT3 on prostate cancer cell lines resulted in downregulation of anti-apoptotic proteins Bcl-2, cIAP-1 and survivin, as well as suppression of proliferative proteins cyclin D1, c-myc, and COX-2. MIA PaCa-2 cells were stably transfected with luciferase and orthotopically

implanted into male athymic nu/nu mice. Bioluminescence imaging was used to monitor tumour growth throughout the study and they showed that tumour volume in the combination group was significantly lower than individual treatments and control ($p < 0.001$). Finally, through HPLC, they also determined that a substantial amount of intact γT3 (94.12 ng/g) was present in tumour xenograft tissue.

2.3 APOPTOSIS

Apoptosis is a process in which cells undergo programmed cell death, in order to eliminate unwanted cells. Those cells may be unwanted for a variety of reasons, including intracellular damage, malfunctioning cells and infected cells. Apoptosis, or altruistic cell suicide, is a normal and important homeostatic mechanism in tissues of multicellular organisms. There are two commonly known pathways to initiate apoptosis – one is the extrinsic, the other the intrinsic. Figure 2.5 is a simplified summary of the two pathways, showing the various components involved in the process. Although both pathways end in apoptosis and several of the proteins involved may have dual roles, both pathways are distinct.

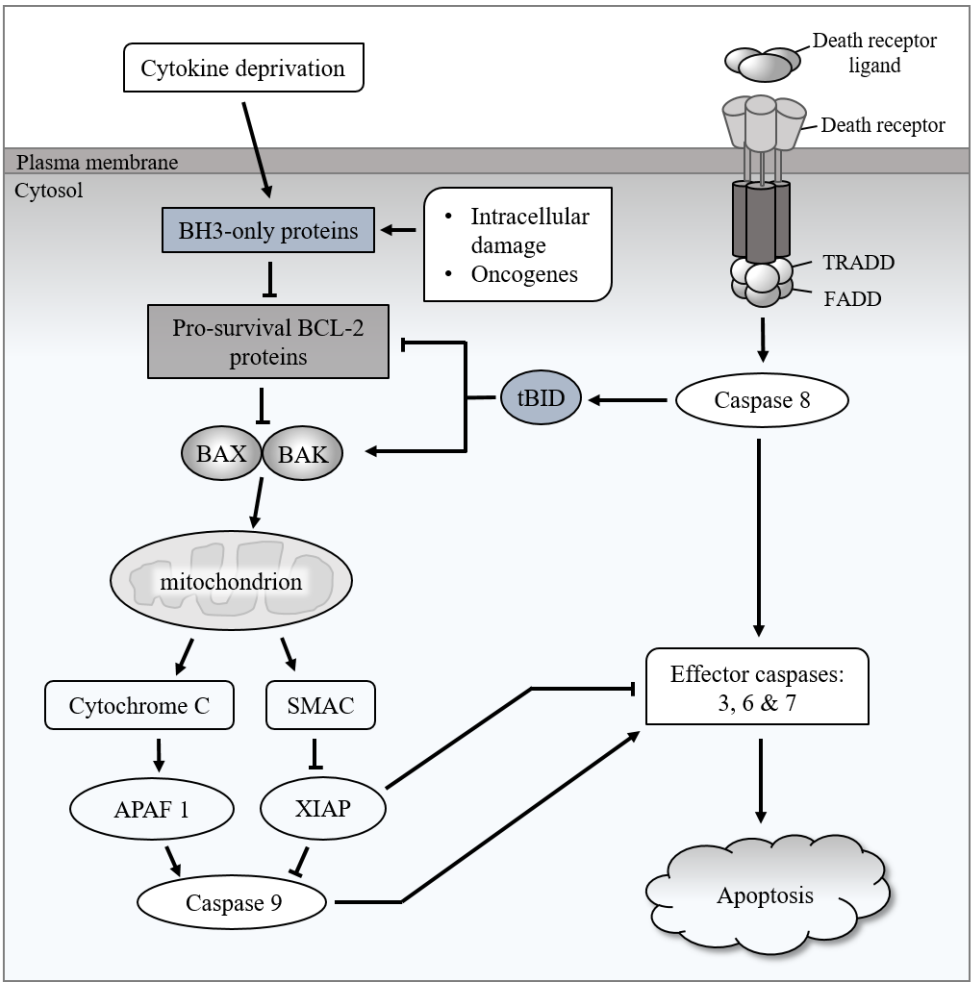

Figure 2.5 Summary of pathways to apoptosis: on the left, the intrinsic (mitochondrial) pathway is initiated by stressors such as cytokine deprivation, intracellular damage or oncogenes. On the right, the extrinsic (death receptor-mediated) pathway is activated by the binding of a death receptor ligand to a death receptor, to begin a cascade where caspase 8, activates the same effector caspases (3,6 and 7) as the intrinsic pathway; in some cells it also activates the intrinsic pathway via tBid (Ashkenazi *et al.*, 2017; Czabotar *et al.*, 2014; Lamers *et al.*, 2012; Adams & Cory, 2007).

In the intrinsic pathway, apoptosis takes place due to the activation of effector caspases 3, 6 and 7 by caspase 9. This happens when cytochrome c is released from the intermembrane space of the mitochondria during mitochondrial outer membrane permeabilization (MOMP), which occurs due to oligomerization of

Bcl-2 associated X protein (Bax) and Bcl-2 antagonist killer 1 (Bak). Cytochrome c then forms a complex with apoptotic protease-activating factor 1 (APAF1) and 2'-deoxyadenosine 5'-triphosphate (dATP), which recruits and activates caspase 9 from procaspase 9. After that, caspase 9 activates procaspases 3 and 7 to form caspases 3 and 7, which then cause apoptosis. Additionally, as cytochrome c is released from the mitochondria, so is another substance called second mitochondria-derived activator of caspase (SMAC). SMAC releases caspase 3 by inhibiting X-linked inhibitor of apoptosis (XIAP), which, when uninhibited, inhibits the caspases and blocks apoptotic signalling (Fesik, 2005; Czabotar *et al.*, 2014; Ashkenazi *et al.*, 2017).

The extrinsic pathway, also seen in Figure 2.5, is activated when a death receptor ligand binds to a death receptor on the cell membrane, triggering the release of caspase 8 inside the cytoplasm, which in turn activates the same caspases 3, 6 and 7 as mentioned in the intrinsic pathway. Caspase 8 can also affect the intrinsic pathway, by way of activating Bax/Bak via tBid (Fesik, 2005; Lamers *et al.*, 2012; Czabotar *et al.*, 2014).

The tumour suppressor protein p53 is also known to activate apoptosis, as a response to cellular stress, including DNA damage and oncogene activation, and is encoded by the *TP53* gene. In an unstressed state, p53 protein levels in cells are low, but when stressors such as DNA damage, activation of oncogenes or nutrient suppression occur, p53 proteins accumulates in the cell. One of the effects of the accumulation of p53 in cells is apoptosis.

According to the review by Aubrey *et al.* (2018), p53 can influence both the intrinsic and extrinsic apoptosis pathways. P53 can induce apoptosis-promoting

factors such Bax, Bid and Apaf1 and specific death receptors. Cytoplasmic or mitochondrial p53 can promote the direct activation of Bax (Thornborrow *et al.*, 2002), neutralise pro-survival Bcl-2 proteins such as Bcl-2 (Bommer *et al.*, 2007), and increase concentration of death receptors (Müller *et al.*, 1998). However, it is not simply accumulation of p53 that leads to apoptosis. The review went on to discuss further mechanisms of p53, however some of those, such as oligomerisation status of p53 and induction of MOMP are currently only proposals, and beyond the scope of this literature review.

The *TP53* gene is known to be mutated in about half of human cancers (Aubrey *et al.*, 2018), and while in neuroblastoma, TP53 gene mutations are rare to uncommon (< 2% in primary tumours, < 15% in relapse) (Van Goethem *et al.*, 2017), there is amplification and increased expression of *MDM2*, which results in increased Mdm2, a p53 inhibitor protein involved in the feedback loop that governs p53 accumulation (Van Maerken *et al.*, 2009). A study by (Van Goethem *et al.*, 2017) found that co-treatment of a panel of neuroblastoma cell lines and orthotopic tumours with the Bcl-2 inhibitor venetoclax (discussed further in *Section 2.3.1.1*) and the Mdm2 antagonist idasanutlin showed a synergistic action to inhibit cell proliferation and tumour growth, and increased action of caspases-3 and -7, compared to individual treatments. In conclusion, the study demonstrated that targeting Bcl-2 and p53 (via Mdm2 antagonist) was an effective approach to the treatment of neuroblastoma.

2.3.1 Bcl-2 protein family

The causes of disrupted apoptosis that can lead to cancer can be summarised into five main groups: impaired death receptor signalling (Fulda *et al.*, 1998; Reesink-Peters *et al.*, 2005), defects or mutations in p53 (Vikhanskaya *et al.*, 2007; Slatter *et al.*, 2011; Avery-Kiejda *et al.*, 2011), reduced expression of caspases (Devarajan *et al.*, 2002; Fong *et al.*, 2006; Shen *et al.*, 2010), increased expression of inhibitor of apoptosis proteins (IAPs) (Lopes *et al.*, 2007; Small *et al.*, 2010) and disrupted balance of Bcl-2 protein members (Goolsby *et al.*, 2005; Miquel *et al.*, 2005). Other researchers have also noted that overexpression of Bcl-2 family proteins was a feature of many cancers (Kelly & Strasser, 2011; Czabotar *et al.*, 2014).

B-cell lymphoma 2 (*BCL2*) is a gene family responsible for encoding over 20 proteins responsible for the regulation of the intrinsic apoptosis pathway (Ashkenazi *et al.*, 2017). The proteins encoded by *BCL2* can be grouped according to function: BH3-only proteins, pro-survival proteins and pro-apoptosis proteins (Table 2.2).

Table 2.2 Summary of selected Bcl-2 family proteins and their roles in programmed cell death (Czabotar *et al.*, 2014).

Initiators	**Guardians**	**Effectors**
BH3-only proteins	Multi-domain pro-*survival* proteins	Multi-domain pro-*apoptotic* proteins
Bad, Bim, Puma, Noxa, tBid, Bik, Hrk, Bmf	Bcl-2, Bcl-X_L, Bcl-w, Mcl-1, A1, Bcl-B	Bax, Bak, Bok

The BH3-only proteins are pro-apoptotic and have two possible mechanisms, either neutralising pro-survival Bcl-2 family proteins or directly activating Bax and Bak, which are both pro-apoptotic proteins. A homologous BH3 region comprising nine amino acids is shared by the BH3 proteins and is essential for their actions. Different BH3-only proteins have different affinities for binding to Bcl-2 family pro-survival proteins – some bind selectively, such as Bad and Noxa, while others, such as Bim and tBid, bind to all pro-survival proteins. Bax and Bak are activated when intracellular steady state levels of BH3 proteins increase (Doerflinger, Glab & Puthalakath, 2015; Czabotar *et al.*, 2014).

Bcl-2 is a member of the Bcl-2 family proteins, with an anti-apoptotic role. It shares structural homology in the Bcl-2 homology (BH) 1, 2, 3, and 4 domains with the other pro-survival proteins. All 6 pro-survival proteins have similar structures, they are globular and comprise of a helical bundle folding to surround a central hydrophobic core helix. This folding forms a groove which can then interact with the BH3 domain of the pro-apoptotic proteins (Czabotar *et al.*, 2014). Examples of these structures can be seen in Figure 2.6.

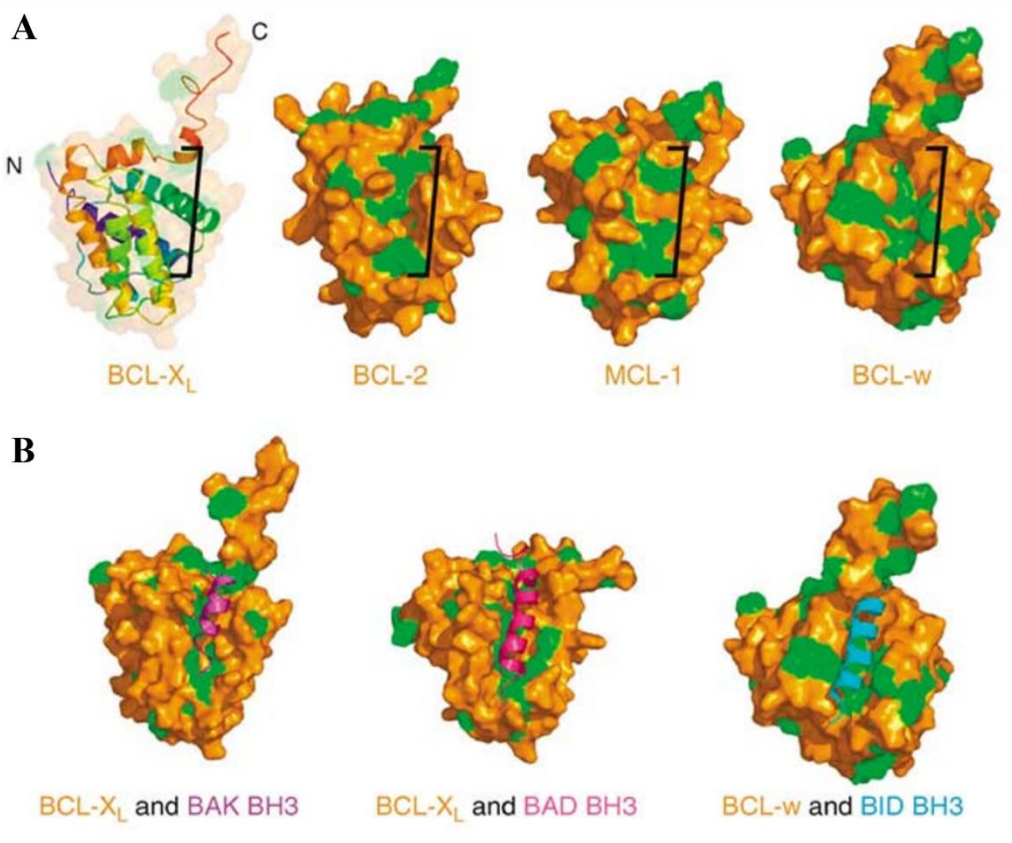

Figure 2.6 Structures of anti-apoptotic Bcl-2 family members (A) and some of the BH3 peptide complexes formed (B). These proteins have two hydrophobic core α-helices surrounded by 6–7 amphipathic α-helices, a flexible N-terminal loop (shown with 'N'), a C-terminal transmembrane domain (shown with 'C') and a surface hydrophobic groove, which is the binding region for α-helical BH3 domains. Green indicates hydrophobic residues, while black brackets indicate BH3 binding grooves. Helical peptides are shown in pink (Bak and Bad) and blue (Bid). (Walensky, 2006).

To briefly describe its actions, Bcl-2 is involved in the intrinsic pathway of apoptosis. Bcl-2 binds to Bax and Bak proteins in the outer mitochondrial membrane, and in so doing, the pore formation that would allow the release of caspase-activating proteins in the cytosol and that eventually leads to apoptosis is prevented (Lamers *et al.*, 2012; Hata, Engelman & Faber, 2015). For more

detail, a review by Czabotar *et al.* (2014) discussed 3 models for the interactions between the Bcl-2 family proteins to control apoptosis. In the direct activation model, BH3-only proteins directly activate Bax and Bak, while pro-survival proteins engage the BH3-only proteins, so preventing their action. In the indirect model, pro-survival proteins bind to any Bax or Bak molecule that becomes activated (exposes its BH3 domain). Finally, in the unified model, both direct and indirect activation theories are combined, suggesting that pro-survival proteins sequester both BH3-only proteins as well as activated Bax or Bak.

An earlier *in vitro* study found that *BCL2* gene expression was connected with an ability to avoid cell death, as well as a possible avenue to develop drug resistance. Researchers found that increased *BCL2* expression in certain cell lines were resistant to common cytotoxic treatments, such as cisplatin and etoposide (Dole *et al.*, 1994).

Neuroblastoma tumours are known to express higher levels of *BCL2* RNA and Bcl-2 protein, compared to other tumours and healthy tissues (Lamers *et al.*, 2012; Goldsmith *et al.*, 2012). Silencing *BCL2* in neuroblastoma cell lines, which had high *BCL2* expression, lead to apoptosis, although a cell line with already low *BCL2* expression, SKNAS, was unaffected by the silencing (Lamers *et al.*, 2012). Other studies using Bcl-2 inhibitors also showed that the level of *BCL2* expression determines the efficacy of the Bcl-2 antagonist. ABT-737 was found to be most effective in vivo against Bcl-2 dependent SMS-SAN xenografts, compared to xenografts that were less dependent on Bcl-2 (Goldsmith *et al.*, 2012), while the higher drug concentrations of the Bcl-2 inhibitor ABT-199 (venetoclax) were needed to achieve therapeutic effects in

cells with low *BCL2* expression levels in another study (Van Goethem *et al.*, 2017).

2.3.1.1 Drugs targeting Bcl-2 proteins

Once the Bcl-2 protein was identified as a potential target, development of selective Bcl-2 antagonists, or more specifically, BH3 mimetics, began. ABT-737, ABT-263 and ABT-199 were three such drugs to selectively target Bcl-2 (Figure 2.7) (Oltersdorf *et al.*, 2005; Tse *et al.*, 2008; Souers *et al.*, 2013). While small molecules targeting other members of the Bcl-2 family, such as Bcl-X_L and Mcl-1 have been synthesised (Ashkenazi *et al.*, 2017), this review will focus on drugs specifically targeting the Bcl-2 protein.

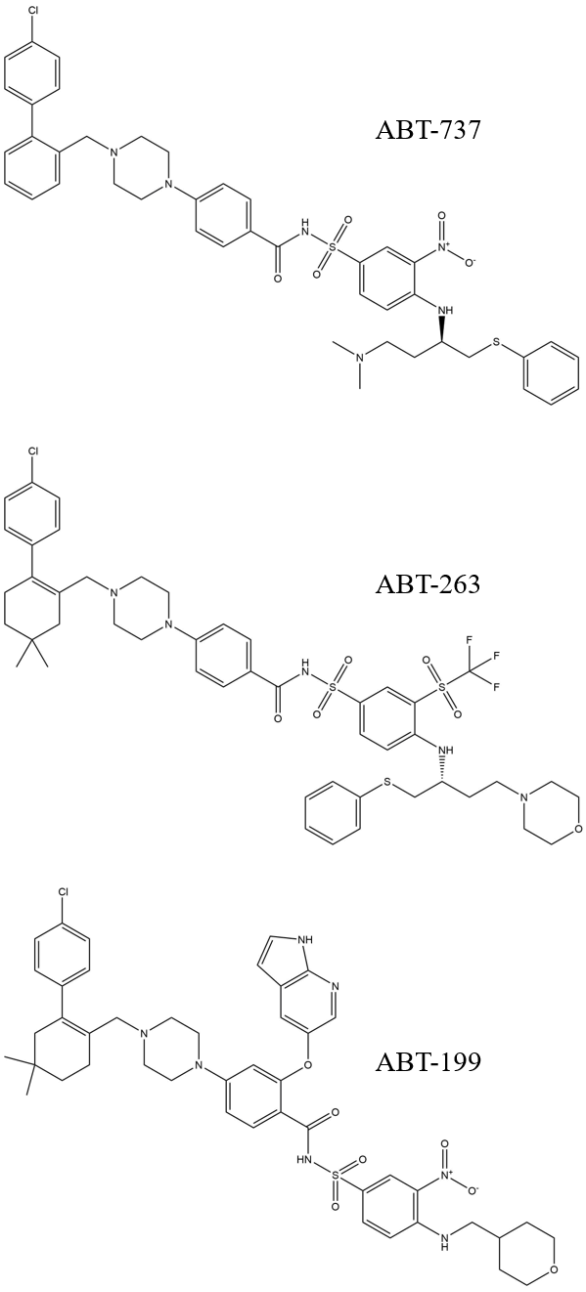

Figure 2.7 Chemical structures of the BH3 mimetics ABT-737, ABT-263 and ABT-199 (PerkinElmer Informatics, 2019).

ABT-737 is a small molecule inhibitor of anti-apoptotic proteins Bcl-2, Bcl-X_L and Bcl-w. It was identified using 'SAR by NMR', which is a high throughput method to screen and identify potential of small molecules in a chemical library, according to protein-ligand interactions, and the most suitable chemical

modified and synthesised using structure-based design. However, two major drawbacks to this inhibitor include lack of oral formulation as well as a major side effect of thrombocytopenia, seen in *in vivo* models (Oltersdorf *et al.*, 2005).

ABT-263 (navitoclax) was used in this study as a known inhibitor of Bcl-2 family proteins. It is the orally bioavailable version of ABT-737 which also has improved affinity to Bcl-2, thus reducing side effects such as thrombocytopenia as seen in *in vivo* studies (Tse *et al.*, 2008). Its properties and actions have been tested on other cancer xenograft models, such as small cell lung cancer (SCLC) (Shoemaker *et al.*, 2008) and non-Hodgkin's lymphoma (Ackler *et al.*, 2012). Additionally, ABT-263 is being investigated in several Phase I and/or Phase II clinical trials, both as a single agent and in combination (Delbridge *et al.*, 2016).

A panel of 11 SCLC *in vitro and in vivo* models was evaluated with ABT-263 as a single agent. They found that the most sensitive cell lines had higher expression of Bcl-2 and other family member proteins such as Bcl-xL and Bim or lower levels of Mcl-1. They also found in that in one tumour xenograft model (H1048 human SCLC cell line, known to be resistant to ABT-263), after a dose of 100 mg/kg/day for 21days, tumour volume was significantly reduced ($p < 0.01$) and comparable to treatment with etoposide. Furthermore, western blotting showed that Bcl-2 levels in H1048 were significantly higher compared to vehicle control, which is comparable to another model, H1963 (human SCLC cell line), which known to be highly sensitive to ABT-263.

In xenograft models of diffuse large B-cell lymphoma (DoHH-2, SuDHL-4), mantle cell lymphoma (Granta 519) and Burkitt's lymphoma (RAMOS), ABT-263 was added to the bendamustine with or without rituximab treatment that is

already in use clinically (Ackler *et al.*, 2012). The results showed that the combination of bendamustine and ABT-263 significantly inhibited tumour growth in all xenografts versus treatment alone. They concluded that addition of ABT-263 to bendamustine with rituximab might be a potential future combination strategy for treatment of non-Hodgkin's lymphoma.

ABT-199 (venetoclax) has been shown to be more selective to Bcl-2 than other members of the Bcl-2 protein family, such as Bcl-xL and Bcl-w (K_i = <0.01 nM compared to K_i = 48 nM and K_i = 245 nM, respectively), and binding to Mcl-1 is not detectable. Similar to ABT-263, ABT-199 is an orally administered drug, but the higher degree of selectivity means that side effects, in particular thrombocytopenia, are only evident at much higher doses, (EC_{50} = 5.5 μM compared to EC_{50} = 0.083 μM with ABT-263) (Vandenberg & Cory, 2013; Souers *et al.*, 2013).

ABT-199 underwent several Phase I, II and III trials, for various lymphomas and leukaemia (Delbridge *et al.*, 2016), and between 2016 and 2019, gained approval from the US Food and Drug Administration for use in various types of leukaemia (Bohl, Bullinger & Rücker, 2019; Wei *et al.*, 2019).

Finally, an orally available Bcl-2 inhibitor called S55746 (Figure 2.8) was shown to be effective against a panel of non- Hodgkin lymphoma cell lines and *in vivo* in subcutaneous Acute Lymphoblastic Leukaemia (ALL) and Diffuse Large B-Cell Lymphoma (Toledo) xenografts in SCID/beige mice, with Casara *et al.*, (2018) observing apoptosis through externalization of phosphatidylserine, caspase-3 activation and PARP cleavage in cell lines, while caspase-3 activity was found to be up to 28 times higher than in vehicle control mice. Tumour volume was significantly lower ($p < 0.05$) in both xenograft models when treated as a single agent at the lowest doses compared to vehicle only control. Additionally, *ex vivo* results showed that apoptosis was induced in primary Chronic Lymphocytic Leukemia and Mantle Cell Lymphoma patient samples.

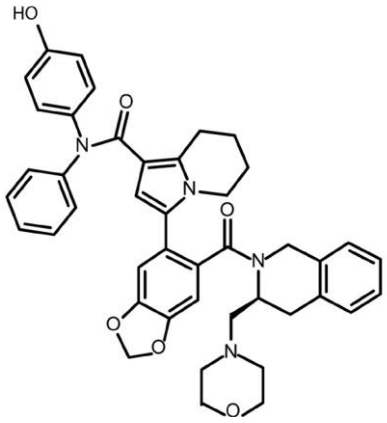

Figure 2.8 Chemical structure of S55746 (Casara *et al.*, 2018)

Following is a table with a summary of the four Bcl-2 inhibitors discussed above:

Table 2.3: Summary of Bcl-2 inhibitors – route of administration, targets, side effects and references.

Name	Route of administration	Targets	Other remarks	References
ABT-737	i.p. injection	Bcl-2, Bcl-X_L, Bcl-w, Mcl-1	Major drawback: severe thrombocytopenia side effect detected in *in vivo* studies	Oltersdorf *et al.* (2005); Mérino *et al.* (2012)
ABT-263 (navitoclax)	oral	Bcl-2 (Bcl-X_L & Bcl-w, but less than ABT-737), Mcl-1	Design based on ABT-737; reduced side effects due to improved Bcl-2 infinity. Tested on SCLC, non-Hodgkin's lymphoma. Promising *in vivo* results alone or in combination treatments.	Tse *et al.* (2008); Shoemaker *et al.* (2008); Ackler *et al.* (2012); Delbridge *et al.* (2015)
ABT-199 (venetoclax)	oral	Bcl-2	Fewer side effects than ABT-263. Underwent Phase I, II & III trials for lymphomas and leukaemia. USFDA approval for use in leukaemias in 2019.	Souers *et al.* (2013); Vandenberg & Cory (2013)
S55746	oral	Bcl-2	Promising *in vitro* and *in vivo* studies for haematological tumour growth.	Casara *et al.* (2018)

2.4 GAMMA-TOCOTRIENOL AND SH-SY5Y

Then et al (2009) showed that gamma-tocotrienol (γT3) in high doses (≥ 100μM) has a stronger pro-apoptosis tendency than alpha-tocopherol (αT) by increasing expression of proteins involved in the apoptosis pathway: p38 and p53 MAPK and reducing the Bcl-2/Bax ratio (Then *et al.*, 2009). γT3 showed pro-apoptotic effects on human DS neurons instead of protective effects as originally predicted, however this was seen in cells that were pre-treated with γT3 and then exposed to hydrogen peroxide (Then *et al.*, 2012). Later, the same research group used molecular docking studies and binding assays (Figure 2.9) to show that γT3 induced apoptosis by active ligand binding to the BH3 domain of the BCL-2 protein, which is a pro-apoptotic domain (Tan *et al.*, 2016).

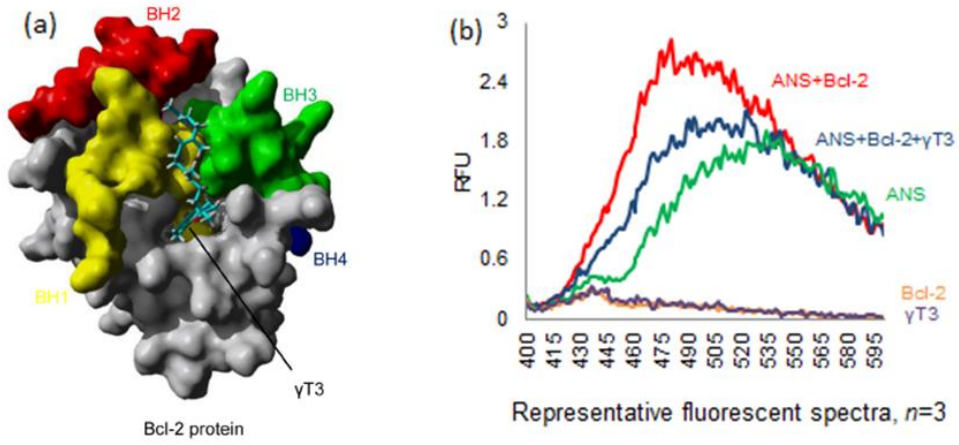

Figure 2.9 Results of *in silico* docking (a) and binding assays (b). γT3 fits in the hydrophobic groove (BH3 domain) of Bcl-2 (a), while in the binding assay (b), the addition of γT3 caused a shift in fluorescence readings. (Tan *et al.*, 2016).

Based on their findings, the researchers proposed a mechanism of action, as seen in Figure 2.10. As shown in Figure 2.9a, γT3 is able to bind to the pro-apoptotic groove of Bcl-2, allowing Bax/Bak to permeabilize the outer mitochondrial membrane and release cytochrome C from the mitochondrial pores. The cascade following that eventually leads to apoptosis. Figure 2.9b shows a shift in fluorescence reading when γT3 is added to Bcl-2, compared to Bcl-2 alone.

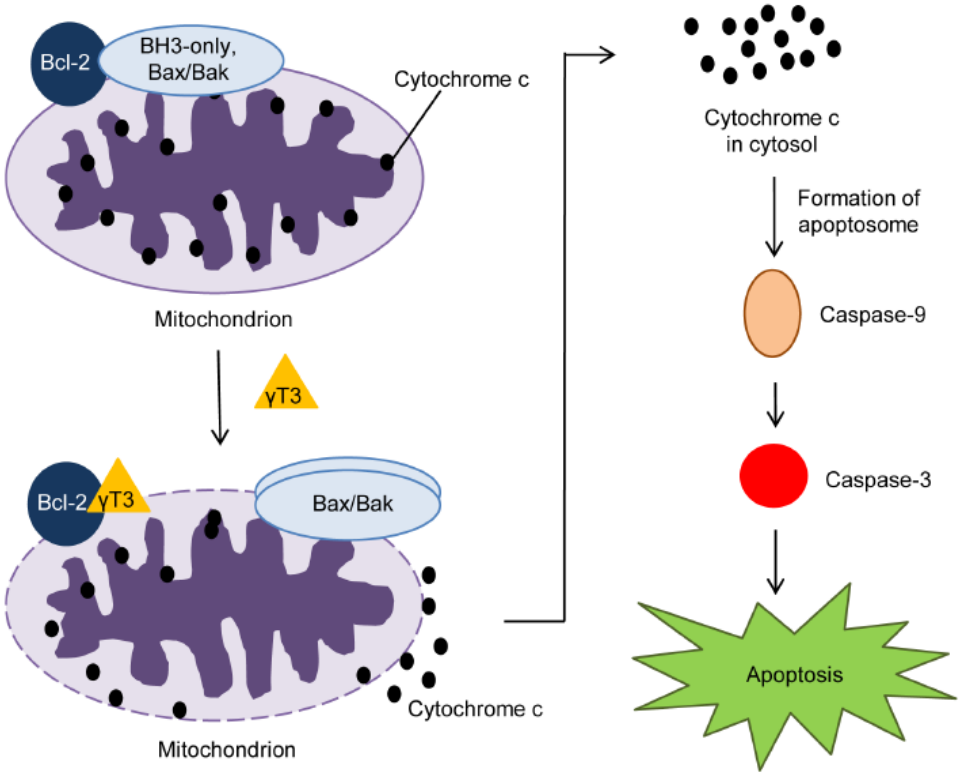

Figure 2.10 Proposed mechanism of action of gamma-tocotrienol**,** based on the results obtained from the study by Tan *et al.* (2016). The γT3 molecule competitively binds to the BH3 domain in Bcl-2, which can be present in higher than normal levels in neuroblastoma (and other cancers) and prevents apoptosis. Binding to Bcl-2 allows Bax/Bak to oligomerize for mitochondrial outer membrane permeabilization, thus leading to cytochrome c release from the mitochondrion, which eventually results in apoptosis.

As discussed in *Section 2.3.1.1*, Bcl-2 is a viable drug target in anticancer treatment. Additionally, based on the synergistic actions of the Bcl-2 inhibitor ABT-263, as well as tocotrienol, there is a possibility that γT3 may also enhance the action of 13cRA. This enhancement could lead to either dose reduction or increased effectiveness of the current dose. Furthermore, 13cRA has been shown to act synergistically with other drugs (Shelake *et al.*, 2015; Milanovic *et al.*, 2015) and there is a possibility that targeting Bcl-2 may help overcome treatment resistance (Niizuma *et al.*, 2006). ABT-263 has been found to work synergistically with all cytotoxic drugs in the neuroblastoma treatment protocol except cisplatin in one cell line (Lamers *et al.*, 2012), as well as bendamustine and bendamustine-rituximab in haematological tumours (Ackler *et al.*, 2012). Guthrie *et al.* (1997)mentioned that tocotrienol increased the potency of tamoxifen in MCF-7 breast cancer cells and more recently, a study showed results of the synergistic actions of γT3 and hydroxyl-chavicol, a plant extract, on glioma cell lines (Abdul Rahman *et al.*, 2014).

Therefore, based on what we know about current neuroblastoma treatments and their drawbacks, as well as the work done by Tan *et al.* (2016) to identify Bcl-2 inhibition as a mechanism of action of γT3 in neuroblastoma, we would like to further investigate the potential of γT3 as an adjunct to 13cRA during the post-consolidation stage of high-risk neuroblastoma therapy using *in vitro* and *in vivo* studies. As stated in the previous section, we will accomplish that with cell viability and cell death assays, analyse apoptosis with flow cytometry and Annexin-FITC/PI staining, and using a neuroblastoma nude mouse model, investigate anti-tumour effects of γT3. Finally, expression of relevant proteins will be evaluated using both *in vitro* and *in vivo* samples.

CHAPTER 3 MATERIALS AND METHODS

3.1 INTRODUCTION

The experiments here can be broadly divided into *in vitro* and *in vivo* work, and were chosen to fulfil the aims and objectives of this research project. *In vitro* work used two neuroblastoma cell lines, SH-SY5Y and SK-N-BE(2), as they represent different stages of neuroblastoma, while *in vivo* work utilized nude mice with SH-SY5Y ectopic tumours.

The aim of the *in vitro* study was to test whether a combination of 13-*cis*-retinoic acid (13cRA) and gamma-tocotrienol (γT3) inhibits neuroblastoma cell growth more effectively than individual treatments. We also wanted to confirm that cell death was caused by apoptosis, and to investigate the hypothesis that the Bcl-2 protein was a target of γT3.

To investigate the first aim, we performed cell viability and cell cytotoxicity assays to elucidate effective doses (IC_{50}) of γT3 and 13cRA. We also investigated ABT-263 as a comparison with known Bcl-2, anti-tumour activity (Oltersdorf *et al.*, 2005). We then performed the same assays on combined treatments to see if there was an improvement in IC_{50} values compared to individual treatments.

In order to confirm that cell death was caused by apoptosis, we carried out flow cytometry with Annexin V-FITC/PI, with both individual and combined treatments, on both cell lines. Western blot tested expression of several proteins, Bcl-2, p53 and MYCN, and compared their relative expression on treated (individual and combination) and untreated cells (Figure 3.1).

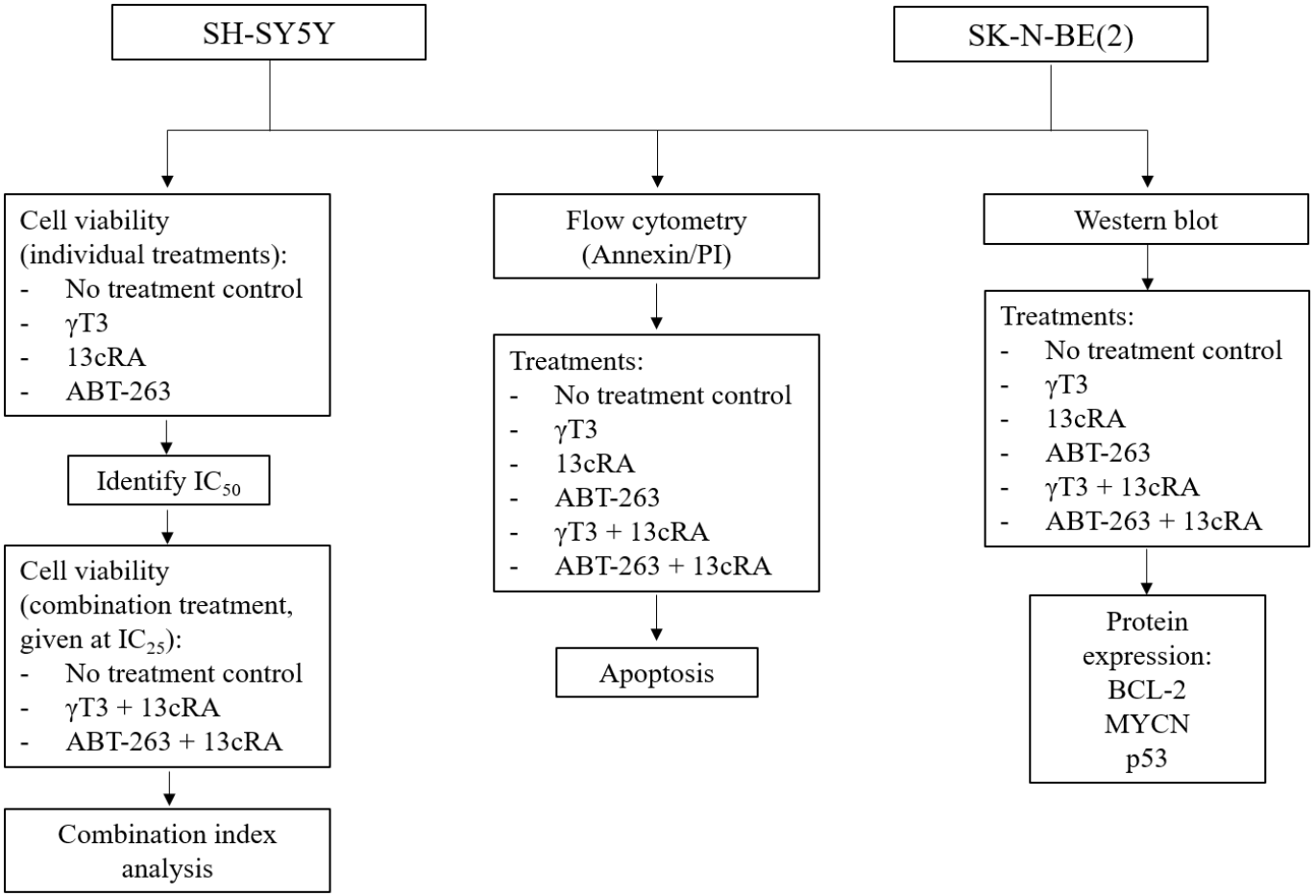

Figure 3.1 Flow chart summary of *in vitro* experiments

The aim of the *in vivo* study (Figures 3.2 and 3.3) was to test whether γT3 is able to inhibit growth of an ectopic NB xenograft alone, in comparison to 13cRA and also whether the combination with 13cRA has a better effect than individual treatments. We also wanted to determine the mechanism of action of γT3, based on earlier computer models that predicted that Bcl-2 was the target, using molecular studies such as western blot. ABT-263, a synthetic Bcl-2 inhibitor, also known as navitoclax, will be used as a comparison to γT3, due to extensively documented mechanism of action indicating a high affinity to Bcl-2, as well as oral route of administration. All 3 pilot studies are summarised in Figure 3.2. First, we wanted to optimise the tumour growth protocol, in particular number of cells injected, time taken for palpable tumour growth and PET scan parameters and workflow. That study was run concurrently with the non-tumour bearing drug tolerability study where we checked if drug doses and vehicles were tolerated by the mice. Finally, results for the first 2 parts of the pilot study were used to run the tumour bearing toxicity study. Tumour growth protocol was finalised and drug doses were deemed non-toxic to mice. A tumour bearing toxicity study was carried out to ensure that there were no adverse effects to tumour bearing test mice. Any final adjustments to the study protocol would be made here.

Mice with ectopic SH-SY5Y tumours were treated with individual and combined treatments, and tumour size measured manually and also with positron emission tomography (PET) scan. Then, protein from tumours were extracted and western blot was used to determine and compare levels of the following proteins: Bcl-2, Bcl-xL, caspase-3, caspase-9, MYCN and p53 (Figure 3.3).

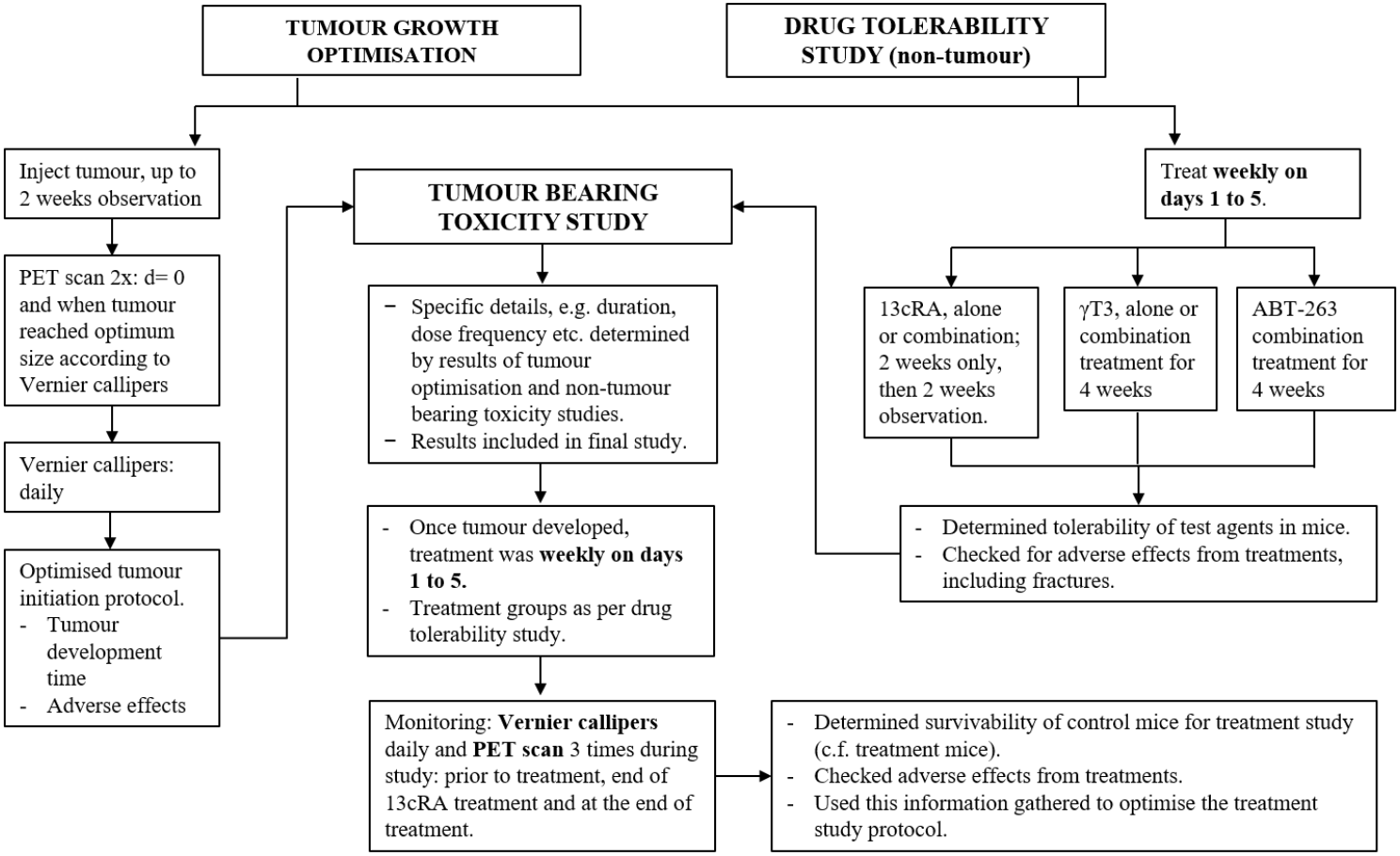

Figure 3.2 Flow chart summary of *in vivo* optimisation and tolerability studies

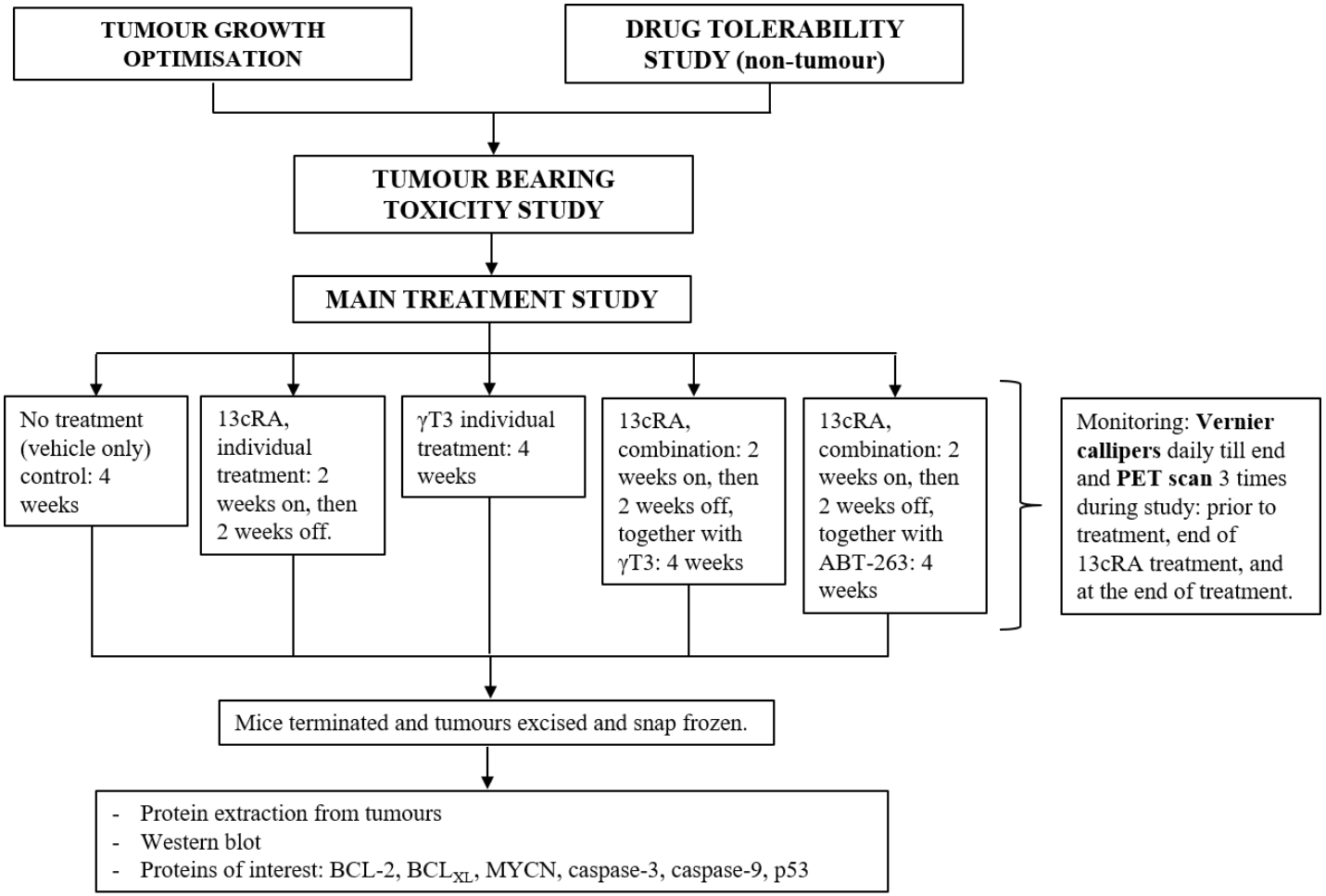

Figure 3.3 Flow chart summary of *in vivo* main study and western blot

3.2 *IN VITRO* EXPERIMENTS

Two human neuroblastoma cell lines were chosen for this: SH-SY5Y (ATCC CRL-2266) and SK-N-BE(2) (ATCC CRL-2271). SH-SY5Y cells have a single copy of *MYCN* and SK-N-BE(2) have more than 100 copies, i.e. SK-N-BE(2) are *MYCN*-amplified, while SH-SY5Y are not (Baj & Tongiorgi, 2009) and so were chosen to represent different risk categories of clinical neuroblastoma (Cohn *et al.*, 2009).

It should also be noted that although γT3 has been shown to have apoptotic effects on cancer cell lines, including neuroblastoma cell lines (Tan *et al.*, 2016), it was shown to only have a toxic effect on non-cancerous cells at high concentrations, for example on primary rat astrocytes above 200µM (Mazlan *et al.*, 2006) and primary rat cerebellar neurons above 100µM (Then *et al.*, 2009). The highest concentration of γT3 used in the *in vitro* investigations was only 30µM.

3.2.1 General cell culture

SH-SY5Y human neuroblastoma cells (CRL-2266) were donated by our collaborators at the Department of Biochemistry, UKM and SK-N-BE(2) human neuroblastoma cells (CRL-2271) were purchased from American Type Culture Collection (ATCC; USA).

Both cell lines were grown in Dulbecco's Modified Eagle's Medium (DMEM) and Ham's F-12 (Sigma, USA) at a 1:1 ratio, supplemented with 10% fetal bovine serum (Sigma, USA) and 50 µg/mL gentamicin (Sigma). 2mM L-

glutamine and 100 µg/mL non-essential amino acid (Sigma) were also added to the complete culture medium. Cell lines were maintained at 37°C in a humidified incubator supplied with 5% CO_2. Medium was changed every four days, and if they were not used for assays, cells were passaged/split when they reached 70 to 80% confluence.

To detach adherent cells in T25 flasks, cells were rinsed twice with 3 mL sterile, 1x phosphate buffered saline (137 mM NaCl, 2.7 mM KCl, 10 mM Na_2HPO_4, 1.8 mM KH_2PO_4) (PBS) and then incubated at 37ºC for 5 minutes in 500 µL of 2.5g/l Trypsin/1mmol/l EDTA solution (Nacalai Tesque, Japan). Then, trypsin was neutralised with an equal volume of complete culture medium before cells were pelleted using 5810R Refrigerated Centrifuge (Eppendorf, Germany) and supernatant removed. Subsequently, cells were resuspended in culture medium before either being counted and then transferred to plates or flasks.

Cell counting was performed after cells were pelleted and then resuspended in 5 mL culture medium. 10 µL of cell suspension was gently mixed with 40 µL 1x trypan blue (Nacalai Tesque, Japan) in a microcentrifuge tube (1 in 5 dilution). 10 µL of this mixture was added to each of two chambers of a glass haemocytometer, under a glass coverslip, using capillary action. Cells were viewed using a TS100 Eclipse microscope (Nikon, Japan). Live, unstained cells in each quadrant of each chamber (4 x 2 chambers = 8) were counted using a hand tally counter and live cell estimate was calculated as below:

$$[(\text{No. of cells}_{\text{Chamber 1}} + \text{No. of cells}_{\text{Chamber 2}} \div 8) \times \text{Vol.}_{\text{original cell suspension}} \times \text{dilution factor} \times 10^4]$$

For cryopreservation, cells were stored in 5% DMSO and 95% complete culture medium (in aliquots of 500 µL per 1.5 mL cryovial). Cells were first stored in -20ºC for 1 hour before transfer to -80ºC overnight. Then, frozen cells were transferred to the liquid nitrogen tank for long term storage. To thaw frozen cells, cryovials containing frozen cells were retrieved from liquid nitrogen storage, then immediately warmed in a 37ºC water bath until almost completely thawed. Cells were gently mixed with a 1 mL pipette in the cryovial before transfer to 4.5 mL warm, complete culture medium in a T25 cell culture flask. Cells were allowed to attach overnight, and then DMSO-containing medium was replaced with fresh, complete culture medium the following day.

3.2.2 Preparation of test reagents

Pure γT3 (Davos, Singapore), a highly viscous substance, was dissolved in 100% ethanol to make a 0.5 M stock solution, which was stored at -20 ºC. A 0.02 M stock solution (diluted in ethanol) was stored at 4 ºC. and the evening before treating cell lines with γT3, the 0.02 M stock solution was incubated overnight at 37 ºC together with 100% fetal bovine serum (Sigma) at a 3:4 ratio of γT3 to FBS. Then, γT3 was further diluted to 100 times the final concentration with complete culture medium containing 50% ethanol before addition to cells to make up the final concentration (Then *et al.*, 2012).

13cRA powder (Sigma, USA) was dissolved in DMSO to make a 100 mM stock solution, stored at -20 ºC. This was later dissolved, again in DMSO, to a 4 mM stock solution, stored at 4 ºC, which was subsequently diluted in complete culture medium.

ABT-263 powder (Toronto Research Chemicals Inc., Canada) was similarly dissolved in DMSO to make a 100 mM stock solution stored at -20 ºC, which was further diluted in DMSO to make a 4 mM stock solution (stored at 4 ºC) which was then diluted to final concentrations in complete culture medium.

3.2.3 Treatment groups

Treatment groups for the cell viability and cell cytotoxicity assays are summarised in the in vitro experiment summary flowchart seen in Figure 3.4 below:

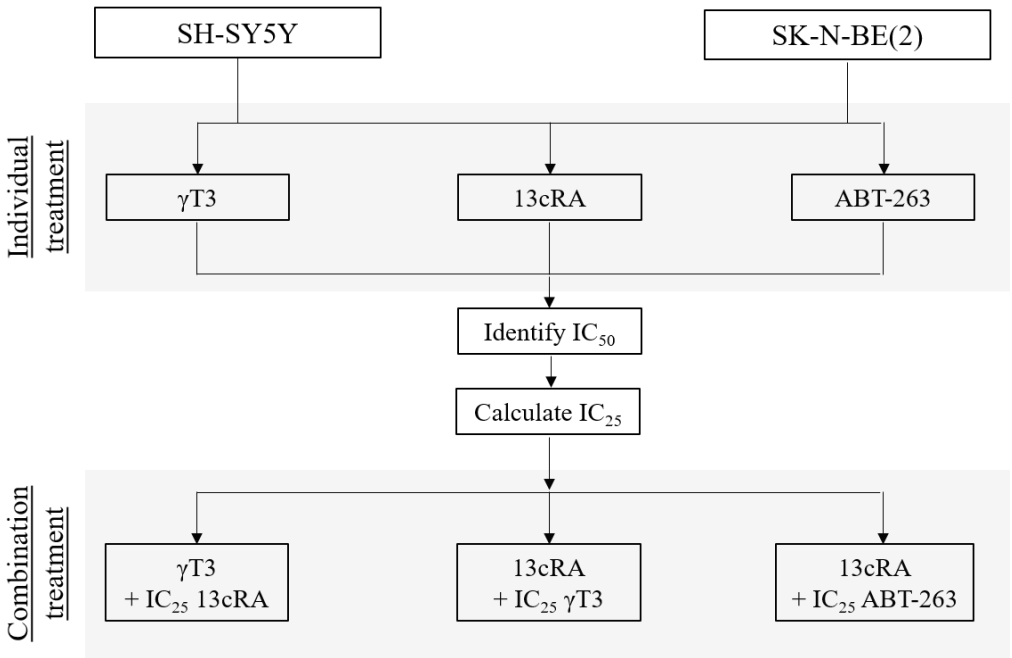

Figure 3.4 Treatments for SH-SY5Y and SK-N-BE(2) cell lines (MTS and LDH assays)

In the individual treatment stage, both cell lines were treated with a dose range, in order to identify the IC_{50}. Once that value was calculated, the IC_{25} was

calculated, and added to the dose range of another treatment, to see how, or if, the combination was able to reduce the original IC_{50}.

For example, the IC_{50} values of γT3 and 13cRA to treat the SH-SY5Y cell line were identified. Then, the IC_{50} value of γT3 was divided to obtain the IC_{25}, in order to have a sub-optimal treatment dose. This IC_{25} dose of γT3 was then added to the dose range of the 13cRA treatment, to see if the IC_{50} value of 13cRA reduced (Abubakar *et al.*, 2017).

3.2.4 Cell viability assay

We measured cell viability using the MTS assay, which uses the tetrazolium compound, 3-(4,5-dimethylthiazol-2-yl)-5-(3-carboxymethoxyphenyl)-2-(4-sulfophenyl)-2H-tetrazolium (MTS) and an electron coupling reagent, phenazine ethosulfate (PES). NADPH or NADH in metabolically active cells convert the tetrazolium compound to a soluble, purple formazan compound. The amount of purple formazan product is directly proportional to the number of living cells present and can be measured at 490 nm wavelength (Promega, 2012).

SH-SY5Y or SK-N-BE(2) cells (2×10^4 cells per well) were seeded in a flat-bottomed 96-well plate and allowed to grow in complete culture medium containing 10% FBS. After 48 hours, medium in wells was replaced with fresh medium containing 1% FBS and no gentamicin along with treatments as described in *Section 3.2.3*. After 24 hours' incubation (Tan *et al.*, 2016), cell viability was measured with the *CellTiter 96® AQ_{ueous} One Solution Cell Proliferation Assay* (MTS) (Promega, USA). 20µL of *CellTiter 96* reagent was added to each well and incubated in dark conditions at 37ºC for 4 hours. Then, absorbance at 490nm was measured using a VarioskanFlash reader (Thermo

Scientific, USA) and the accompanying SkanIt Software (Thermo Scientific, USA).

To calculate cell viability, first, absorbance values were corrected by deducting background absorbance. Average absorbance of blanks (no cells, medium only, performed in triplicate) was deducted from all other absorbance values. Then percentage cell viability of sample cells was calculated as follows:

$$\text{Cell viability (\%)} = \frac{\text{Absorbance of treated sample}}{\text{Absorbance of untreated sample}} \times 100$$

3.2.5 Cell cytotoxicity assay

To evaluate cell death, a lactate dehydrogenase (LDH) release assay kit (Takara Bio Inc, Japan) was used. This assay measures LDH activity in the cell culture supernatant by reducing NAD^+ to NADH (conversion of lactate to pyruvate using LDH catalysis). At the same time, diaphorase catalyst transfers H^+ from NADH to tetrazolium salt, which then reduces to a red formazan product, which can be measured quantitatively with absorbance. Increase in LDH activity, which is released when cell membrane is damaged, is directly correlated with the amount of formazan product formed (Fotakis & Timbrell, 2006).

Following treatments, as described in Section 3.2.3, as well as 2% Triton-X (high control), plates were spun at 140 x g for 5 minutes, then 50µL supernatant was carefully transferred from each well to a new 96-well plate. The transferred supernatant was mixed with an equal volume of reaction mixture (diaphorase/NAD^+ and iodotetrazolium chloride/sodium lactate, 1:45 ratio) and then this mixture was incubated at room temperature in dark conditions. After

30 minutes, absorbance at 490 nm and 610 nm was measured, again, using the Varioskan Flash reader and SkanIt Software.

Average absorbance values (n=3) were calculated and then percentage cytotoxicity was calculated as below, using the other absorbance values:

$$\text{Cytotoxicity (\%)} = \frac{\text{exp. value} - \text{no treatment control}}{\text{TritonX value} - \text{no treatment control}} \times 100$$

3.2.6 Combination Index analysis

There are several ways to investigate the pharmacological interactions between drug combinations, including isobologram, which is a graphical representation, and combination index (CI), which is a quantitative representation (Wali & Sylvester, 2007). Here, we have decided to use CI, the quantitative representation.

The combination index (CI) value indicates whether the combined treatment is synergistic (CI = <1), antagonistic (CI = >1) or additive (CI = 1), and CI can be worked out using the following equation:

$$\text{Combination index (CI)} = d_x/D_x + d_y/D_y$$

Where $d_x = IC_{50}$ of compound X in combination, $D_x = IC_{50}$ of compound X alone, $d_y = IC_{50}$ of compound Y in combination, $D_y = IC_{50}$ of compound Y alone (Chou, 2006).

We determined the effect of combining treatments with the CI method. First, IC_{50} values of individual and combination treatments were determined using non-linear regression curve fit analysis on GraphPad Prism 7.03 Software (GraphPad Software Inc., USA), using results obtained from the cell viability assay (*section 3.2.4*). Then, these IC_{50} values were analysed with CompuSyn software (Chou, 2006) to calculate the CI of each drug combination, in order to

quantitatively measure the pharmacological interaction between combined treatments.

3.2.7 Flow cytometry

Annexin V-FITC was used to detect and quantify apoptosis in SH-SY5Y and SK-N-BE(2) cells after undergoing treatment. Annexin V is a protein which binds preferentially to phosphatidylserine (PS). PS is one of the phospholipids present on the inner surface of the plasma membrane, and is only exposed to the external cellular environment in events such as early apoptosis, where it translocates to the outer layer, or in late apoptosis or necrosis, where the membrane loses integrity and Annexin V can bind to PS still located on the inner surface. Labelling Annexin V with a fluorochrome such as fluorescein isothiocyanate (FITC) allows its detection and thus, quantification by the flow cytometer (Koopman *et al.*, 1994; Wilkins *et al.*, 2002). Propidium iodide (PI) is also used in this assay, to differentiate between early and late apoptosis/necrosis, as PI is excluded by viable cells (with intact cell membrane), while the membranes of dead cells or those in late apoptosis are permeable to PI, thus allowing staining of nucleic acids that resulted from DNA degradation (Riccardi & Nicoletti, 2006). Cells that are viable are both Annexin V and PI negative, while cells in early apoptosis are Annexin V positive, but PI negative. Cells in late apoptosis or necrosis are both Annexin V and PI positive.

SH-SY5Y or SK-N-BE(2) cells were cultured in 6-well plates, with 3.2 x 10^5 cells per well, in 10% FBS-containing cell culture medium. Two wells were used for each treatment group. Cells were allowed to grow for 48 hours before medium was discarded and each well rinsed once with 300 µL warm PBS.

Treatments were added in 1% FBS-containing cell culture medium according to the following groups in Table 3.1.

Table 3.1: Flow cytometry treatment groups

Cell line	Treatment group/concentration (μM)					
	No treatment control	**13cRA**	**γT3**	**ABT-263**	**γT3 + 13cRA**	**ABT-263 + 13cRA**
SH-SY5Y	-	15	8.5	19.5	8.5 + 15	19.5 + 15
SK-N-BE(2)	-	20	12.5	19.5	12.5 + 20	19.5 + 20

Following a 24-hour exposure to treatments, medium from wells were transferred to 15 mL falcon tubes. Wells were rinsed with 300 μL warm PBS and then cells detached as per section 3.2.1, except that 250 μL trypsin was used instead of 500 μL. After trypsin was neutralised, cells were transferred to the aforementioned falcon tubes containing the corresponding supernatant, and then cells were centrifuged at 350 x g for 5 minutes, room temperature. Supernatant was discarded and pellet was resuspended in fresh, room temperature PBS and then centrifuged again using previous settings. Supernatant was discarded again and then pellet was resuspended in 5 mL room temperature PBS. Cells were then filtered using a 40 μm cell strainer (Corning, USA) to ensure a uniform, single cell suspension and then cells were counted, as per section 3.2.1. After cells were counted, they were diluted in cold (4ºC) PBS to a concentration of 1 x 10^7 cells/mL, for each treatment group.

Cells were then immediately stained using the FITC Annexin V Apoptosis Detection Kit I (BD Pharmingen, USA), according to the manufacturer's protocol. Cells were washed twice in cold PBS and then resuspended in 1X

Binding Buffer, containing 0.1 M Hepes/NaOH (pH7.4), 1.4 M NaCl, 25 mM CaCl2, (component no. 51-66121E, provided in kit) to a concentration of 1 x 10^6 cells/mL. From this, 100 µL (1 x 10^5 cells) was transferred to a 1.5 mL Eppendorf tube. Three more Eppendorf tubes, each containing 100 µL solution, were prepared as controls for compensation controls and quadrants.

In the first tube, 5 µL of FITC Annexin V (component no. 51-65874X, provided in kit) and 5 µL Propidium Iodide, PI (component no. 51-66211E, provided in kit) was added, the tube gently vortexed and incubated for 15 minutes at room temperature in the dark. For each treatment group the controls for compensation used were: unstained cells, cells stained with FITC Annexin V only (no PI), and cells stained with PI only (no FITC Annexin V). Nothing further was added to the second tube, 5 µL FITC Annexin V was added to the third tube and 5 µL was added to the fourth tube. After incubation, 400 µL of 1X Binding Buffer was added to each tube, and then samples were analysed using the BD Accuri C6 Flow Cytometer and the BD Accuri Software (BD Biosciences, USA).

3.2.8 Western blot

3.2.8.1 Cell culture

SH-SY5Y or SK-N-BE(2) cells (1.67 x 10^6) were seeded in T25 flasks and allowed to grow for 48 hours in 10% FBS-containing cell culture medium, as described in section 3.2.1. After 48 hours, medium in wells was replaced with fresh medium containing 1% FBS and no gentamicin along with same treatment doses, as described in Table 3.1. Cells were exposed to drug treatments (and no

treatment control) for 24 hours, and then protein was extracted for use in western blot, as described in section 3.2.8.2.

3.2.8.2 Protein extraction and quantification for cell lines

After 24 hours treatment, cells in T25 flasks were transferred to 15 mL falcon tubes and centrifuged at 130 x g, 4°C for 5 minutes. Supernatant was discarded, and then pellets washed in 5 mL ice cold PBS and centrifuged again, at 2500 x g, 4°C for 5 minutes. Supernatant was again discarded and washed for the last time in 5 mL ice cold PBS and centrifuged as before.

After the final wash, supernatant was removed and the cell pellet was resuspended in 50 μL of cold radioimmunoprecipitation assay (RIPA) buffer, containing 10μL/mL each of Halt Protease and Phosphatase Inhibitor Cocktail 100X and 0.5M EDTA (Thermo Scientific, USA). Cell lysate was then transferred to a 1.5 mL tube and kept on ice for 30 minutes, vortexing occasionally. After that, samples were centrifuged at 14000 x g, 4°C for 15 minutes. Supernatant containing total protein lysates was then transferred to a fresh 1.5 mL tube and stored at -80°C.

Protein quantification was performed using Bradford reagent (Sigma, USA). A protein standard was made using bovine serum albumin (BSA) (Affymetrix, USA) diluted in ultrapure water. The stock concentration was 1mg/mL, and this was further diluted to the following concentrations: 0.05, 0.1, 0.2, 0.4, 0.6 and 0.8 mg/mL. 5 μL of each protein standard concentration was added in triplicate to 250 μL Bradford reagent (as per manufacturer instructions). RIPA buffer was diluted 1:1 in ultrapure water and 5 μL of this was used, again in triplicate as previously described, to compensate for background in protein samples.

Absorbance of blank (ultrapure water only) samples were also used to compensate for background readings. 1 μL of each protein sample was added to 4 μL ultrapure water, to make 5 μL sample for use with Bradford reagent. Each sample was tested in triplicate. Protein quantification was carried out in 96 well plates and after addition of samples and Bradford reagent, absorbance was measured using a plate reader (BioTek Instruments, USA) using 595 nm wavelength.

3.2.8.3 SDS-Page and Western Blotting

Expression levels of proteins involved in apoptosis signalling were studied with both *in vitro* and *in vivo* samples. For *in vitro* samples, proteins studied were: Bcl-2, p53, and MYCN. β-actin was used as a loading control.

After determination of total protein concentration (*Section 3.2.8.2*), samples containing 20 μg of total protein was heated for 5 minutes at 95°C together with 4X sample-loading buffer (240 mM Tris-HCl pH 6.8, 8% w/v SDS, 40% v/v glycerol, 0.04% bromophenol blue, 5% w/v 2-mercaptoethanol) in a 3:1 ratio, and then cooled before being loaded into 12% SDS-polyacrylamide gels (Table 3.2). To monitor protein migration and band separation, BLUeye Prestained Protein Ladder (GeneDireX, Taiwan) was also loaded in one well on each gel. Gel electrophoresis was run at 100V, for 90 minutes.

Table 3.2 Composition of one polyacrylamide gel

Components	***Resolving gel (12%)***	***Stacking gel (5%)***
Ultrapure water	1.28 mL	700 μL
30% acrylamide/bis-acrylamide (29:1) solution	1.6 mL	170 μL
1.5 M Tris-HCl, pH 8.8	1.04 mL	-
1.0 M Tris-HCl, pH 6.8	-	130 μL
10 % SDS	40 μL	10 μL
10 % APS	40 μL	10 μL
TEMED	1.6 μL	1 μL
Total volume	4 mL	1 mL

Gels and filter pads (Bio-Rad, USA) were soaked in Bjerrum-Schafer-Nielsen buffer (For 1 L: 48 mM Tris, 39 mM glycine, 10% methanol, 1.3 mM SDS) for 15 minutes. Polyvinylidene fluoride (PVDF) membranes (Membrane Solutions, USA) were soaked in methanol for 1 minute, rinsed in ultrapure water for 5 minutes, and then soaked in cold Bjerrum-Schafer-Nielsen buffer for 10 minutes. A semi-dry blotting system, the Pierce G2 Fast Blotter (Thermo Scientific, USA) was used to transfer proteins from gel to PVDF membrane. Gels, filter pads and PVDF membranes were stacked on the Fast Blotter, which was run for 50 minutes, at 10 V, 1.0 A.

Following protein transfer to PVDF membrane, membranes were soaked in the rapidly reversible protein stain, Ponceau S solution (0.1% w/v Ponceau S in 5% acetic acid, ultrapure water), for 1 minute, to detect presence and location of bands, in order to check protein transfer. Membranes were then rinsed in ultrapure water several times to remove pink Ponceau S stain.

For detection of desired bands, membranes were blocked with 5% BSA dissolved in Tris-buffered saline, TBS (15.2 mM Tris-HCl, 4.6 mM Tris base, 150.6 mM NaCl) for 1 hour at room temperature, then washed in TBST (TBS,

0.1 % Tween-20) for 5 minutes, three times and incubated overnight with primary antibody, diluted at a 1:1000 ratio in 5% BSA/TBST (see Table 3.3 for full list and details) at 4°C, with gentle agitation. Primary antibody dilution ratios were determined using the manufacturer's recommended ratio of 1:1000 and then titrating with ratios of 1:500, 1:1000, 1:2000 and 1:4000.

The following day, membranes were washed with TBST for 5 minutes, five times. Then, membranes were incubated in the corresponding secondary antibody, diluted at a 1:5000 ratio in 5% BSA/TBST (see Table 3.3 for full list and details) for 1 hour at room temperature, with gentle agitation. Secondary antibody dilution ratios were determined in a similar manner to the primary antibodies, but using ratios of 1:2500, 1:5000 and 1:10000. Secondary antibodies were conjugated with horseradish peroxidase (HRP), and therefore, after 1 hour, membranes were washed as after primary antibody incubation and one final wash in TBS for 5 minutes, before addition of Pierce™ ECL Western Blotting Substrate (Thermo Scientific) for 1 minute in dark conditions. Then, membrane was scanned using the Chemidoc MP Imaging System (Biorad) and protein bands analysed using Image Lab Software (Biorad).

Table 3.3 List of antibodies used for western blot (*in vitro* protein samples). All primary antibodies used were polyclonal.

Antibody	Manufacturer	Molecular weight	Dilution
β-actin (source: donkey)	Abcam, UK	42 kDa	1:1000
β-actin (source: rabbit)	Elabscience, Taiwan	42 kDa	1:1000
Bcl-2	Elabscience, Taiwan	26 kDa	1:1000
NMYC	Elabscience, Taiwan	45 kDa	1:1000
p53	Elabscience, Taiwan	43 kDa	1:1000
Anti-rabbit IgG-HRP	Santa Cruz Biotechnology, USA	-	1:5000
Anti-donkey IgG-HRP	Santa Cruz Biotechnology, USA	-	1:5000

3.3 *IN VIVO* MOUSE MODEL

Animal studies are essential to improve our understanding of the mechanisms of diseases, leading to improvements in prevention, diagnosis and treatment. In cancer research, animal, or *in vivo* studies explore both fundamental and translational theories and understanding (Workman *et al.*, 2010; Gargiulo *et al.*, 2012). Rodents, specifically mice, are the most common model in cancer research; in 2008, 96.8% of animals used for cancer research in the UK were mice (Workman *et al.*, 2010).

There are two main models available for cancer research: autochthonous tumour models and transplantation tumour models. Autochthonous tumour models use animals that possess genetic changes that make them more susceptible to tumour development. There is now an increasing range of specific tumour models available, which are created by either inducing expression of oncogenes or inactivating tumour-suppressor genes. Transplantation tumour models involve transplanting and growing tumour cells in mice. If the tumour cells are not of rodent origin, e.g. human tumour cells, then immunodeficient mice are used to prevent rejection (Workman *et al.*, 2010).

An i*n vivo* model can be a necessary step in cancer research as the fundamental interactions between drug, disease, and the rest of the body can be complex. Furthermore, such studies are usually required by regulatory authorities before proceeding to human investigations, in order to better judge the risks of any new interventions (Workman *et al.*, 2010). The promising apoptotic effect of γT3 on SH-SY5Y cells was demonstrated by a recent, *in vitro* study which also

suggested that this is accomplished when γT3 binds to the hydrophobic groove of the Bcl-2 protein (Tan *et al.*, 2016).

Our in vivo study was guided by a similar study published by researchers who induced neuroblastoma tumours in nude mice, in order to observe the effects of combination treatment of retinamide and genistein (Karmakar *et al.*, 2011). We used this paper as a reference for the final methodology which was approved by both the Animal Welfare and Ethical Review Body (AWERB) of The University of Nottingham and the Animal Ethics Committee of Universiti Kebangsaan Malaysia (UKM).

3.3.1 Ethics approval

The use of the animals, the protocol for their care, as well as the study protocol used was reviewed and approved by both the Universiti Kebangsaan Malaysia Animal Ethics Committee (UNMC/2015/THEN SUE-MIAN/25-MAR./663-JUNE-2015-JUNE-2017) and the University of Nottingham Animal Welfare and Ethics Review Board (UNMC0003).

3.3.2 Animals

Male mice [strain: nu/nu nude mouse Crl/Nu-Foxnlnu (albino)] were obtained from Biolasco, Taiwan and Charles River, China, and housed at UKM. Mice used for the tumour optimisation stage were supplied by Biolasco, Taiwan but subsequent batches (of the same strain) were obtained from Charles River, China, due to supply changes by the local distributor.

The study was conducted at the same facility and mice were housed in IVCs with a 12 hours light, 12 hours dark lighting cycle. The room was air-conditioned with a temperature range of 20-22°C. Mice were housed in groups of four during the procedure (tail mark identification), with irradiated bedding, and provided with autoclaved nesting materials and environmental enrichment. Mice were offered sterile irradiated PicoLab Rodent Diet 20 (LabDiet USA, product code 5053) and autoclaved water *ad libitum*. Mice were allowed to acclimatise for 7 to 10 days before any interventions commenced.

3.3.3 Monitoring

In addition to PET/CT scanning and use of Vernier callipers to monitor tumour size in tumour-induced mice, all mice were observed daily for signs of adverse effects. This included recording daily weights, as well as monitoring and recording food and water intake. Tumour bearing mice were observed for potential adverse effects specifically related to the tumour initiation, such as restricted movement due to tumour size. The full list of possible adverse effects can be seen in Appendix A.

3.3.4 Positron emission tomography (PET) scan

Positron emission tomography (PET) is a non-invasive imaging method that detects and measures positron emissions of radionuclides in vivo. In the case of this project, PET imaging was combined with computed tomography (CT) for anatomical reference. The radionuclide we used was 18-flurodeoxyglucose (18-FDG), which is a glucose molecule labelled with the radioactive ^{18}F molecule.

As tumours (and xenografts) are known to exhibit higher glucose uptake than many normal cells, injection of 18-FDG to a xenograft model causes an accumulation of positron emissions at the site of the xenograft, which can be detected by a PET scan (Koba, Jelicks & Fine, 2013). Combining PET scan with computed tomography (CT) provides a direct anatomical image of the test animal (Koba, Jelicks & Fine, 2013).

Training to operate the G8 PET/CT Preclinical Imaging System was provided by Perkin Elmer. A PET scan protocol was developed based on the training.

Anaesthesia of 3% isoflurane and 100% oxygen inhalation was initiated by an induction chamber, then mice were transferred to an imaging cassette on a docking station, which continued to deliver anaesthesia and also contained a heating pad, in order to maintain mouse body temperature. The depth of anaesthesia was monitored by a toe pinch to verify no response before tracer injection.

A trained technician calibrated and calculated the 18-FDG dose, before injecting into mouse via intraperitoneal injection by a trained technician. Dose range was 25 to 75 μCi, and dose was allowed to equilibrate in mouse for 45 minutes before scanning. Following the injection, the syringe was placed back in the dose calibrator to calculate the residual dose remaining in the syringe and recorded. A whole body emission scan will be performed from the head to lower abdomen with a total acquisition time of 10 minutes, followed by CT scan. Initial dose, residual dose and administered dose was recorded.

Images were reconstructed using 3D Maximum Likelihood Estimation Method (MLEM) algorithms. Regions of interest (ROIs) were manually placed on each transverse section of the body. The software (VivoQuant; inviCRO, USA)

utilizes the initial, residual and administered doses, along with the known half-life of the isotope, to convert ROIs into percent injected dose values.

3.3.5 Tumour optimisation study

3.3.5.1 Animals

This study used eight mice that were obtained, housed, fed and monitored as stated in *Section 4.2.3*. Mice were allowed to acclimatise for 7 to 10 days before tumour induction was initiated.

3.3.5.2 Tumour induction

The SH-SY5Y neuroblastoma cell line (CRL-2266) was cultured, detached and counted as per the protocol in Section 3.2.1. A total of 6 x 10^6 cells in 100µL of a 1:1 mixture of complete culture medium and Matrigel was implanted in four mice by subcutaneous injection on the right flank of each mouse, using a sterile 1 mL syringe (Terumo, Japan) and 18G needle (Terumo, Japan). (Karmakar *et al.*, 2011). The remaining four mice were implanted with 4 x 10^6 cells. Mice were sedated with isoflurane anaesthesia during all injection procedures. Mouse conditions (appearance, weight, tumour growth, behaviour) were monitored daily for a period of 14 days.

3.3.5.3 Tumour growth monitoring

Palpable tumours were expected to develop within 6 to 8 days for mice administered 6x10^6 cells (Karmakar *et al.*, 2011), but ended up taking 10 to 14 days. Mice were considered ready for treatment when tumours reached a volume

of about 1cm^3 although final size was ultimately dependent on the growth curve and how long the study could run before the size was reached. For external calliper measurements, the two longest perpendicular axes in the x/y plane of each xenograft tumour were measured to the nearest 0.1cm, by the same person. Volume was calculated using the formula:

$$\frac{4\pi}{3} \times \frac{length}{2} \times \left(\frac{width}{2}\right)^2$$

In addition to callipers, mice were imaged with PET scan twice: prior to tumour induction and at the end of the study when Vernier callipers indicated the tumour size was ready for treatment.

3.3.5.4 Termination

Mice were terminated at the end of the study by cervical dislocation. Then, tumours were removed, weighed and snap frozen in liquid nitrogen, before being transferred to a -80ºC freezer for storage.

3.3.6 Drug tolerability study

The tolerability study had two parts: the first, involving non-tumour bearing mice ran concurrently with the tumour optimisation study. The second part, carried out in tumour bearing mice, ran after the tumour initiation protocol was optimised and doses (frequency and combinations) were confirmed to be tolerated by non-tumour bearing mice. Additionally, due to a concern by the AWERB regarding bone fractures as an adverse effect of 13cRA treatment (Hixson *et al.*, 1979), particular care was taken to monitor CT images of 13cRA treated mice for fractures during both non-tumour and tumour bearing pilot studies.

3.3.6.1 Animals

The pilot study used 20 mice that were obtained, housed, fed and monitored as stated in *Section 3.3.2*. Mice were allowed to acclimatise for 7 to 10 days before any interventions were initiated.

3.3.6.2 Treatment preparation and administration

All drug treatments were suspended in vitamin E stripped palm oil (gift from Malaysian Palm Oil Board, Bangi). Volume of each drug dose was 100µL, i.e. volume of single drug doses were 100µL and combination drug doses were 200µL. Drug treatments were freshly prepared daily from stock solutions (*Section 3.2.2*) according to doses described in Table 3.4, and immediately administered to mice using autoclaved 20 G gavage needles or sterile 20G flexible plastic feeding tubes (both Instech Laboratories Inc, USA) and 1 mL syringe (Terumo, Japan).

3.3.6.3 Non-tumour bearing study

Mice were randomly divided into five groups, and treated as summarised below:

Table 3.4: Non tumour-bearing study groups and treatment doses

Group	Treatment/dose
Group 1 (N=2)	Vitamin E stripped palm oil (γT3, 13cRA & ABT-263 vehicle), PO, weekly on 5 consecutive days, 4 weeks.
Group 2 (N=2)	53mg/kg 13cRA, PO, weekly on 5 consecutive days, 2 weeks on, 2 weeks off.
Group 3 (N=2)	80mg/kg γT3, PO, weekly on 5 consecutive days, 4 weeks.

(continued)

Group	Treatment/dose
Group 4 (N=2)	53mg/kg 13cRA, PO, given together with 80mg/kg γT3, PO, weekly on 5 consecutive days; durations as per Groups 2 & 3.
Group 5 (N=2)	53mg/kg 13cRA, PO, followed immediately by 100mg/kg ABT-263, PO, weekly on 5 consecutive days; durations as per Groups 2 & 3.

13cRA is an orally dosed drug in humans, and γT3 (as well as other tocotrienol-related substances) is commonly administered via the oral route.

The dose of 13cRA used here was calculated based on the human dose of 160mg/m^2/day for 2 weeks on, 2 weeks off (Veal *et al.*, 2013). Using the estimated body surface area (BSA) of a 20g mouse at 0.0066m^2 (Reagan-Shaw, Nihal & Ahmad, 2008; Animal Care and Use Committee, 2015),

160mg x 0.0066m2 = 1.056 mg/day

= 1.056 mg per 20g mouse

As 1kg = 1000g, which is 20g x 50,

1.056 mg x 50 = 52.8 mg /kg/day, which was rounded up to a dose of 53mg/kg/day.

There is so far insufficient evidence to clearly establish a dose for γT3. The IC_{50} calculated of γT3 alone on SH-SY5Y cells in our in vitro studies was around 20μM. However, the pharmacokinetics of γT3 are still unclear and it is difficult to predict the behaviour of γT3 in a mouse. So far, intravenous (*iv*) and intraperitoneal (*ip*) routes have shown low bioavailability and considerable work is currently being carried out to investigate formulations including liposomes and nanoparticles (Fu *et al.*, 2014). Doses in other studies vary greatly: 1mg/kg, ip for ectopic gastric cancer xenografts (Manu *et al.*, 2012); 80mg/kg, intratumoral, currently used by our collaborators for glioblastomas; 125mg/kg,

gavage, three times a week to treat ectopic prostate cancer xenografts (Jiang *et al.*, 2012); 400mg/kg daily for 4 weeks for orthotopic pancreatic tumour xenografts (Kunnumakkara *et al.*, 2010). Eventually we decided to use a dose of 80mg/kg/day, PO, for 4 weeks in the drug tolerability and optimisation stage. The results obtained here would then be used to establish a safe and effective dose for the treatment stage.

The dose of ABT-263 (100mg/kg/day, PO) was the same dose as used in another study that treated neuroblastoma tumours in mice (Lamers *et al.*, 2012).

3.3.6.4 Tumour bearing study

Tumours were induced based on the outcomes of S*ection 3.3.4.2*. As tumour induction using only 4 x 10^6 cells was unsuccessful, ectopic tumours were initiated as described in *Section 3.3.5.2* using 6 x 10^6 SH-SY5Y cells per tumour and mice dosed according to the groups and numbers described in Table 3.4.

3.3.6.5 Monitoring

General mouse monitoring was carried out as described in *Section 3.3.3*. Tumour growth monitoring was carried out as described in *Section 3.3.5.3*, with the addition of PET imaging performed thrice per mouse: pre-tumour induction, pre-treatment initiation and at the end of the study just before termination.

3.3.6.6 Termination

Mice were terminated at the end of the experiment as described in *Section 3.3.5.4*.

3.3.7 Main treatment study

3.3.7.1 Animals

40 mice were used in this portion of the study. Mice were randomly selected and grouped in groups of 8 per group, with treatment groups as described in Table 3.4.

3.3.7.2 Tumour induction

Tumours were induced as described in *Section 3.3.5.3*.

3.3.7.3 Monitoring

Monitoring was carried out as described in *Section 3.3.6.5*.

3.3.7.4 Treatment

Treatment was prepared and administered to mice as described in *Section 3.3.6.2*.

3.3.7.5 Termination and tumour collection

Termination and tumour collection was conducted as described in *Section 3.3.5.4*.

3.3.8 Western Blot

3.3.8.1 Antibodies

Antibody dilution ratios were determined as per description in *Section 3.2.8.3*.

Table 3.5 List of antibodies used for western blot (*in vivo* protein samples)

Antibody	Manufacturer	Molecular weight	Dilution
β-actin (source: donkey)	Abcam, UK	42 kDa	1:1000
Bcl-2	Elabscience, Taiwan	26 kDa	1:1000
Bcl-xL	Elabscience, Taiwan	30 kDa	1:1000
Caspase 3	Elabscience, Taiwan	35 kDa	1:1000
Caspase 9	Elabscience, Taiwan	46 kDa	1:1000
MYCN	Elabscience, Taiwan	45 kDa	1:1000
p53	Elabscience, Taiwan	43 kDa	1:1000
Anti-rabbit IgG-HRP	Santa Cruz Biotechnology, USA	-	1:5000
Anti-donkey IgG-HRP	Santa Cruz Biotechnology, USA	-	1:5000

3.3.8.2 Tumour sample preparation

Frozen tumours were weighed and then pulverised, on ice, into a fine powder in a chilled, autoclaved mortar, using liquid nitrogen and a chilled, autoclaved pestle. Powders were then transferred to ice cold RIPA buffer, containing 10μL/mL each of Halt Protease and Phosphatase Inhibitor Cocktail 100X and 0.5M EDTA, as described in *Section 3.2.8.2*. For every 5 mg of tissue, 300 μL of RIPA buffer was used. Then, tissue/RIPA buffer mixture was agitated using a vortex for 2 hours at 4°C. Following that, mixture was centrifuged at 12000

rpm for 20 minutes, at 4°C. Supernatant was collected and aliquots of 20 µL per tube were made and the pellet discarded. Aliquots were stored at -80°C.

3.3.8.3 Protein concentration determination

Protein concentration was determined using Bradford Assay, as described in *Section 3.2.8.2*.

3.3.8.4 Western blot procedure

Western blot was carried out as described in *Section 3.2.8.3*, using 25 µg protein lysate per sample. For *in vivo* samples, proteins studied were: BCL-2, BCL-xL, p53, caspase-3, caspase-9 and MYCN. β-actin was again used as a loading control. Titration of antibody dilutions were performed as described in *Section 3.2.8.3*.

However, a further protein quantification step was carried out after scanning membranes with the Chemidoc Imager.

Membranes were transported in TBS to a dark room. After removal from TBS, Pierce™ ECL Western Blotting Substrate was added again for 1 minute, before membranes were covered in transparent plastic and exposed to film (Amersham Hyperfilm™ ECL, GE Life Sciences, UK) for 15 minutes in an autoradiography cassette (Hypercassette, GE Life Sciences, UK). The film was then washed in Carestream® Kodak® Autoradiography GBX Developer (Sigma, USA) for 30 seconds, washed in water for 1 minute, and finally washed in Carestream® Kodak® Autoradiography GBX Fixer (Sigma, USA) for 10 seconds. Film was fully dried before proceeding to densitometric analysis.

3.3.8.5 Densitometry

Protein bands on films were scanned using the GS-800 Calibrated Imaging Densitometer (Bio-Rad, USA) and accompanying software, Quantity One (Bio-Rad, USA). Prevention of saturated film was accomplished by earlier trial and error of film exposure length. Image analysis was performed using the same software.

Next, relative protein expression was calculated. First, the treated protein band intensity of interest was divided by its sample control band intensity (β-actin) for normalisation (A). Non-treated protein band intensity was also divided by its sample control band intensity (β-actin) for a normalised non-treated protein band intensity (B). Finally, relative protein expression was calculated:

$$\text{Relative protein expression} = \frac{\text{Normalised treated protein band intensity}}{\text{Normalised untreated protein band intensity}}$$

3.4 STATISTICAL ANALYSIS

Differences between treated and untreated controls were compared using two-tailed paired t-test with Dunnett's post-hoc test, except for tumour reduction data, where differences were compared using the Kruskal-Wallis test with uncorrected Dunn's test. Data was presented with error bars to indicate mean ± SD, representative of at least 3 independent experiments. Statistical significance was set at $p < 0.05$. All statistical analysis was carried out using GraphPad Prism 7.03 Software (GraphPad Software Inc., USA).

CHAPTER 4 RESULTS

4.1 *IN VITRO* RESULTS

This section will present the results obtained from cell culture work. First, cell viability results on individual and combination treatments of 13cRA, γT3 and ABT-263 on SH-SY5Y and SK-N-BE(2) cell lines (Sections 4.1.1.1 and 4.1.1.2), and comparison of IC_{50} values in individual and combination treatments (Section 4.1.1.2). Next, combination index values obtained from analysis by Compusyn software in Section 4.1.2, followed by flow cytometry results from treatments on both cell lines to determine effects of the abovementioned treatments on apoptosis (Section 4.1.3), and finally protein expression results from western blots (Section 4.1.4).

4.1.1 Cell viability

4.1.1.1 Individual treatments

Both SH-SY5Y and SK-N-BE(2) cells showed a significant increase in cell viability when treated with lower doses of 13cRA (below 10 µM), as seen in Figure 4.1. Thereafter, cell viability decreased. SH-SY5Y cells had a slightly steeper slope. Both cell lines showed very significant decrease in cell viability at 50 µM ($p \leq 0.0001$), compared to no treatment control. The IC_{50} for 13cRA in both cell lines was 39 µM.

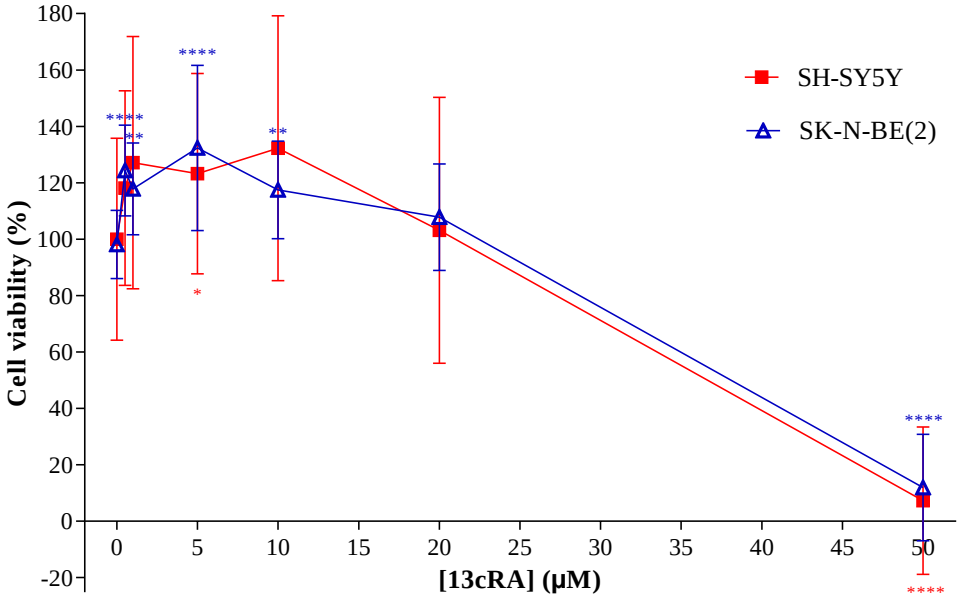

Figure 4.1: Cell viability of SH-SY5Y and SK-N-BE(2) cells treated individually for 24 h with 0 to 50µM 13cRA, as measured by MTS assay. Results are represented as mean ± SD from N= ≥3 (biological replicates); *significant when compared with untreated cells *$p \leq 0.05$, **$p \leq 0.01$, ***$p \leq 0.001$, ****$p \leq 0.0001$.

In contrast to 13cRA treatment, treatment with γT3 did not result in significant increase in cell viability at low concentrations (Figure 4.2). SH-SY5Y cell lines responded to treatment earlier than SK-N-BE(2) cell lines, with significant decrease in cell viability at 7.5 µM ($p \leq 0.01$), while SK-N-BE(2) cell lines only showed the same significant decrease in cell viability at 30 µM. IC_{50} for γT3 in the SH-SY5Y cell line was 20 µM and 26 µM in the SK-N-BE(2) cell line.

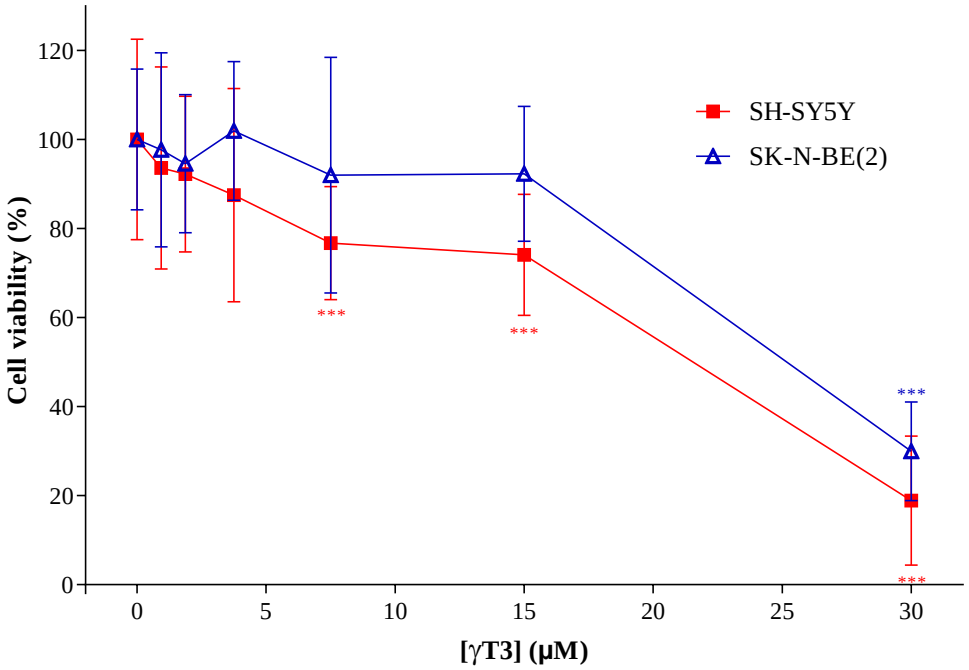

Figure 4.2: Cell viability of SH-SY5Y and SK-N-BE(2) cells treated individually for 24 h with 0 to 30µM γT3, as measured by MTS assay. Results are represented as mean ± SD from N= ≥3 (biological replicates); *significant when compared with untreated cells *$p \leq 0.05$, **$p \leq 0.01$, ***$p \leq 0.001$.

In Figure 4.3, treatment with ABT-263 showed a slight, although not significant increase in cell viability in SH-SY5Y cell lines followed by a steady decline in cell viability which was not significant until 40 µM ABT-263 ($p \leq 0.001$). In the same graph, SK-N-BE(2) cell lines showed a slight and significant increase in cell viability at 12.5 µM ($p \leq 0.001$), followed by steady but not significant decrease until 50 µM, when the reduction in cell viability compared to no treatment became significant ($p \leq 0.001$). IC_{50} for ABT-263 in both cell lines was 40 µM.

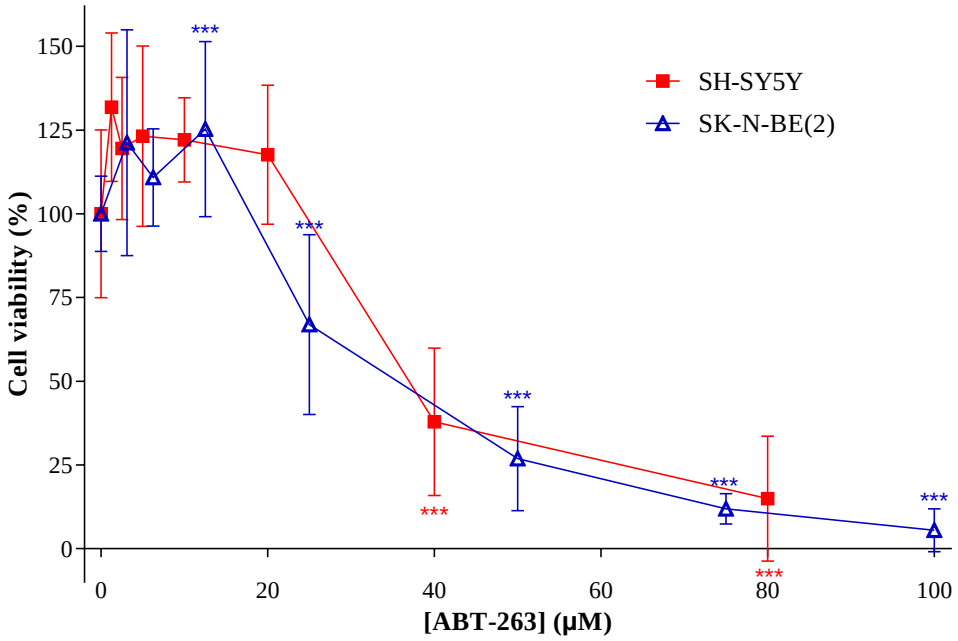

Figure 4.3: Cell viability of SH-SY5Y and SK-N-BE(2) cells treated individually for 24 h with 0 to 80µM or 0 to 100µM of ABT-263, respectively, as measured by MTS assay. Results are represented as mean ± SD from N= ≥3 (biological replicates); *significant when compared with untreated cells *$p \leq 0.05$, **$p \leq 0.01$, ***$p \leq 0.001$.

4.1.1.2 Combination treatments

As shown in Figure 3.4 (Section 3.2.3), the sub-optimal concentrations used for combination treatment was chosen by calculating IC_{25} values from the IC_{50} values obtained from the individual treatment assay. It should however be noted that the sub-optimal concentrations used and the final calculated IC_{50} values may not completely correspond, as later data was added to the IC_{50} calculations (to reduce error bars) after sub-optimal value calculation and subsequent experiment was carried out.

SH-SY5Y cells showed a much more rapid decline in cell viability than SK-N-BE(2) cell lines when treated in combination with 0 to 40μM 13cRA and either 8.5μM or 12.5μM γT3, respectively (Figure 4.4). In the SH-SY5Y cell line, addition of 8.5 μM of γT3 caused the IC_{50} of 13cRA to drop by 74% from 39μM, while in the SK-N-BE(2) cell line, the IC_{50} of 13cRA dropped from 39 μM by 59%.

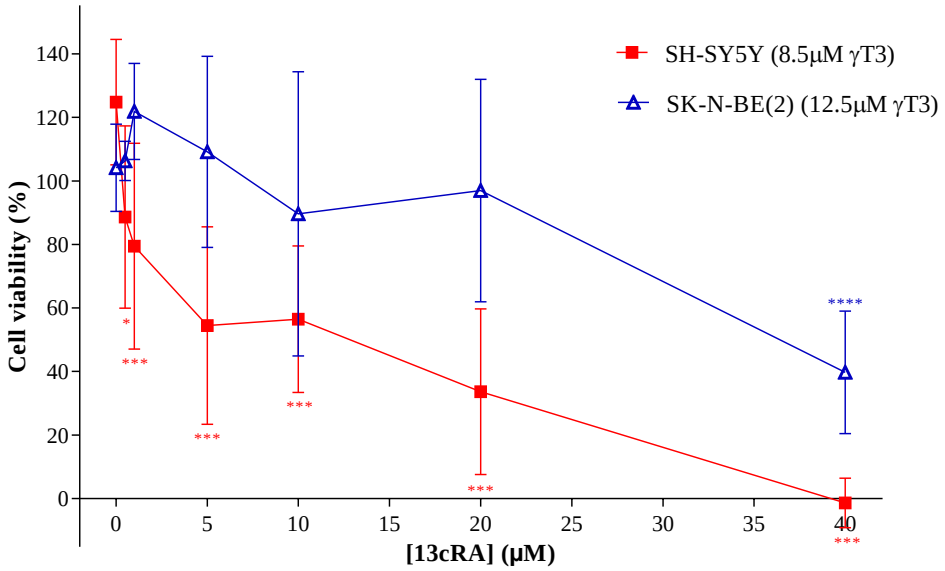

Figure 4.4: Cell viability of SH-SY5Y and SK-N-BE(2) cells treated individually for 24 h with 0 to 40µM 13cRA and either 8.5µM or 12.5µM γT3, respectively, as measured by MTS assay. Results are represented as mean ± SD from N= ≥3 (biological replicates); *significant when compared with untreated cells *p≤0.05, **p≤0.01, ***p≤0.001, ****p≤0.0001.

Figure 4.5 shows a similar pattern, where SH-SY5Y cell lines showed a more rapid decline in cell viability than SK-N-BE(2) cells when treated with 0 to 25µM γT3 and either 15µM or 20µM 13cRA, respectively. Addition of 15 µM 13cRA caused IC_{50} of γT3 (20 µM) to decrease by 90% in the SH-SY5Y cell line, while addition of 20 µM of 13cRA to treat the SK-N-BE(2) cells reduced the IC_{50} by 23%.

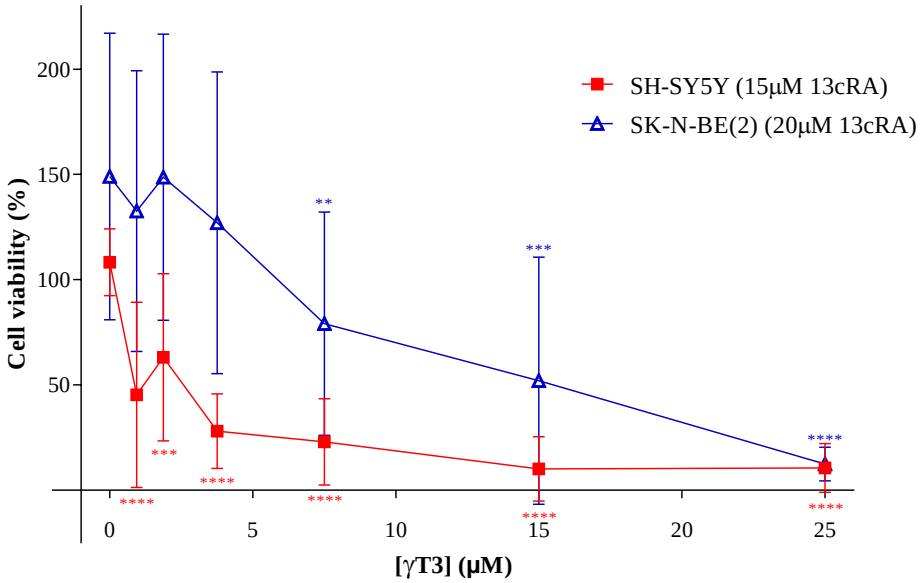

Figure 4.5: Cell viability of SH-SY5Y and SK-N-BE(2) cells treated individually for 24 h with 0 to 25µM γT3 and either 15µM or 20µM 13cRA, respectively, as measured by MTS assay. Results are represented as mean ± SD from N= ≥3 (biological replicates); *significant when compared with untreated cells *p≤0.05, **p≤0.01 , ***p≤0.001, ****p≤0.0001.

However, when SH-SY5Y and SK-N-BE(2) cells were exposed to 0 to 40µM 13cRA and 19.5µM ABT-263, SH-SY5Y only showed a visible and significant decline in cell viability at 10 µM 13cRA, and while SK-N-BE(2) showed a drop in cell viability at the same 13cRA concentration, significance was only observed at 40 µM 13cRA (Figure 4.6). The IC_{50} of 13cRA dropped by 26% from 39 µM in the SH-SY5Y cell line after addition of 19.5 µM ABT-263, while in the SK-N-BE(2) cell line, the reduction in IC_{50} was less, at 15%.

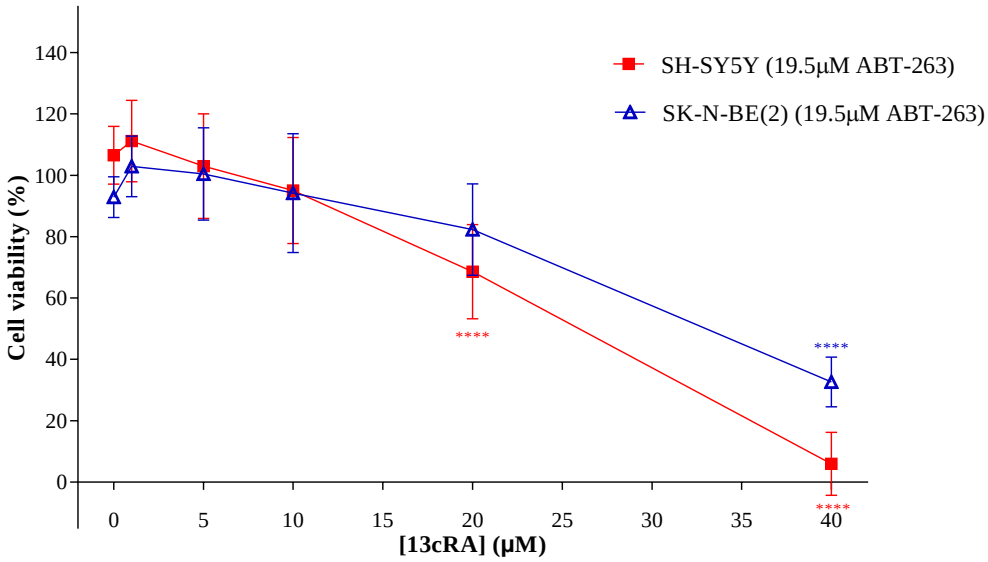

Figure 4.6: Cell viability of SH-SY5Y and SK-N-BE(2) cells treated individually for 24 h with 0 to 40µM 13cRA and 19.5µM ABT-263, as measured by MTS assay. Results are represented as mean ± SD from N= ≥3 (biological replicates); *significant when compared with untreated cells *p≤0.05, **p≤0.01 , ***p≤0.001, ****p≤0.0001.

When IC_{50} figures of combination treatments were compared, a significant decrease in IC_{50} was observed when SH-SY5Y cell lines were treated with 0 to 25µM γT3 only or 0 to 40µM 13cRA only, compared to combination treatments (Figure 4.7).

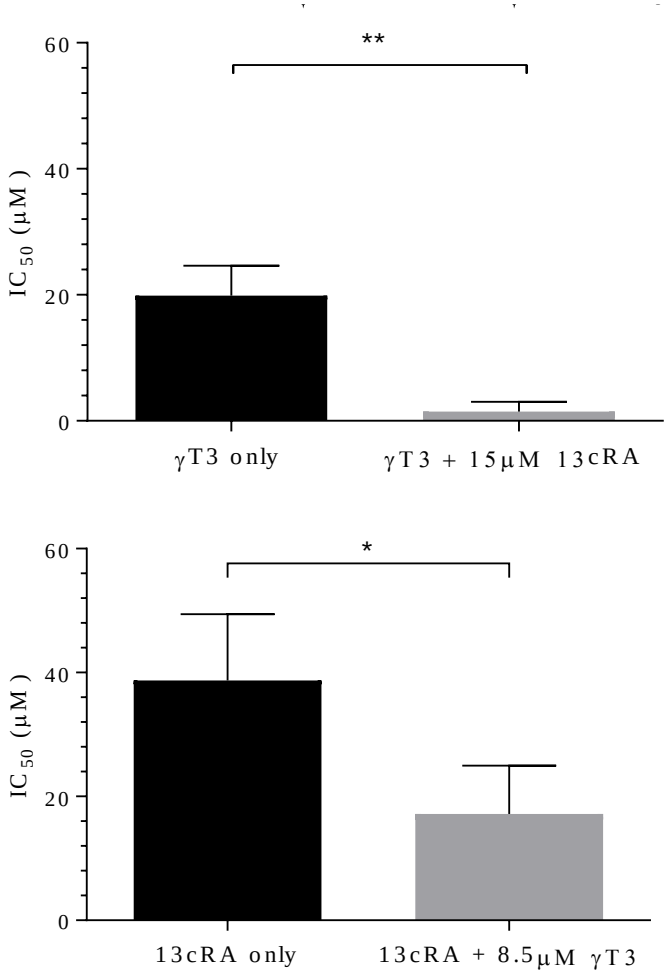

Figure 4.7: Comparison of IC_{50} in SH-SY5Y cells treated for 24 h with individual treatments (0 to 25µM γT3 only or 0 to 40µM 13cRA only) compared to combination treatments, as measured by MTS assay. Results are represented as mean ± SD from three biological replicates and significance between individual and combination treatments shown as * $p \leq 0.05$.

Figure 4.8 shows a similar, significant difference between IC_{50} of individual and combination treatments in SK-N-BE(2) cell lines.

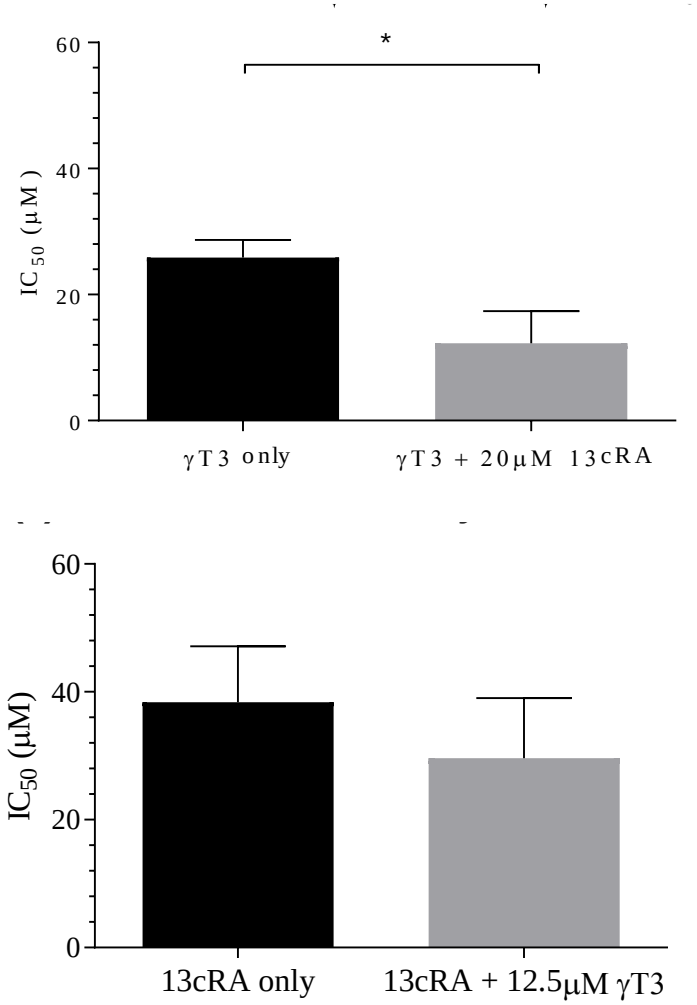

Figure 4.8: Comparison of IC_{50} in SK-N-BE(2) cells treated for 24 h with individual treatments (0 to 25μM γT3 only or 0 to 40μM 13cRA only) compared to combination treatments, as measured by MTS assay. Results are represented as mean ± SD from three biological replicates and significance between individual and combination treatments shown as * $p \leq 0.05$.

However, no significant change in IC_{50} was observed when ABT-263 was combined with 13cRA to treat either cell line, although the addition of ABT-263 to 13cRA did result in a slight reduction of IC_{50} for 13cRA (Figure 4.9).

A. SH-SY5Y

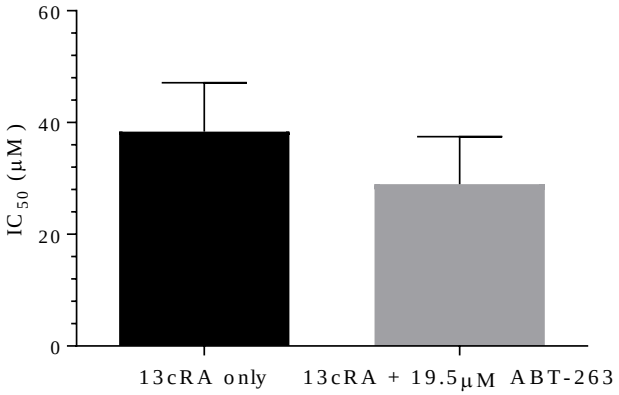

B. SK-N-BE(2)

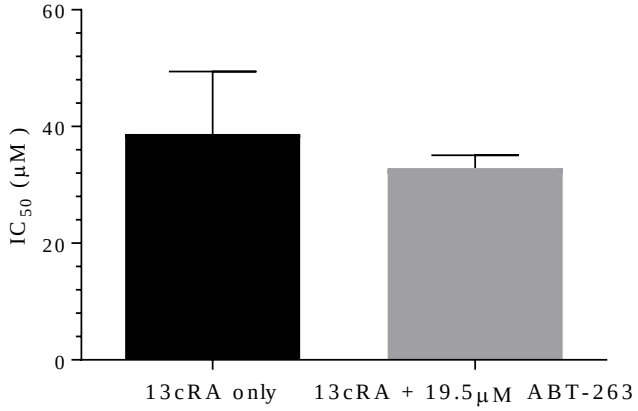

Figure 4.9: Comparison of 13cRA IC_{50} in SH-SY5Y cells (A) and SK-N-BE(2) cells (B) treated for 24 h with individual treatment (0 to 40µM 13cRA only) and combination treatment (additional 30µM or 40µM ABT-263), as measured by MTS assay. Results are represented as mean ± SD from three biological replicates. No statistical significance.

Table 4.1: Comparison of IC_{50} values of individual and combination 13cRA or γT3 treatments in SH-SY5Y and SK-N-BE(2) cell lines. Cells were exposed to treatment for 24h with individual treatments (0 to 25μM γT3 only or 0 to 40μM 13cRA only) or combined with either 13cRA or γT3, and cell viability was measured by MTS assay.

	IC_{50} value (μM)	
Treatment group	**SH-SY5Y**	**SK-N-BE(2)**
13cRA only	39	39
γT3 only	20	26
13cRA + 8.5 μM γT3	10	-
γT3 + 15 μM 13cRA	2	-
13cRA + 12.5 μM γT3	-	16
γT3 + 20 μM 13cRA	-	20

4.1.2 Combination index

Combination index values obtained after processing IC_{50} values using Compusyn software are summarised in Tables 4.2, 4.3 and 4.4.

The addition of γT3 to 15 μM of 13cRA showed immediate synergy in SH-SY5Y cell lines (from the lowest concentration of γT3, 0.975 μM), while in SK-N-BE(2) cell lines, synergy was only observed at the higher concentration of 7.5 μM γT3 added to 20 μM 13cRA (Table 4.2).

Table 4.2: Effect of 0.9375 - 25 μM of γT3 combined with 13cRA on SH-SY5Y and SK-N-BE(2) cells; n≥3. If CI is >1: antagonism; **<1: synergism**; = 1: additive effect. Values indicating synergism are underlined.

	Cell line	**γT3 (μM)**					
		0.9375	**1.875**	**3.75**	**7.5**	**15**	**25**
Combination index	**SH-SY5Y** (15 μM 13cRA)	<u>0.091</u>	<u>0.232</u>	<u>0.120</u>	<u>0.162</u>	<u>0.125</u>	<u>0.203</u>
	SK-N-BE(2) (20 μM 13cRA)	84.355	156.842	301.816	<u>0.239</u>	<u>0.198</u>	<u>0.088</u>

The addition of 13cRA to 8.5 μM γT3 in SH-SY5Y cell lines only showed synergy with 5 μM of 13cRA, while in SK-N-BE(2) cell lines, 10 μM 13cRA and 12.5 μM γT3 was needed to show synergy (Table 4.3).

Table 4.3: Effect of 0.5 - 40 μM of 13cRA combined with γT3 on SH-SY5Y and SK-N-BE(2) cells; n≥3. If CI is >1: antagonism; **<1: synergism**; = 1: additive effect. Values indicating synergism are underlined.

	Cell line	**13cRA (μM)**					
		0.5	**1**	**5**	**10**	**20**	**40**
Combination index	**SH-SY5Y** (8.5 μM γT3)	3.729	1.683	<u>0.445</u>	<u>0.488</u>	<u>0.168</u>	<u>1.7 x 10^{-12}</u>
	SK-N-BE(2) (12.5 μM γT3)	30467	30468	30470	<u>0.378</u>	<u>0.786</u>	<u>0.125</u>

Interestingly, treatment with ABT-263 and 13cRA in both cell lines had similar effects (Table 4.4). Synergy was observed at the same concentration of 13cRA (10μM) in both SH-SY5Y and SK-N-BE(2) when 0 to 40 μM 13cRA was added to 19.5 μM ABT-263.

Table 4.4: Effect of 10 - 40 μM of 13cRA combined with ABT-263 on SH-SY5Y and SK-N-BE(2) cells; n≥3. If CI is >1: antagonism; **<1: synergism**; = 1: additive effect. Values indicating synergism are underlined.

	Cell line	**13cRA (μM)**				
		1	**5**	**10**	**20**	**40**
Combination index	**SH-SY5Y** (19.5 μM ABT-263)	3.085	5.458	<u>0.230</u>	<u>0.183</u>	<u>0.121</u>
	SK-N-BE(2) (19.5 μM ABT-263)	4.665	7.039	<u>0.472</u>	<u>0.423</u>	<u>0.339</u>

4.1.3 Cell cytotoxicity results

LDH assay was performed on SH-SY5Y and SK-N-BE(2) cell lines, using individual and combination γT3 and 13cRA treatments.

In Figure 4.10, a statistically significant increase in % cytotoxicity was seen at the highest concentrations of γT3 ($p \leq 0.01$) and 13cRA ($p \leq 0.001$) although prior to that, % cytotoxicity was calculated at 0% or below.

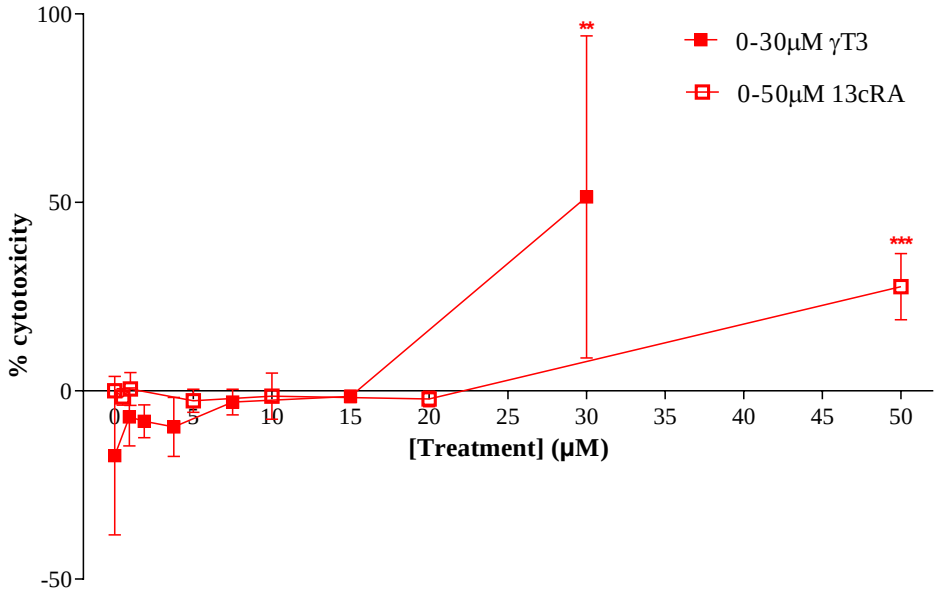

Figure 4.10: Cell death of SH-SY5Y cells treated individually with 0-30µM γT3 and 0-50µM 13cRA, as measured by LDH release assay. Results are represented as mean ± SD from N= ≥3 (biological replicates). *significant when compared with untreated cells: **$p \leq 0.01$, ***$p \leq 0.001$.

In Figure 4.11, there was a rise in % cytotoxicity at the highest concentrations of γT3 and 13cRA in the SK-N-BE(2) cell line, but no statistically significant results were seen.

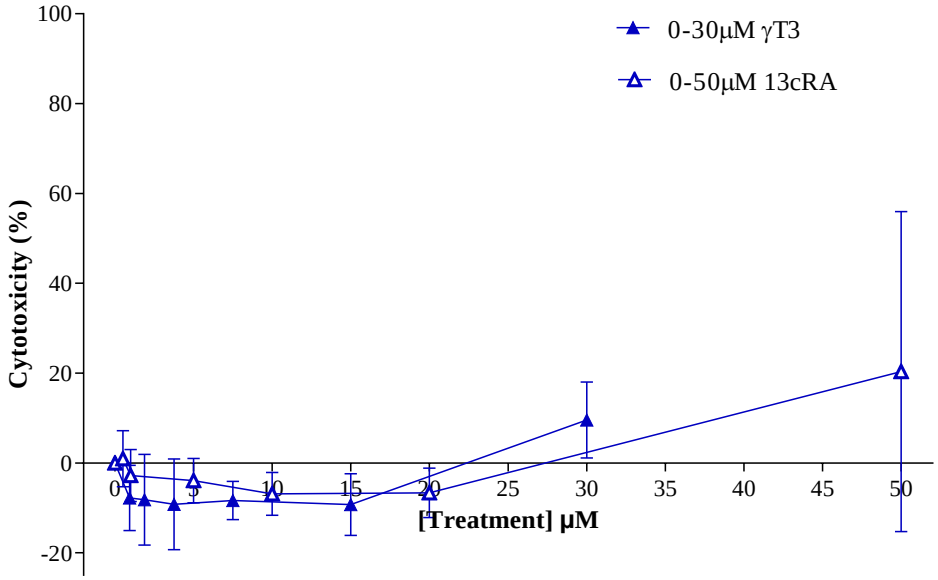

Figure 4.11: Cell death of SK-N-BE(2) cells treated individually with 0-30µM γT3 and 0-50µM 13cRA, as measured by LDH release assay. Results are represented as mean ± SD from N= ≥3 (biological replicates). No significant results.

The combination treatments on SH-SY5Y cells in Figure 4.12 show a concentration dependent rise in % cytotoxicity in the 0 to 25µM γT3 and 15µM 13cRA group, with a statistically significant increase at 7.5µM γT3 when 15µM was added ($p \leq 0.05$), with statistical significance increasing at each subsequent γT3 concentration $p \leq 0.01$ at 15µM and $p \leq 0.001$ at 25µM. However, the 0 to 40µM 13cRA and 8.5µM γT3 treatment group displayed high % cytotoxicity throughout, even at 8.5 µM γT3 only (~75% cytotoxicity), with the % cytotoxicity remaining at around this level throughout.

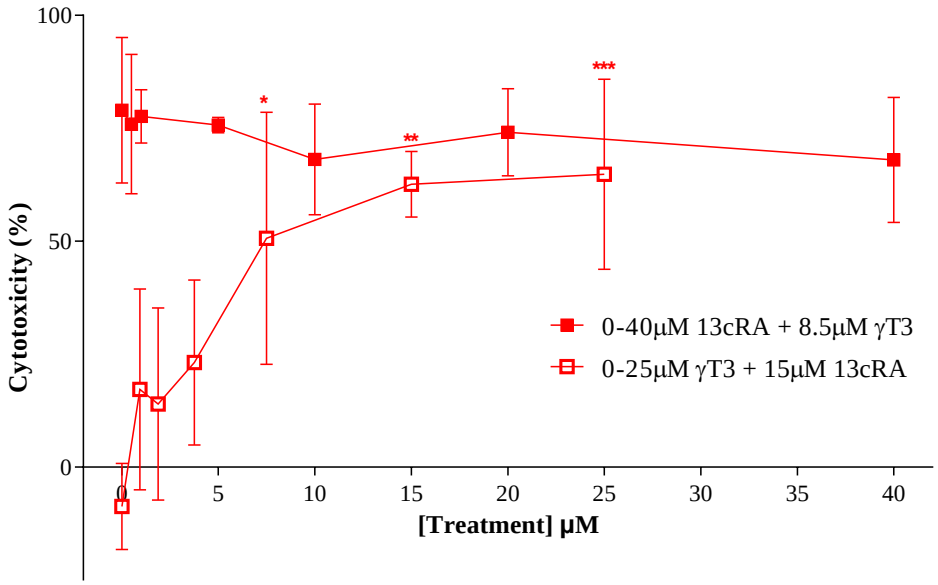

Figure 4.12: Cell death of SH-SY5Y cells treated in combination with either 0 to 40µM 13cRA and 8.5µM γT3 or 0 to 25µM γT3 and 15µM 13cRA, as measured by LDH release assay. Results are represented as mean ± SD from N= ≥3 (biological replicates). *significant when compared with untreated cells: *$p \leq 0.05$, **$p \leq 0.01$, ***$p \leq 0.001$.

Figure 4.13 shows no statistically significant results from the combination treatments on the SK-N-BE(2) cell line, although the 0 to 25µM γT3 and 20µM 13cRA treatment group does indicate a concentration dependent increase in % cytotoxicity. The 0 to 40µM 13cRA and 12.5µM γT3 group starts at about 25% cytotoxicity at 0µM 13cRA and 12.5µM γT3 and dips slightly below, only rising to about 30% cytotoxicity at 40µM 13cRA.

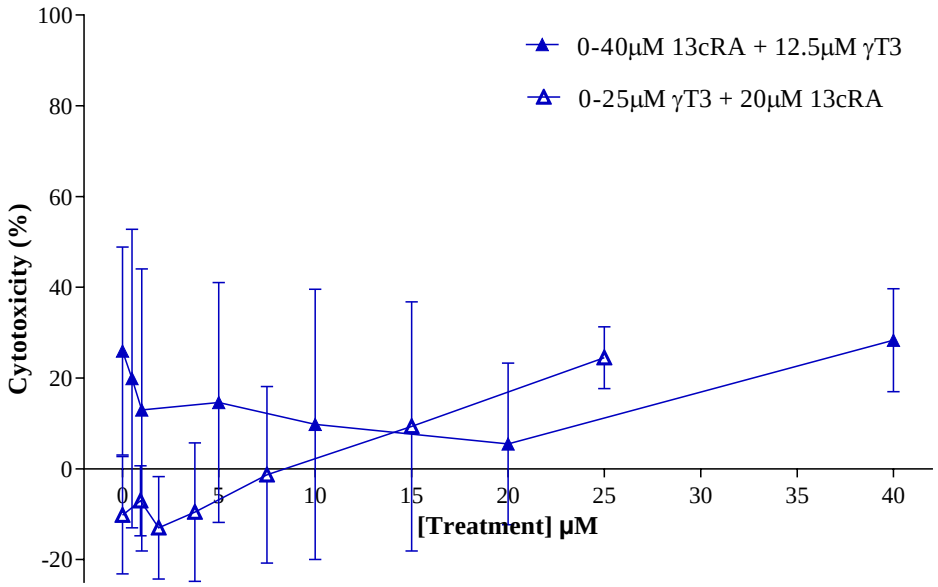

Figure 4.13: Cell death of SK-N-BE(2) cells treated in combination with either 0 to 40µM 13cRA and 12.5µM γT3 or 0 to 25µM γT3 and 20µM 13cRA, as measured by LDH release assay. Results are represented as mean ± SD from N= ≥3 (biological replicates). No significant results.

4.1.4 Flow cytometry

Figures 4.14A and 4.15A are dot plots of control cells, 13cRA only-treated cells, γT3 only- and γT3/13cRA-treated cells, and ABT-263 only- and ABT-263/13cRA-treated cells in SH-SY5Y and SK-N-BE(2) cell lines, respectively. Figures 4.14B and 4.15B summarise percentage number of the previously mentioned cells at each stage of apoptosis, with the values obtained from the dot plots shown in Figures 4.14A and 4.15A.

In the SH-SY5Y cell line none of the changes in viable cells were statistically significant when comparing treated to non-treated cell groups (Figure 4.14). There was an increase in number of cells in early apoptosis after treatment with γT3 combination treatment in the SH-SY5Y cell line, from 3.2% to 5.6%, although it was not statistically significant (Figure 4.1A). There was also a slight drop to 1.8% and 1.9% respectively for ABT-263 only and ABT-263 combination groups. In the late apoptosis stage, there was an statistically insignificant increase from 5% in vehicle only control cells to 10.3%, 8.8%, 9.9% and 6.3% in γT3 only, γT3 combination, ABT-263 only and ABT-263 combination treatment cells, respectively. Necrosis also showed increases, although statistically insignificant, in percentage number of cells in γT3 only, γT3 combination, ABT-263 only and ABT-263 combination treatments, with values of 4.3%, 5%, 3.6% and 3.9%, respectively, up from 0.8% in the control treatment group.

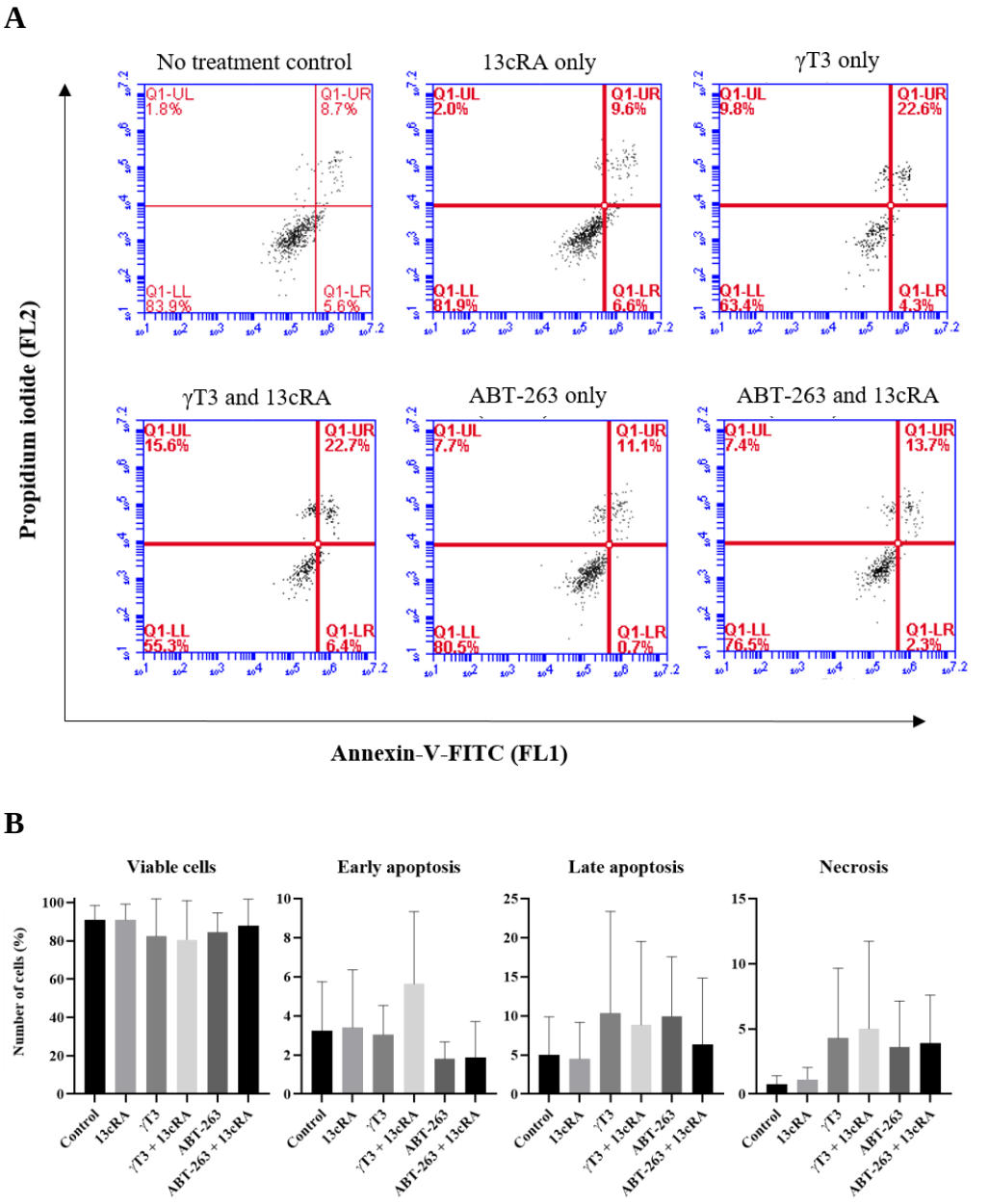

Figure 4.14: Comparison of apoptosis in SH-SY5Y cells after individual or combinations with 13cRA, γT3 or ABT-263, using flow cytometry with Annexin V-FITC/PI assay kit. Dot plots of cells with no treatment control, 13cRA only, γT3 only, γT3 and 13cRA, ABT-263 only and ABT-263 and 13cRA shown in (A). Data in (B) shows % number of cells at each stage of apoptosis, comparing treatment groups to no treatment control, as well as individual compared to combination treatment groups. Results in (B) are represented as mean ± SD from N=3 (biological replicates). No significant changes found.

Samples from the SK-N-BE(2) cell line (Figure 4.15) showed one statistically significant change in the late apoptosis stage: from 0.3% of control cells to 1.8% of cells in the ABT-263 combination treatment group (Figure 4.15B).

Otherwise, like the SH-SY5Y cell line, there were some changes in percentages of cell distribution but they were not statistically significant. In the early apoptosis stage, the ABT-263 combination group once again showed an increase compared to the control group cells, 4.5% vs 1.9%, respectively, while the γT3 combination group in early apoptosis showed an even lesser increase of 3.4%. In late apoptosis and necrosis, changes in cell percentage were even more slight, with the exception of the ABT-263 combination group in late apoptosis.

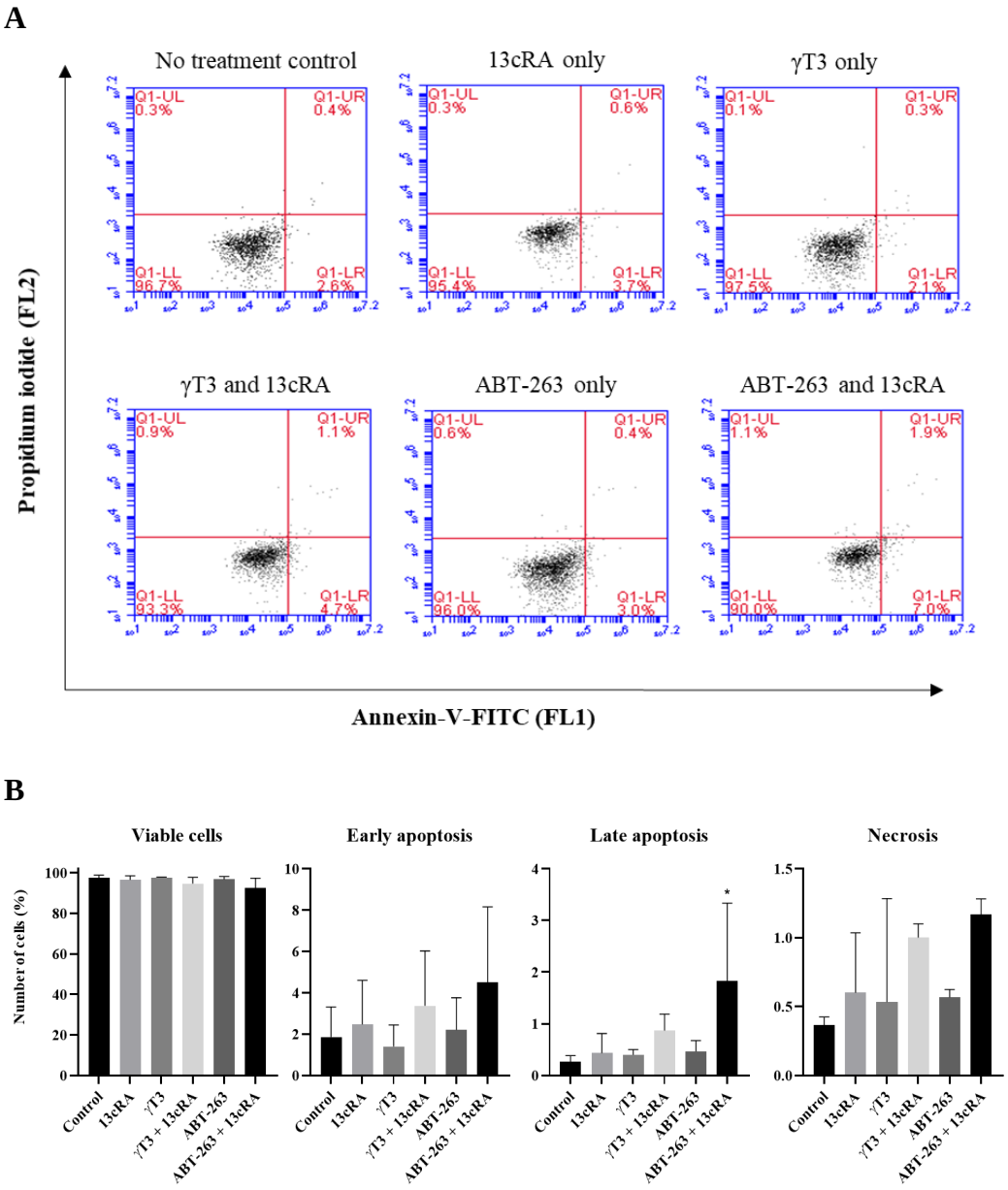

Figure 4.15: Comparison of apoptosis in SK-N-BE(2) cells after individual or combinations with 13cRA, γT3 or ABT-263, using flow cytometry with Annexin V-FITC/PI assay kit. Dot plots of cells with no treatment control, 13cRA only, γT3 only, γT3 and 13cRA, ABT-263 only and ABT-263 and 13cRA shown in (A). Data in (B) shows % number of cells at each stage of apoptosis, comparing treatment groups to no treatment control, as well as individual compared to combination treatment groups. Results in (B) are represented as mean ± SD from N=3 (biological replicates), *significant when compared with untreated cells *p≤0.05.

4.1.5 Western blot (*in vitro*)

A significant decrease in MYCN protein expression was observed in ABT-263 individual and combination groups in the SH-SY5Y cell line, * $p \leq 0.05$ (Figures 4.16 and 4.17A). While increases in Bcl-2 protein expression were observed in the 13cRA and γT3 combination group (Figures 4.16 and 4.17B), they were not statistically significant.

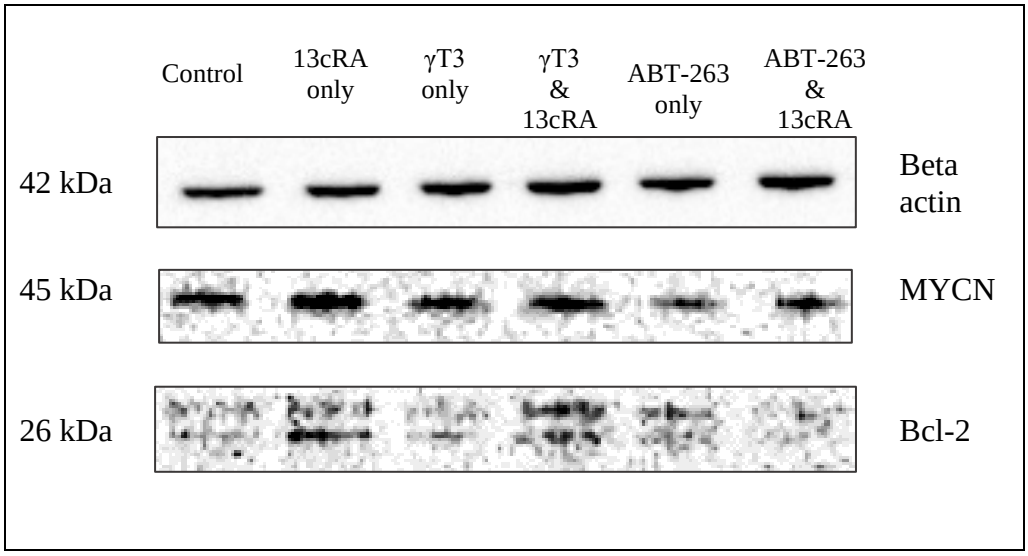

Figure 4.16: Effect of 13cRA and γT3, alone and in combination, and ABT-263 alone and in combination with 13cRA, compared to vehicle only control on protein expression of Bcl-2 and MYCN in SH-SY5Y neuroblastoma cell lines. Beta actin was used as the loading control, and results are representative of three independent experiments.

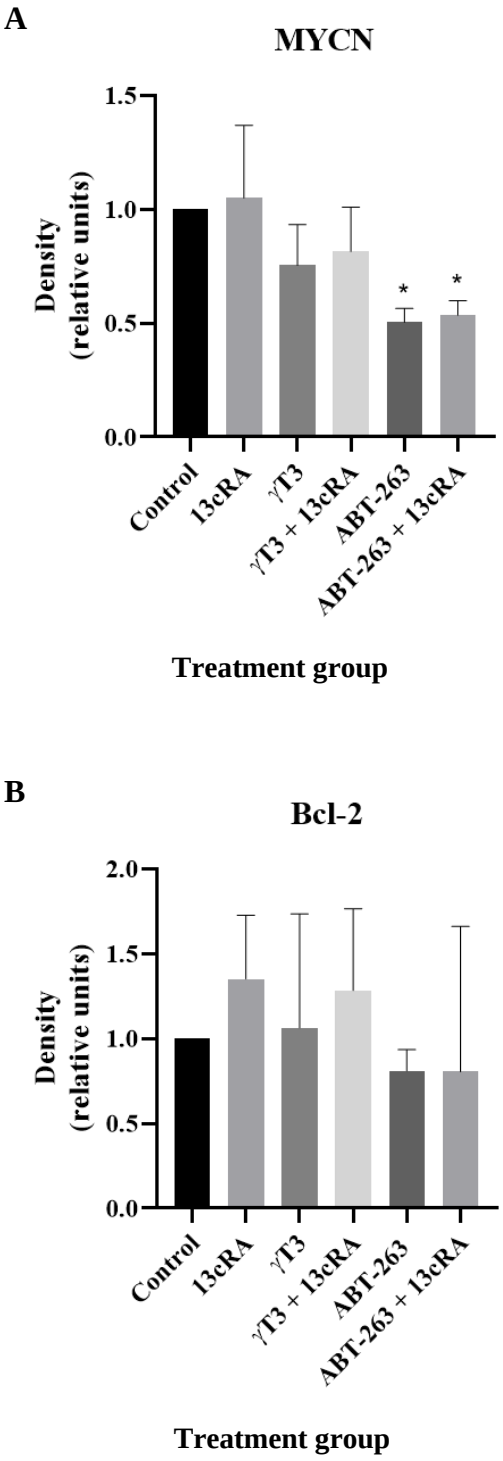

Figure 4.17: Comparison of relative density profiles obtained from western blot protein bands after individual and combination treatment of SH-SY5Y cell lines, as seen in Figure 4.16 of A) MYCN and B) Bcl-2. Results are represented as mean ± SD from three biological replicates and significance between treated and untreated shown as * $p \leq 0.05$.

In the SK-N-BE(2) cell line, protein expression of MYCN was not significantly altered in all treated samples compared to untreated samples (Figures 4.18 and 4.19A). However, there were significantly elevated Bcl-2 protein expression levels in γT3 combination, and ABT-263 individual and combination groups (Figures 4.18 and 4.19B). There was also a reduction in Bcl-2 protein expression in the 13cRA only treatment group for the SK-N-BE(2) cell line, but this was not significant (Figure 4.19B).

No bands were obtained for samples tested against p53, and therefore no results are presented.

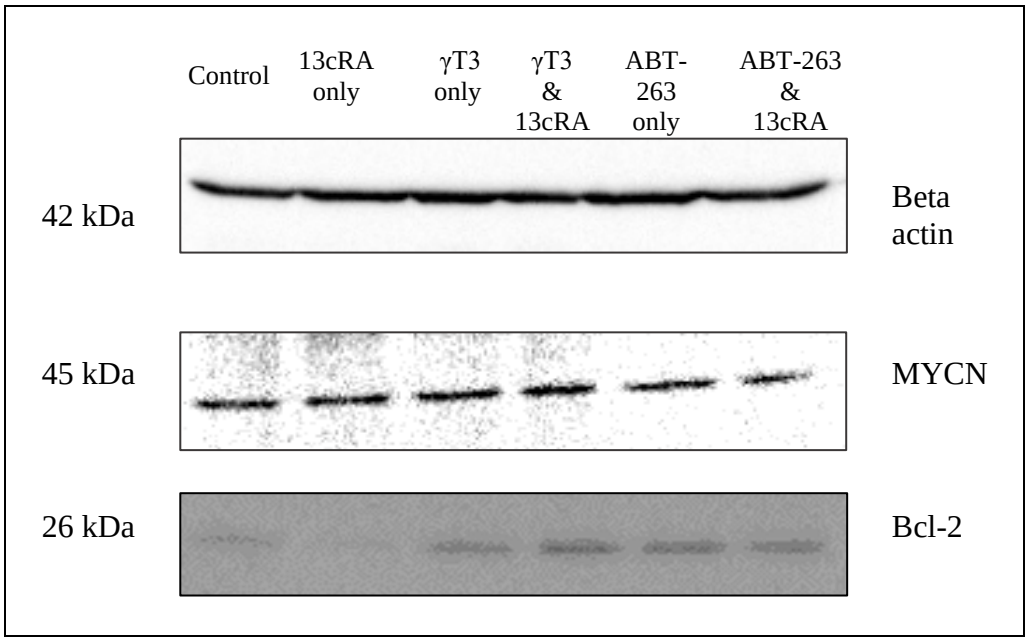

Figure 4.18: Effect of 13cRA and γT3, alone and in combination, and ABT-263 alone and in combination with 13cRA, compared to vehicle only control on protein expression of Bcl-2 and MYCN in SK-N-BE(2) neuroblastoma cell lines. Beta actin was used as the loading control, and results are representative of three independent experiments.

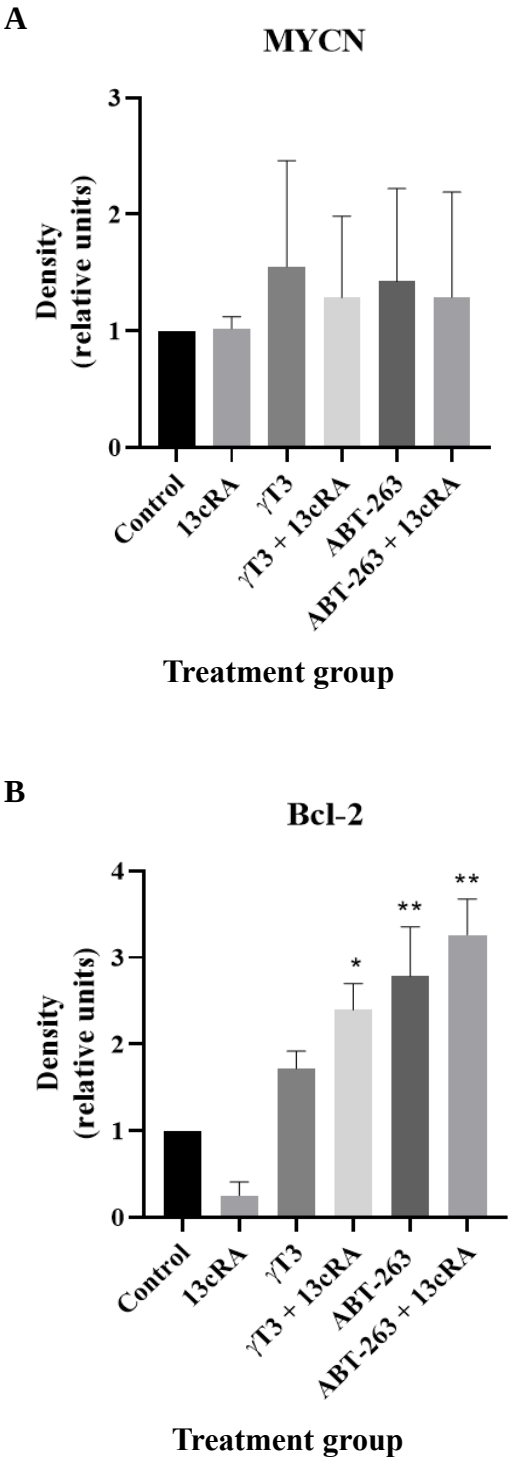

Figure 4.19: Comparison of relative density profiles obtained from western blot protein bands after individual and combination treatment of SK-N-BE(2) cell lines, as seen in Figure 4.18 of A) MYCN and B) Bcl-2. Results are represented as mean ± SD from three biological replicates and significance between treated and untreated shown as * $p \leq 0.05$, ** $p \leq 0.01$, with CI = 95%.

4.2 *IN VIVO* RESULTS

This section presents results obtained from *in vivo* experiments. Treatment combinations were selected based both on prior *in vitro* work as well as published literature for guidance on dosage and frequency.

Section 4.2.1 shows results of the effect of individual and combination treatments on tumour volume of tumours grown from SH-SY5Y cell lines in nude mice (Figure 4.20) and representative PET images to show position of tumour growth, as well as relative sizes at the end of treatment (Figure 4.21).

Western blot results using protein samples extracted from the previously mentioned tumours – both the images of representative protein bands, as well as data from quantification are shown in Section 4.2.2.

4.2.1 Tumour size reduction

Using readings from daily calliper measurements, significantly smaller tumour sizes ($p \leq 0.05$) were observed in two treatment groups (13cRA only and γT3 combined with 13cRA), when compared to vehicle only control (Figure 4.20). Average final tumour volume of 13cRA only group and γT3 combination group were reduced by about half (2.2 cm^3), and three quarters (1.1 cm^3), respectively, compared to the vehicle only control (3.9 cm^3). However, all treatment groups demonstrated a lower final tumour volume when compared to vehicle only control.

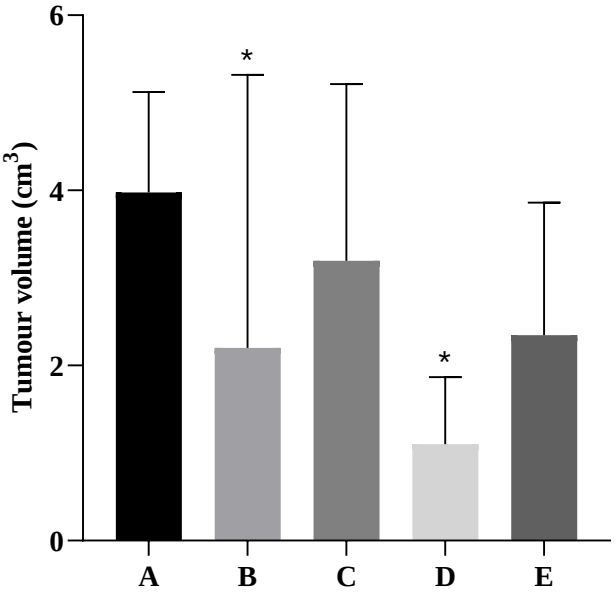

Figure 4.20: Comparison of treatment effects on tumour volume, vs. vehicle only control. N= 4 to 8. * indicates significance, where $p \leq 0.05$, with CI = 95%.

Figure 4.21 is a qualitative representation of tumours observed in PET scan images. Using the VivoQuant software, each image is built from the combination of two scans: one is a CT scan, which provides a direct anatomical image of the mouse, while the ^{18}F--FDG PET image visualises the biodistribution and uptake of ^{18}F-FDG. Increasing brightness indicates higher uptake of ^{18}F--FDG, i.e. pale yellow or white shows high levels of ^{18}F--FDG uptake and blue shows low levels of ^{18}F—FDG uptake. The images in Figure 4.21 show high uptake of ^{18}F-FDG in the bladders of all images, as well as in the hearts of images A to C, but low uptake in tumours. Further PET/CT images are available in Appendix C.

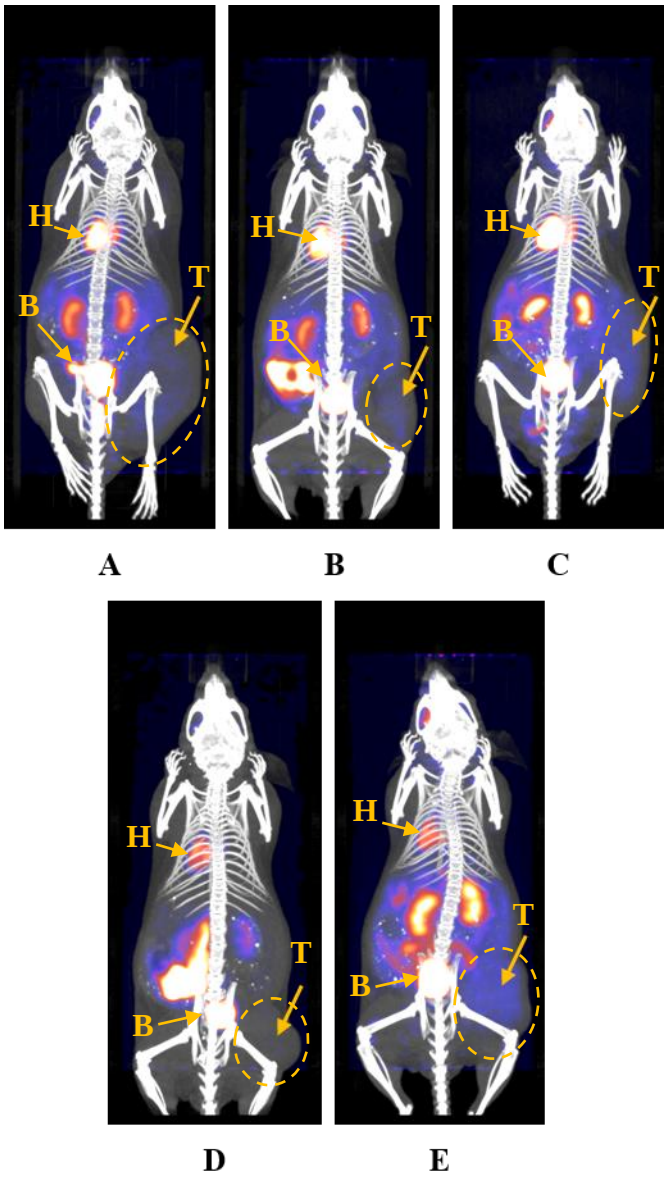

Figure 4.21: Representative images to show effects of treatments on tumour volume. Images were obtained by PET/CT scan and processed using Vivoquant software. T indicates position of tumour, H is the heart and B is the bladder. Yellow dotted line indicates area of tumour.

Key: A: Vehicle only control; B: 13cRA (53mg/kg); C: γT3 (80mg/kg); D: γT3 (80mg/kg) and 13cRA (53mg/kg); E: ABT-263 (100mg/kg) and 13cRA (53mg/kg).

4.2.2 Western blot (*in vivo*)

When compared to the no treatment group, the only significant change in protein expression was observed with an increase in caspase-9 for tumours treated with 13cRA only (Figures 4.22 and 4.23B).

MYCN protein bands were not observed from western blots (Figure 4.22).

Figure 4.23A shows an increase in p53 expression in all treatment groups, however, this was statistically not significant (p-value ranged from 0.7 to 0.9). Caspase-9 showed a slight reduction in protein expression for γT3 + 13cRA and ABT-263 and 13cRA groups, but this was not statistically significant (p=0.98 and p=0.95, respectively). Caspase-3 expression had the highest, but not statistically significant increase in the 13cRA only group (p=0.211) while the γT3 only and ABT-263+13cRA combination groups showed lesser and also statistically insignificant increases (p=0.464 and p=0.926, respectively) (Figures 4.22 and 4.23C). Slight increases in Bcl-xL expression was observed for all treatment groups (p-value ranging from 0.399 to 0.899) except ABT-263+13cRA combination, which had a slight decrease (p=0.980) and increase in Bcl-2 was observed in all treatment groups, with the γT3 + 13cRA group having the highest increase (p=0.268) (Figures 4.22, 4.23D and E); however, all changes in expression of both proteins was not statistically significant (Figures 4.23D and E).

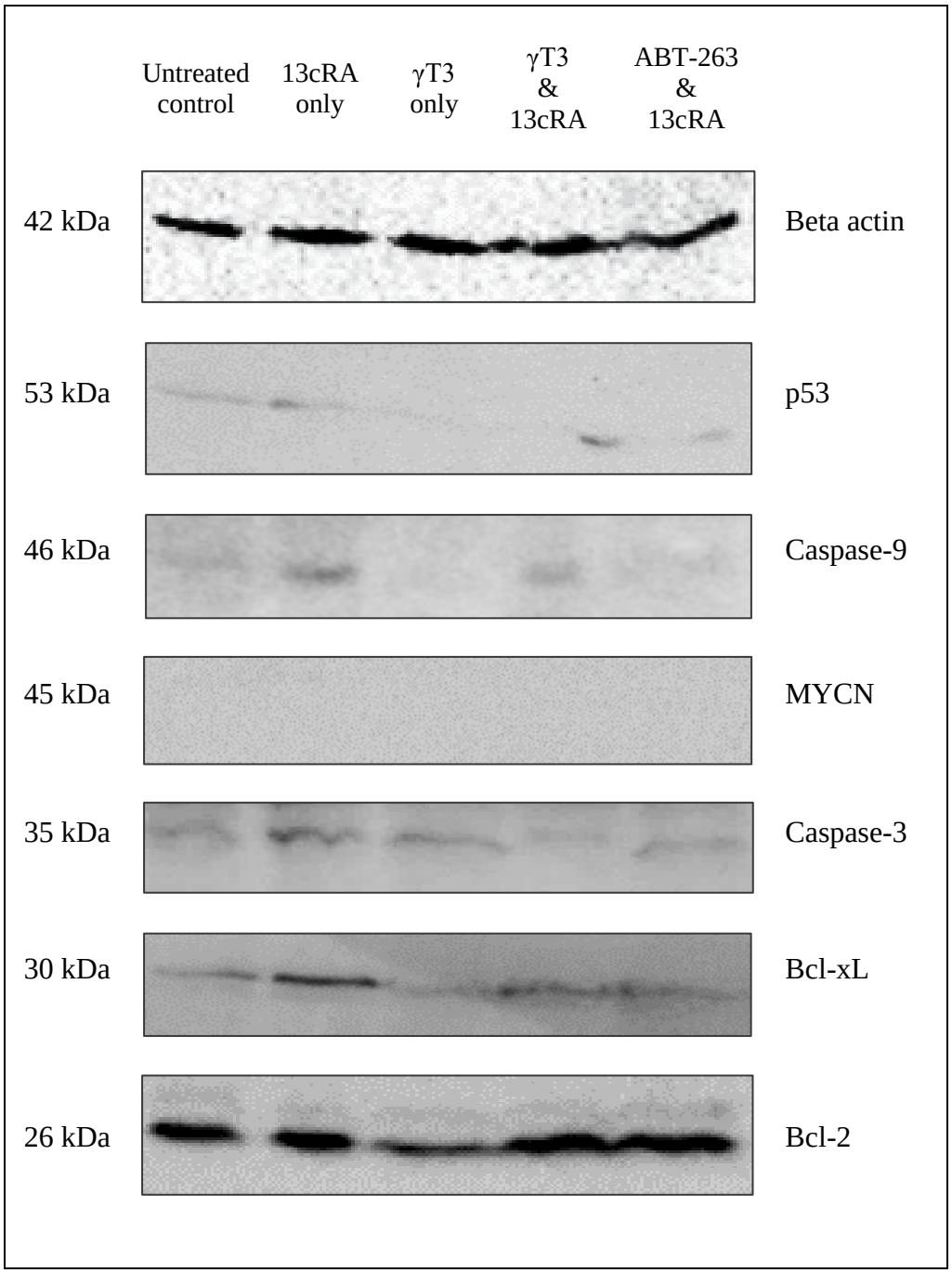

Figure 4.22: Effect of 13cRA and γT3, alone and in combination, and ABT-263 in combination with 13cRA, compared to vehicle only control on protein expression of Bcl-2, Bcl-xL, caspases-3 and -9, MYCN and p53 in ectopic tumours grown in nude mice from an SH-SY5Y neuroblastoma cell line. Beta actin was used as the loading control, and results are representative of three independent experiments.

A

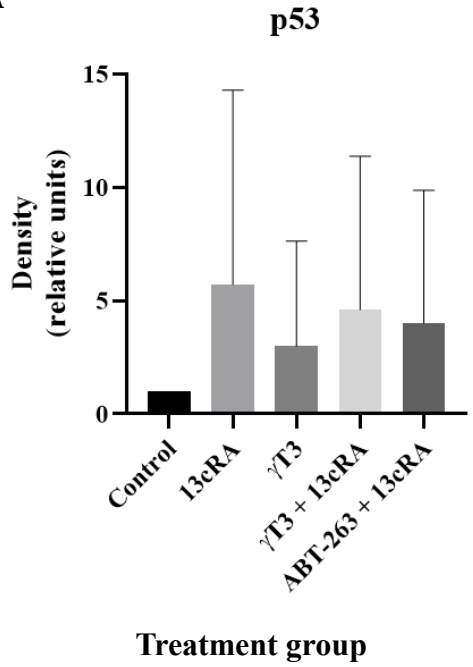

B

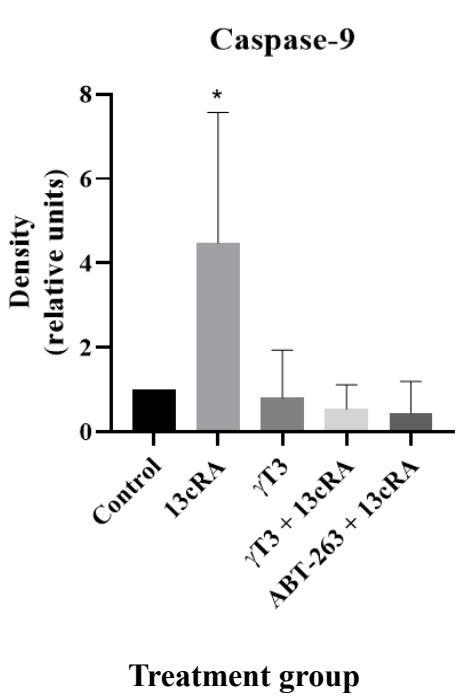

Continued…

C

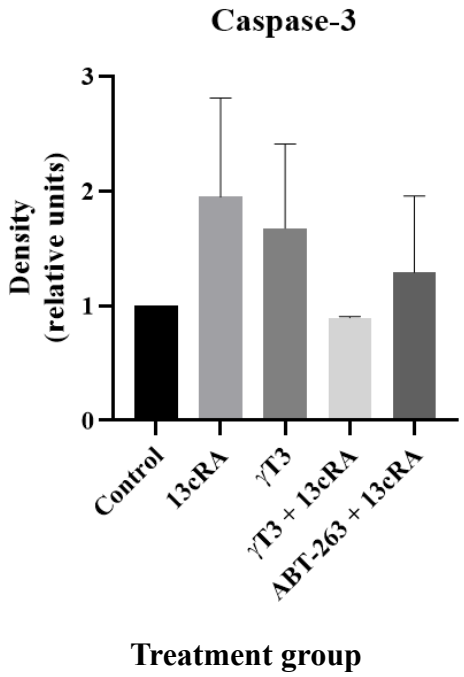

D

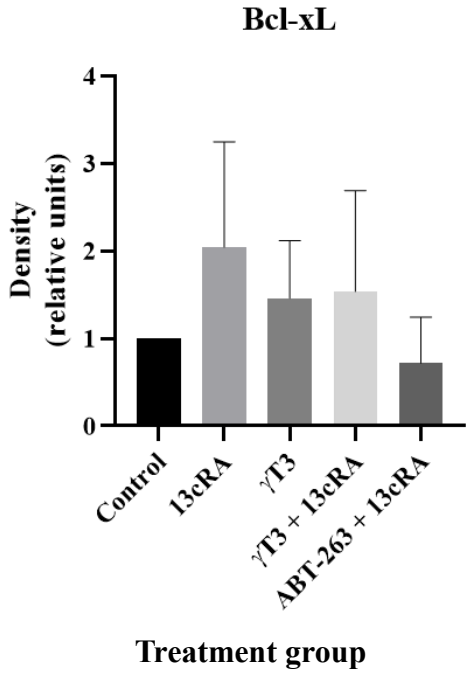

Continued…

E

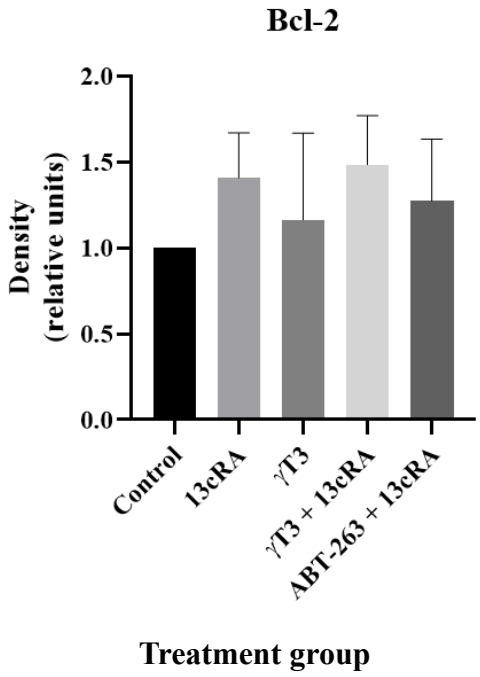

Figure 4.23: Comparison of relative density profiles obtained from western blot protein bands as seen in Figure 4.22 of A) p53, B) caspase-9, C) caspase-3, D), Bcl-xL, and E) Bcl-2. Results are represented as mean ± SD from three biological replicates and significance between treated and untreated was set at $p \leq 0.05$; $*p \leq 0.05$ with CI= 95%.

CHAPTER 5 DISCUSSION

Our hypothesis, as mentioned in the introduction, is that γT3 has significant anti-tumour effects on neuroblastoma, and one possible mechanism is by binding to the Bcl-2 protein to initiate the intrinsic apoptosis cascade. We also hypothesised that the combination drug treatment of γT3 together with 13cRA will demonstrate a synergistic effect.

In order to investigate our hypothesis, we carried out experiments to determine effects of γT3 on cell viability and death in SH-SY5Y and SK-N-BE(2) cell lines, and used the obtained IC_{50} values to calculate the combination index (CI) in order to determine if the combinations were synergistic. ABT-263 was also used as we wanted to compare the theorised Bcl-2 inhibitory action of γT3 to a known selective Bcl-2 inhibitor. Additionally, cytotoxicity was evaluated using the LDH assay.

To investigate apoptotic action of γT3, we carried out *in vitro* flow cytometry experiments with Annexin V-FITC/PI staining as well as protein investigations with western blot, using *in vitro* and *in vivo* samples. The *in vivo* protein samples themselves were extracted from ectopic tumours grown in nude mice, treated with individual or combination treatments of 13cRA, γT3 or ABT-263. Tumour growth was monitored using callipers and PET scan in order to ascertain anti-tumour effects of γT3.

5.1 EFFECTS ON NEUROBLASTOMA CELL LINES

5.1.1 Gamma-tocotrienol as an individual agent

So far, several studies have investigated the anti-cancer properties of γT3, although not in neuroblastoma. Instead, studies have primarily focused on using tocotrienols to treat the most common cancers such as breast, prostate and liver (Sailo *et al.*, 2018; Aggarwal *et al.*, 2019), although one study, by Tan *et al.* (2016) has shown a potential mechanism of action of γT3 in neuroblastoma. Few CNS cancers have been studied with tocotrienols, although tocotrienols have been shown to cause apoptosis in glioblastoma (Lim *et al.*, 2014; Abubakar *et al.*, 2017). Tocotrienols have been found to have many targets including, but not limited to inflammatory cytokines, enzymes such as COX-2, transcriptional factors such as PPAR-γ and anti-apoptotic proteins such as Bcl-2 and Bcl-xL (Kannappan *et al.*, 2012).

This study investigated the effects of γT3 and 13cRA as individual treatments, in the SH-SY5Y and SK-N-BE(2) cell lines. SH-SY5Y, with its single copy of *MYCN*, was chosen to represent lower risk stages of neuroblastoma, while SK-N-BE(2) represents the high risk group of neuroblastoma patients, as *MYCN* is amplified (over 100 copies) (Baj & Tongiorgi, 2009).

The IC_{50} value of 20μM γT3 in SH-SY5Y cells (Figures 4.2 and 4.7) is the same as that found in the study by Tan *et al.*, (2016). The results also show that γT3 has an earlier effect on SH-SY5Y cells than SK-N-BE(2) cells (Figure 4.2), as cell viability begins to drop at 0.975μM (c.f. ≥5μM in SK-N-BE(2) cells). The IC_{50} value of γT3 in SK-N-BE(2) cells is 26μM (Figures 4.2 and 4.8).

The higher concentrations required to treat SK-N-BE(2) cell lines compared to SH-SY5Y is not completely unexpected, due to the *MYCN* amplification in SK-N-BE(2) cells, which is well documented as a cause of resistance to therapy in high-risk neuroblastoma (Matthay *et al.*, 1999), compared to a cell line such as SH-SY5Y, which only has a single copy *MYCN*. Nevertheless, these results show that γT3 is able to reduce cell viability in a concentration dependent manner in both cell lines. This confirms findings with the SH-SY5Y cell line from a previous study (Tan *et al.*, 2016) and gives new information about its effects on a resistant neuroblastoma cell line, SK-N-BE(2). The dose dependent reduction in cell viability also adds to our knowledge about the action of γT3 in cancer cell lines, as it is similar to observations in A549 human lung adenocarcinoma and U87MG glioblastoma cell lines (Lim *et al.*, 2014; Abubakar *et al.*, 2017).

Cell lines showed a viability of over 100% when treated with only 13cRA, until approximately 20μM, when viability reduced in a dose dependent manner (Figure 4.1). The increase in cell viability at low doses can be attributed to the known effect of 13cRA to differentiate cancer cells, where changes in apoptosis signalling in the cells in order to ensure viability have been observed, such as increase in p53 or increases in Bcl-2 family expression in SH-SY5Y cells treated with low doses of 13cRA (Waetzig *et al.*, 2019; Hadjidaniel & Reynolds, 2010).

The current high dose, pulsed frequency of 13cRA administration for the maintenance stage of high risk neuroblastoma was based on studies to provide optimal 13cRA plasma levels while limiting dose-dependent side effects such as mucocutaneous toxicity, skin dryness and cheilitis (Reynolds *et al.*, 2003;

Matthay, 2013). Unfortunately, while initial trial results showed that 13cRA was a beneficial adjuvant therapy in high risk neuroblastoma (46±6% patients with event free survival rate, 3 years post randomisation vs 29±5% patients without, p=0.027) (Matthay *et al.*, 1999), a follow up study showed that the 5 year event free survival rate for those patients who received the 13cRA intervention was not statistically significant against the placebo group (p=0.1219) even though the survival rate of the treatment group was still higher than the placebo group (Matthay *et al.*, 2009). Furthermore, it is well documented that high risk neuroblastoma with MYCN amplification is prone to developing treatment resistance (Canete *et al.*, 2009; Cohn *et al.*, 2009; Yalçin *et al.*, 2013).

5.1.2 Synergy with other treatments

As the current dosing schedule of 13cRA is limited by toxicity, it is necessary to explore ways of improving the efficacy of 13cRA without compromising the safety of patients. Many other cancers have developed resistance to drug therapy, and one approach to overcome this barrier is by administering a multi-target drug, or administering a combination of treatments that will affect multiple targets (Cole & Maris, 2012; Lu *et al.*, 2012). Another is by identifying drug combinations that are synergistic, where the effects of lower, usually sub-optimal doses of two drugs are amplified when combined (Han *et al.*, 2017).

Past studies have shown the synergistic effects of tocotrienols were combined with other drugs. Synergy was demonstrated with TRF and tamoxifen in MCF7 and MDA-MB-435 breast cancer cells (Nesaretnam *et al.*, 2010), γT3 and a plant extract, hydroxyl-chavicol in several glioma cell lines (Abdul Rahman *et al.*, 2014), and γT3 and another plant extract, jerantinine A in U87MG glioblastoma

cells (Abubakar *et al.*, 2017). Based on available evidence, we assessed the effects of combining γT3 and 13cRA (and ABT-263 and 13cRA) to treat SH-SY5Y and SK-N-BE(2) cell lines for synergy.

Compared to individual treatments with 13cRA and γT3, the results of the combination treatments show a much larger difference when comparing both cell lines. When 8.5μM γT3 was added to 13cRA in the SH-SY5Y cell line, the IC_{50} of 13cRA dropped by 74% from 39μM (Figures 4.4 and 4.7), while addition of 12.5μM γT3 was added to 13cRA in the SK-N-BE(2) cell line, the IC_{50} of 13cRA dropped by a lower degree, by only 23% from 39μM (Figures 4.4 and 4.8). Addition of 15μM of 13cRA to γT3 caused a 90% reduction of γT3 IC_{50} in the SH-SY5Y cell line (Figures 4.5 and 4.7) while addition of 20μM 13cRA to the SK-N-BE(2) cell line caused γT3 to drop by 53% (Figures 4.5 and 4.8).

Additionally, in Figure 4.4, the SK-N-BE(2) cell line appears to increase in cell viability much more than the SH-SY5Y cell line, where there is an almost immediate dose-dependent drop upon initiation of combination treatment. Although SK-N-BE(2) cell viability remains below 100% at higher dose than 10μM, it does not substantially drop until above 20μM and the reduction is not significant until 40μM. In Figure 4.5, there is once again a large rise to almost 150% in cell viability for the SK-N-BE(2) cell line at the 0μM γT3 with 20μM 13cRA treatment point, compared to the rise to only about 110% SH-SY5Y cell line when exposed to 0μM γT3 combined with 15μM 13cRA. Cell viability in the SK-N-BE(2) cell line reduces below 100% at a point between 5μM and 7.5μM (with added 20μM 13cRA), which follows a similar pattern as seen in

Figure 4.4 where SK-N-BE(2) cell viability only dropped below 100% at the 20μM 13cRA point (with added 12.5μM γT3).

As 13cRA and γT3 both have different targets (Waetzig *et al.*, 2019; Tan *et al.*, 2016), it is possible that the reduction in IC_{50} when cells were exposed to a combination treatment compared to individual treatment is simply due to the fact that the treatment was affecting multiple targets. As a comparison, ABT-737, an early generation Bcl-2 inhibitor, was able to antagonise the protective effects of low dose 13cRA in pre-treated SMS-KCNR neuroblastoma cells, and re-sensitise the cells respond to treatment with the cytotoxic agent etoposide, resulting in increased apoptosis (from 8% to 52%) (Hadjidaniel & Reynolds, 2010). ABT-737 is much more specific than γT3 (van Delft *et al.*, 2006; Kannappan *et al.*, 2012), and so potentially, there might also be pathways other than just Bcl-2 interacting in this combination treatment. An alternative reason for this observation is that the combination was synergistic.

In order to obtain CI results from the software, average cell viability percentage of each concentration in the individual and combination treatment assays (Figures 4.1 to 4.6) was keyed into Compusyn software (Chou, 2006). According to the Chou-Talalay method for drug combination (Chou, 2010), a synergistic effect is seen when combination index (CI) is calculated at less than 1. CI larger than 1, indicates antagonism and a CI equal to indicates an additive effect.

From the results calculated by the software, there is strong synergy between 8.5μM γT3 and 5μM 13cRA in the SH-SY5Y cell line, CI=0.445, while in the SK-N-BE(2) cell line, 12.5μM γT3 and 10μM 13cRA slightly higher doses are required for synergy (Table 4.3). This data was obtained from the cell viability

results in Figures 4.1, 4.2 and 4.4. We also performed the CI calculation based on data from Figures 4.1, 4.2 and 4.5. Table 4.2 shows synergy between 15μM 13cRA and 0.975μM γT3 in the SH-SY5Y cell lines (CI=0.091) as well as between 20μM 13cRA and 7.5μM γT3 in the SK-N-BE(2) cell line (CI=0.239).

For comparison, we were also interested in the CI value between 13cRA and the selective Bcl-2 inhibitor, ABT-263. Using cell viability results from Figures 4.1, 4.3 and 4.6, we found synergy at 19.5μM ABT-263 and 10μM 13cRA in SH-SY5Y and SK-N-BE(2) cell lines (CI=0.230 and CI=0.472 respectively).

From these results, it is clear that the combination of γT3 and 13cRA is synergistic. Furthermore, despite the non-significant reduction in cell viability, the addition of ABT-263 to 13cRA is also synergistic. Similarities between the mechanism of action of γT3 and ABT-263 have been observed, as they have both been shown to bind to the Bcl-2 protein (Tan *et al.*, 2016; Tse *et al.*, 2008).

According to *in vitro* results published by Reynolds *et al.*, (2003), 5 to 10μM 13cRA therapy over 2 weeks is sufficient to show sustained growth arrest in neuroblastoma cell lines without toxicity. This was the *in vitro* work that lead to the currently prescribed high dose, pulsed frequency of 13cRA therapy as maintenance in high risk neuroblastoma (Matthay, 2013). However, that alone is still prone to treatment failure and recurrent disease, and clinically, does not show a statistically significant improvement in 5 year survival rate (Yalçin *et al.*, 2013).

A synergistic effect was observed by the addition of 12.5μM γT3 to 10μM 13cRA in the MYCN amplified cell line, SK-N-BE(2), which was chosen as the model for high risk neuroblastoma. This a similar level of 13cRA that was found

to be ideal for sustained growth arrest, with as little side effects as possible (Reynolds *et al.*, 2003). Furthermore, this dose of γT3 is well below what has been found to be toxic to normal cells, as only doses above 100μM were found to be neurotoxic in primary cultures of cerebellar neurons from rats (Then *et al.*, 2009).

In our cell viability assays, the dose of only 10μM 13cRA in SK-N-BE(2) cell lines did not decrease cell viability, but rather increased it to well above 100% (Figure 4.1), and in combination, there was still no significant dose dependent reduction in cell viability until 13cRA reached 40μM (Figure 4.4). However, as previously discussed, the SK-N-BE(2) cell line is overall more resistant to treatment than the SH-SY5Y, and while the dose reduction at concentrations of more than 10μM 13cRA with combined γT3 did not significantly reduce the cell viability, it did prevent cell viability rising above 100%.

Low dose 13cRA is commonly used to differentiate cancer cell lines, which is the principle behind the usage of 13-cis retinoic acid as an adjuvant treatment (Reynolds *et al.*, 2003). Unfortunately, as this is only effective in about 50% of high risk neuroblastoma patients (Matthay *et al.*, 2009), this approach needs to be improved. With the addition of a non-toxic dose of γT3 to 10μM 13cRA in SK-N-BE(2) cells, cell viability dropped below 100% (Figure 4.4), unlike in the individual treatment where cell viability at the 10μM 13cRA treatment point remained at nearly 120% and only dropped below 100% at more than twice the dose. This finding, if replicated in a clinical setting, can potentially enhance the potency of 13cRA adjuvant treatment in high risk neuroblastoma without the additional side effects that come with increasing the dose.

In addition to this potential benefit to 13cRA treatment in high risk neuroblastoma adjuvant therapy, these observations add weight to the evidence that γT3 can act synergistically with other drugs. This is important, as when drug combinations are synergistic, lower concentrations of drugs would be needed, meaning enhanced action but with less risk of dose-dependent toxicity. Furthermore, as anti-cancer therapies work more effectively when targeting multiple mechanisms, this is a logical approach to improving the efficacy of high risk neuroblastoma adjuvant therapy (Sylvester, 2012).

5.2 MECHANISM OF ACTION

The Bcl-2 protein family is made up of over 20 proteins that are responsible for regulating the intrinsic apoptosis pathway. Their functions can be broadly split into 3 groups: BH3-only proteins, pro-survival proteins and pro-apoptosis proteins. The BH3-only proteins are either responsible for directly activating pro-apoptotic proteins, or neutralising pro-survival Bcl-2 family proteins; i.e. the BH3-family proteins work towards initiating apoptosis. If there were an excess of pro-survival Bcl-2 family proteins, then apoptosis, or natural cell death, would be hindered (Ashkenazi *et al.*, 2017).

Deregulation of Bcl-2, either by amplification of the *BCL2* gene or overexpression of pro-survival Bcl-2 protein family members, such as Bcl-2 and Bcl-xL, has been linked to cancers as diverse as breast cancer (Schott *et al.*, 1995), large B cell lymphoma (Monni *et al.*, 1997), small lung carcinoma (Olejniczak *et al.*, 2007), and of course, neuroblastoma (Dole *et al.*, 1995; Tanos *et al.*, 2016). In all these cancers, the Bcl-2 deregulation contributes directly or indirectly to the development of the initial cancer or to its resistance to treatment, or both. Delbridge *et al.*, (2016) reviewed small molecules that have been developed over the past 30 years with the Bcl-2 regulated apoptotic pathway (intrinsic pathway) as a target, with the aim to "directly activate apoptosis of malignant cells", and all these small molecules have been developed as BH3-mimetics. One of the most common actions of natural BH3-only proteins is to bind to pro-survival Bcl-2 proteins in order to neutralise them, and thus allow normal apoptosis to resume (Doerflinger, Glab & Puthalakath, 2015).

Tan *et al.*, (2016) concluded from evidence seen in their *in silico* docking analysis that γT3 binds to the hydrophobic groove of the pro-survival Bcl-2 protein, acting very much like a BH3-only protein. Therefore, an assessment of the action of γT3 should include an apoptosis assay. In their paper, the researchers showed, using the LDH assay, that γT3 significantly induced cell death compared to an untreated control ($p<0.05$). Additionally, they evaluated depolarised mitochondrial membrane potential (using JC-1 staining) and found a significant increase ($p<0.05$) in % cells containing green JC-1 monomer (an indication of apoptosis) between the no treatment control and SH-SY5Y cells treated with 15μM γT3 cells.

In this study, the potential of combination treatments of γT3 and 13cRA to cause apoptosis over individual treatments was investigated. Also, as our hypothesis is that γT3 acts on neuroblastoma cells by binding to the BH3 domain of the Bcl-2 protein to initiate the intrinsic apoptosis cascade (Tan *et al.*, 2016), a direct comparison with a Bcl-2 inhibitor was required. The Bcl-2 inhibitor ABT-263 was used as a comparison to γT3 due to a higher affinity to Bcl-2 than Bcl-X_L and Bcl-w compared to its predecessor, ABT-737 (Oltersdorf *et al.*, 2005; Tse *et al.*, 2008).

5.2.1 Gamma-tocotrienol and apoptosis

In the SH-SY5Y cell line, individual treatment with both 13cRA and γT3 lead to statistically significant increases in cytotoxicity at the highest doses of treatment, at 50μM ($p\leq0.001$) and 30μM ($p\leq0.01$), respectively (Figure 4.10). In the SK-N-BE(2) cell line, although sharp rises in cytotoxicity were seen at the

highest concentrations (30μM γT3 and 50μM 13cRA), these increases were not statistically significant (Figure 4.11).

Adding 15μM of 13cRA to γT3 in the SH-SY5Y cell line resulted in the first statistically significant increase in cytotoxicity, recorded at 7.5μM ($p \leq 0.05$), showing an obvious dose-dependent trend in cytotoxicity. The next two concentrations are also statistically significant: 15μM ($p \leq 0.01$) and 25μM ($p \leq 0.001$). A similar combination (20μM 13cRA added to γT3) in the SK-N-BE(2) cell line shows a similar dose-dependent trend, although there are no statistically significant changes in cytotoxicity (Figure 4.13).

The more significant response of the SH-SY5Y when compared to the SK-N-BE(2) cell lines in both individual and combination treatments mirrors that of the cell viability assay results discussed in Section 5.1. As previously stated, the SK-N-BE(2) cell line is known to be more resistant to treatment due to its overexpression of the *MYCN* gene, while SH-SY5Y has only a single copy of *MYCN* and is therefore much more susceptible to treatment (Baj & Tongiorgi, 2009).

The lactate dehydrogenase (LDH) assay was performed on *in vitro* cell cultures: SH-SY5Y and SK-N-BE(2). The LDH assay measures LDH activity in the supernatant, or leakage of LDH from the cell into the culture medium, which then reacts with the assay reagents to form a red formazan product which can be measured, as the amount of formazan is directly correlated to the amount of LDH released because of cell membrane damage, which indicates irreversible cell death (Fotakis & Timbrell, 2006). While the MTS assay only measures changes

in overall cell proliferation, the LDH assay is able to differentiate between cell cycle inhibition and cell death (Smith *et al.*, 2011).

Compared to cell viability results, the cell cytotoxicity (cell death) results show a sudden spike in cytotoxicity at higher concentrations, as opposed to the more gradual decline in cell viability seen in the MTS assay. It should be noted that the LDH assay can be considered to be a measure of the extent of plasma membrane breakdown (a sign of cell death), as LDH is normally confined to the inside of the cell (Fotakis & Timbrell, 2006; Galluzzi *et al.*, 2009) while the MTS assay for cell viability measures metabolically active cells, by measuring the amount of formazan formed by conversion of the tetrazolium compound using NADPH or NADH (Promega, 2012). However, these metabolic alterations might be caused by factors other than cell death (Galluzzi *et al.*, 2009). Thus, it is possible that while cell cycle inhibition occurred at lower drug concentrations and was detected with the MTS assay, the cell plasma membrane did not break down sufficiently to release LDH and cause irreversible cell death until higher drug doses were administered to the cells.

Interestingly, when γT3 was added to 13cRA (8.5μM in the SH-SY5Y and 12.5μM in the SK-N-BE(2) cell lines), instead of a dose-dependent increase in cytotoxicity, the cells started at a heightened level of cytotoxicity (when exposed to either 8.5μM or 12.5μM γT3 only) and stayed mostly at that same level as the dose of 13cRA increased (Figures 4.12 and 4.13). In the SH-SY5Y cell line, the cells were mostly at about 75% cytotoxicity throughout, while in the SK-N-BE(2) cell line, the cells stayed level at about 30% cytotoxicity.

This observation might be explained by other parameters not covered by the LDH assay (and might be answered if another cytotoxic assay, e.g. neutral red) was also used to confirm), as the equivalent γT3 dose in the individual cytotoxicity assays did not show a similar rise in cytotoxicity (Figures 4.10 and 4.11). In the SK-N-BE(2) cell line (Figure 4.11), there is no statistically significant change, although cytotoxicity levels do drop very slightly when 13cRA is added at low concentration, before rising again at the highest dose, 40μM. This somewhat ties in with the MTS assay results seen in Figure 4.4, where the same treatment group and cell line showed increase in cell viability at low doses of 13cRA (with added 12.5μM γT3) before dropping as the 13cRA concentration increased.

5.2.2 Flow cytometry

While the LDH assay, along with the MTS assay are acceptable as preliminary screening assays in order to evaluate the anti-cancer effects of γT3 on neuroblastoma cells, a more specific apoptosis assay was required in order to specifically determine how γT3 (individually and in combination) caused cell death. Based on the evidence of past work, as discussed earlier, we hypothesised that one possible mechanism of γT3 was apoptosis.

Annexin V-FITC/PI and flow cytometry was used to assess the degree of apoptosis in both cell lines after either individual or combination treatments. Annexin V is a protein that binds preferentially to phosphatidylserine (PS), which is usually expressed on the inner surface of the plasma membrane, but in early apoptosis, is exposed to the outer surface, although the plasma membrane

is still intact. FITC is a fluorochrome attached to Annexin V that allows the detection and quantification of the Annexin V. PI only stains nucleic acids of dead cells with compromised cell membranes as intact cell membranes exclude it (Riccardi & Nicoletti, 2006; Wilkins, Kutzner, Truong, Sanchez-Dardon, & McLean, 2002). Thus, unlike the LDH assay which quantifies LDH released from cells where the membrane is damaged, Annexin V-FITC can differentiate between different stages of cell death.

We measured and then compared the apoptotic changes of the plasma membrane of treated to untreated SH-SY5Y and SK-N-BE(2) cells after staining with Annexin V-FITC/PI and analysis with the flow cytometer. There was only one statistically significant change in number of cells (Figure 4.15B: ABT263 combination group had a significant increase compared to control). This could be due to a large variability in values within each group between repeats. Despite the lack of statistical significance, there was still a visible qualitative shift in cell populations when comparing the no treatment control cells to treatment cell populations, which will be discussed.

While generally, treatment groups for both the SK-N-BE(2) and the SH-SY5Y cell lines showed a shift in the cell population towards apoptosis, the overall shift in cell population for all treatment groups was far less drastic in SK-N-BE(2) cells compared to SH-SY5Y. The results here echo those of the cell viability and cell cytotoxicity assays, where IC50 of γT3 in SH-SY5Y cells was lower than in SK-N-BE(2) cells (20μM vs 26μM). Additionally, the amount of cells undergoing late apoptosis in the individual 13cRA and γT3 treatment groups was very similar to that of the no treatment control group, unlike in the SH-SY5Y

cell line (Figure 4.14 A and B) where about twice as many late apoptotic cells as viable cells are visible. In the cell viability assays, especially in combination treatment, the SH-SY5Y cell lines were far more responsive to treatment than SK-N-BE(2) cells (Figures 4.4 and 4.5), and the same can be said of the cell cytotoxicity results, where treatments were more cytotoxic in SH-SY5Y cells than SK-N-BE(2) cells (Figures 4.10 to 4.13). The overall lesser response of SK-N-BE(2) cells to treatment compared to SH-SY5Y cells can be easily explained by the treatment resistance that is common in cells with amplified MYCN expression, which is a feature of the SK-N-BE(2) cells. As the SK-N-BE(2) cell line was selected as a model for high risk neuroblastoma, the observations here are supported by literature and clinical observations that high risk neuroblastoma has more treatment resistance than lower risk groups of neuroblastoma (Baj & Tongiorgi, 2009; Park et al., 2013).

When comparing the no treatment control cells to the five treatment groups in Figure 4.14A, there is a visible increase in the number of double- and PI-only stained SH-SY5Y cells, which indicates late apoptotic and necrotic cell death, respectively, with the exception of the 13cRA only group. Interestingly, in the SK-N-BE(2) cell line, 13cRA showed a slight, although not statistically significant increase in apoptotic cells compared to control. However the percentage of cells undergoing necrosis in the SK-N-BE(2) cell line was very low – the highest was just over 1% (Figure 4.15B) while in SH-SY5Y cells, the highest was around 5% (Figure 4.14B).

These observations could be attributed to the fact that the dose of 13cRA used here was well below its IC50, according to our cell viability assay, and low dose

13cRA has been shown to augment survival signalling in SH-SY5Y cell lines (Waetzig et al., 2019) and even antagonise the action of cytotoxic drugs such as etoposide (Hadjidaniel & Reynolds, 2010) in SH-SY5Y cell lines. In a TUNEL assay, (which assesses proportion of cells with sub-G1 DNA content in response to treatment, as a measure of apoptotic cell death), addition of 13cRA to a cell population treated with etoposide reduced apoptosis from 68% to 4.5% (Hadjidaniel & Reynolds, 2010), while Waetzig et al., (2019) found that cell viability was increased due to reduction in p53 protein levels in SH-SY5Y cells after treatment with low dose 13cRA. While the SK-N-BE(2) cell line is less commonly studied than the SH-SY5Y cell line, a study investigating the effect of ATRA on SK-N-BE(2) and SH-SY5Y cells by analysing morphological changes and cell cycle, found that low dose (10μM) caused more differentiation in SK-N-BE(2) cells than in SH-SY5Y cells (Redova et al., 2010). In a study investigating the role of *MYCN* in neuroblastoma cell differentiation, researchers found that overexpressing *MYCN* in a normally poorly differentiating neuroblastoma cell line, SK-N-AS, increased number of cells with neurite outgrowth (measure of differentiation) by approximately 90% compared to wild type, single copy *MYCN* cells after exposure to 10μM ATRA (Guglielmi et al., 2014). The *MYCN* overexpression of the single copy *MYCN* SK-N-AS cell line mimics that of the SK-N-BE(2) and SH-SY5Y cell lines used here, respectively. They also showed, using BrdU/PI staining and flow cytometry, that after treatment with ATRA, more LAN-5 neuroblastoma cells (overexpressed *MYCN*) were arrested in the G0/G1 phase of the cell cycle (indicating differentiation) than control cells (71.5% vs 50.4%). These observations are also supported by the cell viability data in Figure 4.1, where there is a significant increase in cell

viability of SH-SY5Y and SK-N-BE(2) cells to over 100% at low doses of 13cRA (<10μM). Additionally, from the slope of the curve, cell viability continues to remain above 100% in SH-SY5Y and SK-N-BE(2) up till approximately 20 and 25μM, respectively, which means the sub-optimal doses of 13cRA used here (15μM and 20μM) was within the dose range where cell viability was higher than no treatment control cells.

Compared to the other treatment groups, there were more Annexin V stained cells, i.e. apoptotic cells, in both the γT3 individual and combination treatment groups in the SH-SY5Y cell line (Figures 4.14A and B) and in the SK-N-BE(2) cell line, there were more apoptotic cells in the γT3 combination treatment group than the other groups apart from ABT-263 (Figures 4.15A and B). There were also more necrotic cells in the PI positive quadrant (necrosis) of the γT3 treatment groups in the SH-SY5Y cells than in the other groups Figure 4.14B).

Tocotrienols, and specifically γT3, have been shown to cause apoptosis in other cancer cell lines, as well as the SH-SY5Y cell line. In a mitochondrial membrane potential measurement, a significant increase ($p<0.05$) in % cells containing green JC-1 monomer (an indication of apoptosis) was seen in SH-SY5Y cells treated with 15μM γT3 compared to the no treatment control (Tan et al., 2016). In another study, using Annexin V-FITC/PI, Abdul Rahman et al., (2014) found significantly more ($p<0.05$) SW1783 and LN18 glioma cells in early apoptosis when treated with γT3 compared to no treatment control. Additionally, they found a significant increase ($p<0.05$) in necrotic cells for the γT3 treatment group in the SW1783 cells compared to the control. In another study on the effect of γT3 on cancer cells, 67.7% ($p<0.001$) of U87MG glioblastoma cells showed

induction of G0/G1 cell cycle arrest (apoptosis) after treatment with γT3 for 24 hours, compared to control treatment (Abubakar, Lim, Kam, & Loh, 2017).

This study therefore reflects previous work on the apoptotic effect of γT3. 13cRA alone, especially at a low dose did not lead to apoptosis compared to γT3 alone or in combination (Figures 4.14 and 4.15). The fact that the γT3 combination group had a higher number of cells in the apoptosis stages than individual 13cRA and γT3 groups in both cell lines (Figures 4.14 and 4.15) is encouraging, as it lends support to the idea of enhancing the effects of 13cRA without increasing the dose, and with it, the side effects, by adding a low dose of γT3, many times lower than levels known to be toxic (Then, Mazlan, Mat Top, & Wan Ngah, 2009).

There was also more apoptotic effect in the γT3 groups than in the ABT-263 individual and combination groups in the SH-SY5Y cell line (Figure 4.14B), while in the SK-N-BE(2) cell line, the ABT-263 combination group showed a significant increase in late apoptotic cells compared to control (Figure 4.15B). While the SH-SY5Y cell line is not a cell line normally associated to treatment resistance, it is, as discussed in Section 4.1, uniquely non-sensitive to specific Bcl-2 antagonists such as ABT-263, due to its relatively (compared to primary tumours) low level of Bcl-2 expression (Lamers et al., 2012). Thus, while other treatments showed a more drastic shift in SH-SY5Y cell populations towards the apoptotic quadrants (Figure 4.14A), both ABT-263 treatment groups had more muted responses. In the SK-N-BE(2) cell line, the ABT-263 groups had more apoptotic cells than in the γT3 groups (Figure 4.15B). Comparing this to the lower numbers of apoptotic cells for the ABT-263 groups against the γT3 groups

in the SH-SY5Y cell line, it highlights the insensitivity of the SH-SY5Y cell line to Bcl-2 antagonists such as ABT-263. This insensitivity will be examined at a later point in the discussion. Despite the specific insensitivity of SH-SY5Y to Bcl-2 antagonists, ABT-263 has been shown to cause apoptosis in neuroblastoma cells with PI staining and analysis by flow cytometry showing an increase in sub-G1 fraction compared to control (Lamers *et al.*, 2012).

From the observations made in this study, it is clear that γT3 causes cell death in both neuroblastoma cell lines. Furthermore, when used in combination with 13cRA, sub-optimal doses of both drugs can be used for a greater effect than when used individually, as seen in the cell cytotoxicity results. Based on the flow cytometry results, is not conclusive whether apoptosis is the definite mechanism of action of γT3 in neuroblastoma cells, due to statistical insignificance. However, using the observations here, as well as other studies (Abdul Rahman *et al.*, 2014; Tan *et al.*, 2016; Abubakar *et al.*, 2017), there is good evidence to indicate that apoptosis is at least one of the mechanisms used by γT3 to kill neuroblastoma cell lines, and this should be further studied in additional experiments for confirmation, using different assays and more variety of cell lines.

Although the experiments using Annexin V-FITC/PI and flow cytometry were used to confirm apoptosis as a possible mechanism of γT3 in neuroblastoma cell lines, that method would not give further details on the precise pathway involved. In order to do that, the effects of γT3 on protein expression were investigated, *in vitro* as well as *in vivo*.

The proteins of interest were chosen based on several factors, including past evidence that indicated that γT3 caused apoptosis in SH-SY5Y cell lines via the intrinsic apoptosis pathway, specifically as a BH3 mimetic that bound to the Bcl-2 anti-apoptosis protein (Tan *et al.*, 2016). Thus, we used Bcl-2 and caspases-9 and -3. The activation of caspase-3 by caspase-9 in the intrinsic pathway is considered the initiation of apoptosis (Würstle *et al.*, 2012). We also chose MYCN as its overexpression, and that of its gene, *MYCN*, is used as a clinical definition of high risk neuroblastoma (Cohn *et al.*, 2009). The p53 protein was chosen because p53 is known to activate apoptosis due to external stress, and be involved in regulation of various components of the apoptosis cascade (Aubrey *et al.*, 2018). Finally, Bcl-xL was used because ABT-263, used in this study as a Bcl-2 inhibitor, is also known to (to a lesser degree) affect the Bcl-xL protein (Mérino *et al.*, 2012).

In this investigation, the effects of γT3 and 13cRA, used alone and together, on those proteins, were assessed. Protein samples were obtained from both *in vitro* and *in vivo* sources and the changes or lack of changes were evaluated in order to further elucidate the mode of action of γT3 in neuroblastoma.

5.2.3 Expression of apoptosis proteins

5.2.3.1 MYCN

In this study, we compared the expression of MYCN protein in two cell lines, SH-SY5Y and SK-N-BE(2), after individual and combination treatments of 13cRA, γT3 and ABT-263. Like the study by Tan *et al.* (2016), we found that 24 hours treatment of γT3 reduced MYCN expression in SH-SY5Y cells

compared to control (Figure 4.17A). However, unlike that study, the reduction here was slight and not statistically significant. In the SK-N-BE(2) cell line, there was a slight, statistically insignificant increase in MYCN expression after treatment with γT3 individually or in combination with 13cRA (Figures 4.18 and 4.19A). Further study is required to determine if the difference in response is due to normal protein expression of cell lines, as these properties have been shown to significantly influence the response to treatments (Ham *et al.*, 2016; Lamers *et al.*, 2012).

We also found that 13cRA, unlike ATRA, does not increase MYCN expression in SH-SY5Y cells (Figures 4.16 and 4.17A), which was what was observed by Tan *et al.* (2016). The same lack of change in MYCN expression after 13cRA treatment was also observed in SK-N-BE(2) cells (Figures 4.18 and 4.19A). Current known actions of retinoic acids on MYCN expression in neuroblastoma cells seem to vary. In contrast to the findings by Tan *et al.* (2016), another study found that treating IMR-32 and Kelly neuroblastoma cells (both overexpress *MYCN*) with 100 nM ATRA for 6 days caused a visible drop in MYCN expression compared to no treatment control (Otsuka *et al.*, 2019). The main differences between the study by Tan *et al.* (2016) and Otsuka *et al.* (2019) is that the former used a higher dose, 10 μM (although this dose is still considered low) compared to 100 nM, over a shorter time (24 hours vs 6 days), and SH-SY5Y cells are non-MYCN amplified, unlike IMR-32 and Kelly cells.

SH-SY5Y cell lines showed a statistically significant drop in MYCN expression after 24 hours treatment with ABT-263 ($p \leq 0.05$), both as a single agent or in combination with 13cRA (Figure 4.17A). There was no corresponding literature

that studied the SH-SY5Y cell line and MYCN expression after treatment with a Bcl-2 inhibitor such as ABT-263, however, we can extrapolate from a study by Ham *et al.* (2016), where the SK-N-F1 neuroblastoma cell line, which possesses wild-type *MYCN*, as does SH-SY5Y, did not show any visible changes in MYCN protein expression after treatment with ABT-199, a Bcl-2 inhibitor, of which ABT-263 is a predecessor. Unfortunately, the significant reduction in MYCN expression due to ABT-263 treatment cannot be explained at this point and more studies are needed to further elucidate the mechanism.

In comparison, the *MYCN* amplified neuroblastoma cell line, SK-N-BE(2), used in our study did not show a notable change in MYCN expression after 24 hours treatment with ABT-263 (Figure 4.19A). This lack of change in MYCN expression in the SK-N-BE(2) cell line correlates with findings in the same study by Ham *et al.* (2016), which aimed to enhance the action of ABT-199 by combining it with other drugs. SK-N-BE(2) and other *MYCN*-amplified neuroblastoma cell lines were treated with ABT-199, but no significant changes in MYCN protein expression were observed with ABT-199 only treatment, although addition of other drugs with different targets did reduce MYCN levels. This would indicate that drugs that target Bcl-2 do not necessarily affect MYCN levels.

Unfortunately, the *in vivo* samples did not yield any results for analysis with traditional western blot. However, we sent one set of protein samples (five treatment groups, including control) for analysis with a Jess capillary protein assay (Appendix B). As this assay only used one biological repeat, we cannot fully rely on the results. However, it showed no large changes of MYCN

expression in all treatment groups compared to control, except γT3 only, which almost doubled (Table B2). Chapter 5.4 will discuss future work, including an outline for specific investigations involving MYCN expression.

5.2.3.2 Bcl-2

Bcl-2 was identified as a possible target of the vitamin E isomer, γT3 (Tan *et al.*, 2016). Using simulated docking analysis, the study found that γT3 binds to the hydrophobic groove of Bcl-2, and the researchers proposed that γT3 acts by binding to anti-apoptotic Bcl-2, which is highly expressed in many cancers and prevents natural cell death. Thus, the Bcl-2 protein, and its expression following treatment with γT3, was of great interest to this study.

In this study, Bcl-2 expression in SH-SY5Y cell lines after treatment with γT3, alone or combined with 13cRA did not change significantly when compared to control. The same observation was seen in the *in vivo* study, which used SH-SY5Y cell lines for ectopic tumour induction. This lack of change in Bcl-2 expression in the SH-SY5Y cell line was very similar to the observations in the study by Tan *et al.*, (2016). In that study, the researchers also found insignificant changes in Bcl-2 expression after treating SH-SY5Y cell lines for 24 hours in γT3 alone or combined with ATRA. The groups with added retinoic acid for both this and the study by Tan *et al.*, (2016) had very slightly higher Bcl-2 expression than the γT3 only groups. However, the study focused on the binding assay results, which showed that γT3 was able to bind preferentially to the BH3 domain in the Bcl-2 protein compared to αT3, and did not discuss the observations in Bcl-2 protein expression.

While there were no significant changes to Bcl-2 levels in the SH-SY5Y cell line, the ABT-263 alone and combined groups did appear to cause a non-significant drop in Bcl-2 expression compared to control. It is interesting to note that the *in vivo* study, which used the SH-SY5Y cell line to induce tumour growth, also showed an insignificant change, but it was a very slight increase of Bcl-2 expression in the ABT-263 with 13cRA group. However, these results are supported by observations in the study by Van Goethem *et al.* (2017), where treatment with the similarly Bcl-2-selective drug ABT-199 did not cause any downregulation to Bcl-2 protein abundance compared to vehicle control. In fact, the Bcl-2 protein expression of SH-SY5Y, treated or untreated, was very low compared to several other neuroblastoma cell lines, although higher than many cancer cell lines, evidence of which was shown by another study on Bcl-2 expression in neuroblastoma cell lines (Lamers *et al.*, 2012).

While the results in the SH-SY5Y cell line and tumours were all insignificant, the *in vitro* results of the SK-N-BE(2) cell line were not. Bcl-2 protein expression was significantly increased compared to control when cells were treated for 24 hours with γT3 and 13cRA ($p \leq 0.05$), ABT-263 alone ($p \leq 0.01$), and ABT-263 combined with 13cRA ($p \leq 0.01$). Bcl-2 after treatment with γT3 alone rose almost two times more than control, although this was insignificant, and 13cRA only treatment caused an also insignificant, but visible drop in Bcl-2 expression.

As previously mentioned, Bcl-2 has an anti-apoptotic role (Czabotar *et al.*, 2014), and neuroblastoma cell lines with increased *BCL2* expression were found to be resistant to common cytotoxic treatments (Dole *et al.*, 1994), while

silencing *BCL2* in neuroblastoma cell lines with high BCL2 expression lead to apoptosis (Lamers *et al.*, 2012).

A study by Lasorella *et al*., (1995) showed that when neuroblastoma cells are treated with low dose (5 μM) ATRA for 6 days, changes in cell Bcl-2 expression varies depending on specific cell line. The study showed that SH-SY5Y and SK-N-SH cells responded with a substantial increase in Bcl-2 expression compared to no treatment control, while SMS-KCNR had about half the increase of Bcl-2 compared to SH-SY5Y and SK-N-SH, and IMR-32 cells did not show a visible increase in Bcl-2 expression. While the first 3 cell lines showed evidence of differentiation after 6 days ATRA exposure, the IMR-32 cells did not differentiate.

In addition to being used as a differentiating agent, retinoic acid, and in particular, 13cRA, is a known cause of apoptosis in many cancer cell lines. For example, using cell cycle and DNA analysis experiments, Toma *et al.* (1997) showed that 13cRA was an effective apoptosis-inducing drug in MCF-7 and MDA-MB-231 breast cancer cell lines, with cell populations in DNA histograms of 13cRA-treated cells showing a reduction of G_1/G_2 cells in the cell population, compared to control. Treatment with 1 μM of 13cRA for 6 days also resulted in reduced Bcl-2 protein for 13cRA-treated MCF-7 cells compared to untreated when analysed by immunofluorescence flow cytometry. Reduced Bcl-2 is an indication of improved apoptosis.

In this study, the SK-N-BE(2) cell line was treated with 20 μM 13cRA over 24 hours, which is both a higher dose and a shorter treatment period than for the MCF-7 cells in the abovementioned study. The reduction of Bcl-2 protein

(Figure 4.19), while not statistically significant, was still more than half of the protein expression in the vehicle control, which points towards treatment with 13cRA alone demonstrating improved apoptosis in SK-N-BE(2), as shown in MCF-7 in the study by Toma *et al.* (1997).

However, following that logic, the statistically significant increase of Bcl-2 in SK-N-BE(2) after treatments with γT3 combination, and ABT-263, alone and in combination, indicate that these treatments inhibit apoptosis. However, as seen in the cytotoxicity experiments, these treatments clearly reduce cell proliferation and while not statistically significant, did demonstrate an increase in apoptotic cells from the flow cytometry experiments.

One factor that was not investigated in this study was the effect of these treatments on the protein expression of Bax. While a simple approach is to study only Bcl-2 protein expression, apoptosis is regulated by the interactions between the proteins, with Bcl-2 being anti-apoptotic and Bax pro-apoptotic. A change in the balance of both Bcl-2 and Bax can affect cell apoptosis. Bax is involved in the formation of channels in the mitochondrial membrane to allow cytochrome c release when apoptosis is triggered; however, this can be inhibited by overexpression of Bcl-2 (Teijido & Dejean, 2010). So, further studies should also investigate Bax protein expression. While the study by (Tan *et al.*, 2016) did not show any conclusive effects on Bax protein expression after treatment of γT3 combined with retinoic acid, their retinoic acid of choice was ATRA, which has been shown to have different effects compared to the other commonly used isomer, 13cRA (Reynolds *et al.*, 2003). Additionally, they only used SH-SY5Y cell lines, and as has been demonstrated here, as well as in published studies

(Lamers *et al.*, 2012; Ham *et al.*, 2016; Goldsmith *et al.*, 2012) the choice of neuroblastoma cell line can vastly change treatment responses.

An explanation for the statistically significant increased Bcl-2 expression after γT3 combination and ABT-263 single and combination treatment groups in the SK-N-BE(2) cell line is still unclear. However, binding of γT3 to the hydrophobic groove in the Bcl-2 protein was shown by *in silico* docking, and therefore further studies using a greater diversity of cell lines and further protein studies are necessary in order to comprehensively investigate the action of γT3 in neuroblastoma.

5.2.3.3 Other apoptosis proteins

We evaluated protein expression levels in the tumour samples obtained from the *in vivo* study to investigate the hypothesised apoptosis caused by γT3. The proteins we chose to study were all proteins associated with apoptosis, in addition to Bcl-2, which was discussed in the previous section. The proteins discussed in this section are: p53, caspases-9 and -3 and Bcl-xL.

Results from protein extracted from tumour samples showed only one statistically significant change in protein expression: caspase-9 in the 13cRA treatment group, $p \leq 0.05$ (Figures 4.22 and 4.23B). The other *in vivo* protein expression results were not significant, however those findings will nevertheless still be discussed in this section.

Caspase-9 is part of a group of molecules known as “initiator caspases”, known as such because they activate the “effector caspases”, such as caspase-3, which

are directly responsible for morphological and biochemical changes that occur during apoptosis (Würstle *et al.*, 2012). Precursor caspase-9 exists as a 46kDa protein, which is activated when Apaf-1 oligomerises (with cytochrome c and dATP) to form a large apoptosome complex. At the apoptosome complex, the activated caspase-9 activates procaspase-3, which goes on to execute apoptotic cell death. When caspase-9 dissociates from the apoptosome, it is deactivated (Kuida, 2000; Fesik, 2005; Würstle *et al*., 2012). In short, release of caspase-3 is an indicator of the initiation of apoptosis, and activated caspase-9 is required in order to activate caspase-3. In this study, we observed the protein expressions of caspases-9 and -3 as markers of apoptosis. Both are common proteins used in apoptosis studies.

In a study that used LA1-55n and SH-SY5Y neuroblastoma cells to examine the ability of the small molecule tolfenamic acid to improve the action of 13cRA on neuroblastoma, 20 μM of 13cRA alone was shown to cause significant caspase-3 and -7 activation ($p<0.05$), when tested with a Caspase-Glo 3/7 kit (Shelake *et al.*, 2015). As previously mentioned, caspase-3 is a downstream or effector caspase, activated by caspase-9. Release of caspase-3 is an indicator of the initiation of apoptosis, and activated caspase-9 is required in order to activate caspase-3 (Fesik, 2005; Würstle *et al.*, 2012). The same study also used Annexin V-PE/7-AAD to investigate apoptosis in both cell lines, and found that addition of 13cRA caused a shift of the LA1-55n cell population from viable to late apoptosis (14.2% in 13cRA treated cells vs 3.2% in control cells).

In comparison, although the 13cRA treatment group tumour samples in this study showed nearly 6 times more caspase-9 protein compared to control

($p \leq 0.05$), there was also a slightly elevated, although not significant increase in caspase-3 protein (approximately 2 times more compared to control). Based on these results, none of the treatments used in this study caused apoptosis in the *in vivo* tumours.

However, it should be noted that the caspase-3 used in this study was inactive (procaspase-3), so perhaps not fully reflective of the induction of apoptosis via either the intrinsic or extrinsic apoptosis pathways. As previously mentioned, activation of caspase-3 is a clear indicator of apoptosis induction, in addition to caspases-6 and -7 (Kepp *et al.*, 2011; Würstle *et al.*, 2012).

The flow cytometry experiments showed only one statistically significant increase in apoptotic cells (late apoptosis, ABT-263 combination group), however, there was a visible increase (at least double) of apoptotic cells in the γT3 combination group in both SH-SY5Y and SK-N-BE(2) cell lines, compared to vehicle control (Figures 4.14 and 4.15). Although not conclusive, the pattern shown here suggests that further investigation into the apoptotic action of γT3 is necessary. For further evidence, using a caspase kit such as the one used by Shelake *et al.* (2015) for *in vitro* samples and an activated caspase-3 primary antibody to investigate protein expression from *in vivo* tumour samples may be helpful in fully understanding apoptotic action of γT3 in neuroblastoma.

The tumour suppressor protein p53 is a known activator of apoptosis, and has been a focus of past research neuroblastoma (Van Goethem *et al.*, 2017; Zhang *et al.*, 2013; Chen *et al.*, 2010). It is present in low levels in an unstressed state but accumulates when the cell is stressed, for example, following DNA damage, oncogene activation or nutrient suppression (Aubrey *et al.*, 2018). Van Goethem

et al. (2017) found that suppressing the natural p53 inhibitor Mdm2 in neuroblastoma cell lines and orthotopic tumours led to inhibition of cell proliferation, and increased action of caspases-3 and -7 indicated that the mode of action was apoptosis.

In this study, there were no statistically significant changes in p53 protein expression, when compared to the control group. However, all the treatment groups showed an increase in p53 protein expression compared to the control group (Figure 4.22A). Compared to the control group, p53 expression was increased by more than 5 times, while the γT3 combination group increased by just under 5 times, with a similar result from the ABT-263 combination group. γT3 alone showed the lowest increase in p53 expression at about 2.5 times more than control.

In a study investigating retinoic acid treatment resistance, SH-SY5Y cell lines treated with 5 μM 13cRA for 72 hours showed increased cell viability by reducing p53 protein levels, although 5 μM 13cRA for 24 hours did not significantly affect p53 expression (Waetzig *et al.*, 2019). However, lower doses of retinoic acid, such as 10 μM ATRA, over several days, have been commonly used to differentiate SH-SY5Y cells for investigations that require viable, neuron-like cells (Encinas *et al.*, 2000; Jämsä *et al.*, 2004; Dwane *et al.*, 2013). The dose used in our study was 3 times higher than that used by Waetzig *et al.* (2019), and our study cells were only exposed to treatment for 24 hours. Perhaps the differences found between this study and that by Waetzig *et al.* (2019) could be therefore attributed to different dose and length of exposure to the treatment.

Tan *et al.* (2016) also found a statistically insignificant increase in p53 expression when they treated SH-SY5Y cell lines with γT3 or γT3 combined with ATRA. However, unlike with 13cRA, ATRA alone did not show a change in p53 expression, when compared to the control group. Niizuma *et al.* (2006) concluded that neuroblastoma cells possess resistance against ATRA, but that study did not use 13cRA as a comparison. Also, while ATRA and 13cRA are both retinoic acid isomers, and therefore have similar chemical properties, 13cRA has been shown to have better *in vitro* activity in neuroblastoma cell lines than ATRA, because it acts as a prodrug for ATRA. This means more drug can be delivered into tumour cells, leading to higher potency (Reynolds *et al.*, 1994). Therefore, an increase in p53 expression due to 13cRA treatment, in contrast to the lack of change due to ATRA treatment is not unexpected. The results for p53 expression after treatment with γT3 is similar to the *in vitro* findings by Tan *et al.* (2016). Expression of p53 was increased in both studies by γT3 alone, as well as in combination with retinoic acid - 13cRA here, and ATRA in the study by Tan *et al.* (2016), and this increase was statistically insignificant in both studies when compared to untreated control.

There were no significant changes in Bcl-xL protein expression from treated samples compared to vehicle control in this study. Bcl-xL is a member of the Bcl-2 protein family and was found to be expressed in most neuroblastoma cell lines, although expression levels of both Bcl-xL and Bcl-2 were variable (Dole *et al.*, 1995). Additionally, the researchers inserted an expression vector containing Bcl-xL into the SHEP-1 neuroblastoma cell line, which normally expresses negligible levels of Bcl-xL, and found that sufficient levels of Bcl-xL,

like Bcl-2, were able to inhibit chemotherapy-induced apoptosis where the SHEP-1 cell line previously could not.

We chose to study Bcl-xL protein expression because after Bcl-2, it is one of the most actively bound targets of ABT-263, although to a much smaller degree than Bcl-2 (Mérino *et al.*, 2012). Kunnumakkara *et al.* (2010) found that γT3 alone did not reduce levels of Bcl-xL in an orthotopic nude mouse model of human pancreatic cancer compared to vehicle only control, although neither did gemcitabine, which is commonly used in pancreatic cancer treatment. However, used together, there was a dramatic reduction in Bcl-xL expression, where the combination treatment band on the blot was almost entirely gone, compared to thick, visible bands for other treatment groups. The results found by both this study and Kunnumakkara *et al.* (2010) could mean that γT3 does not alter Bcl-xL protein levels in either neuroblastoma or pancreatic cancer cell lines. Future studies investigating the mechanism of action of γT3 in both these cancers could therefore consider Bcl-xL a lower priority than other proteins.

5.3 GAMMA-TOCOTRIENOL EFFECTS *IN VIVO*

One of our objectives was to assess anti-tumour effects of 13cRA and γT3 as single agents or in combination in a nude mouse model. We monitored the tumour development using both manual callipers as well as PET/CT scan. ABT-263 combined with 13cRA was used as a selective Bcl-2 antagonist comparison to the γT3 combination with 13cRA.

In this section, the effects of γT3 on the volume of an ectopic neuroblastoma tumour in a nude mouse model will be discussed, in addition to an evaluation of the non-invasive tumour monitoring methods used here.

5.3.1 Effects on tumour volume

Pre-clinical, *in vivo* studies in rodents are commonly used in cancer research and can be used to further our understanding of the actions of drugs and other substances of interest in a model more complex than a simple *in vitro* study (Workman *et al.*, 2010). The *in vitro* study on effects of γT3 on the viability of neuroblastoma cancer cell lines produced promising results, including results that indicated that the addition of γT3 to 13cRA was synergistic, thus requiring lower doses of each drug in order to achieve a comparable or improved result. Due to this promising data, as well as the promise shown in the study by Tan *et al.* (2016), further experiments were conducted in order to study the effects *in vivo*. It should be noted that apart from the study by Tan *et al.* (2016), there have been no other published studies on the actions of tocotrienols on neuroblastoma,

either *in vitro* or *in vivo*. However, there are several *in vitro* and *in vivo* studies of the actions of tocotrienols, whether γT3 or TRFs, in other cancer models.

The *in vivo* results showed that the combination of γT3 and 13cRA resulted in a significant reduction in tumour volume compared to the vehicle only control ($p \leq 0.05$), but was not shown by either the γT3 only or ABT-263 combination groups. Additionally, while the 13cRA only group also showed a significant reduction in tumour volume ($p \leq 0.05$), the final tumour volume in this group was still twice that of the γT3 combination group.

While the γT3 only group showed very little reduction in tumour volume compared to the vehicle control group, the combination of γT3 and 13cRA had the lowest tumour volume out of the 5 groups and was statistically significant ($p \leq 0.05$). These results appear to confirm the *in vitro* results that showed a drastically improved degree of cytotoxicity of combined γT3 and 13cRA compared to individual treatments of both. A similar study by Manu *et al.*, (2012) also found that combining γT3 with another drug substantially improved the effects of the drug action compared to individual treatments.

They treated SNU-5 gastric cancer ectopic tumours in athymic nu/nu mice with 1mg/kg bodyweight of γT3, dissolved in corn oil and delivered via intraperitoneal (i.p.) injection 3 times weekly. This was given either alone or in combination with oral capecitabine (60mg/kg, oral). In their study, they found much better results with combined drug treatments compared to γT3 only. However, unlike in this study, the γT3 only group in the study by Manu *et al.*, (2012) significantly reduced the tumour volume compared to control ($p<0.001$), and capecitabine alone was similarly effective compared to control ($p<0.001$).

However, the most dramatic reduction in tumour volume was seen in the γT3 and capecitabine combination group, where tumour volume was approximately 20 times smaller than control group ($p<0.001$), and approximately 5 to 7 times smaller than capecitabine only and γT3 only groups ($p<0.001$). This result was reflected in this study, where combining γT3 with the standard clinical treatment (13cRA) improved the effects.

One main point of difference between this study and that by Manu *et al.*, (2012) is that this study focuses on the post-consolidation stage of treatment (13cRA), while the study by Manu *et al.*, (2012) focused on the induction chemotherapy (capecitabine). The post-consolidation stage of high-risk neuroblastoma treatment aims to treat any residual disease which was not successfully eliminated during earlier intensive treatment stages, with the aim being to prevent relapse (Smith & Foster, 2018). Capecitabine, as part of the first-line chemotherapy regimen in gastric cancer (Wagner *et al.*, 2017), is normally used to target tumours rather than residual disease, and as such has higher efficacy (as well as toxicity) than 13cRA. So although the individual treatments in this study (γT3 or 13cRA) were not significant, while individual treatments in the study by Manu *et al.*, (2012) were (γT3 and capecitabine) were, the relative change in tumour size reduction between individual and combination treatments for both studies were similar.

Similar to the study by Manu *et al.*, (2012), luciferase-transfected MIA PaCa-2 pancreatic cancer cells were treated with either γT3 or a chemotherapy drug, or both together (Kunnumakkara *et al.*, 2010). In this study, 400mg/kg/day of oral γT3 and the chemotherapeutic agent gemcitabine (25mg/kg, twice weekly, i.p.)

were used to treat orthotopic pancreatic cancer tumours, and at the end of the study, the researchers found that although the individual drug groups did not have any significant effects on the tumour volume, combined γT3 and gemcitabine made a significant change ($p<0.001$). This result, where the action of individual drug groups was improved upon combination, is similar to the results seen when combining 13cRA and γT3 in this study.

In our study, all treatments, including γT3, were administered orally only after subcutaneous tumours reached a size of approximately 1 cm^3, as described in Section 3.3.5.3. Our results therefore indicate that only the γT3 and 13cRA combination was able to stall further tumour growth, as final tumour volume of this treatment group was 1.10 cm^3. The 13cRA only treatment group had a significantly smaller final tumour volume compared to the vehicle control group (2.20 cm^3 vs 3.98 cm^3, $p\leq0.05$) but treatment with this group did not prevent tumour growth. Despite this, it should be noted that our study used solid tumours, while in a clinical setting, the use of 13cRA is to prevent relapse of tumour growth after chemotherapy and radiotherapy (Peinemann *et al.*, 2015). In a clinical setting, 13cRA would only be used when there is minimal tumour presence, and the ability of retinoic acid to differentiate cancer cells is a major reason that its use was first proposed in trials to improve high risk neuroblastoma treatment protocols (Reynolds *et al.*, 2003). Thus, it could be argued that because the addition of γT3 to 13cRA was able to reduce the size of a solid tumour, *in vivo*, significantly more than 13cRA alone, this could be a beneficial addition to 13cRA in the maintenance stage of high risk neuroblastoma.

5.3.2 Tumour monitoring methods

The *in vivo* protocol here used two methods to measure tumour growth in the mouse models: Vernier callipers and PET imaging Sections 3.34 and 3.3.7.3. Measurements using callipers were taken daily, while PET imaging was performed thrice per mouse – before tumour induction, just before treatment was initiated and at the end of the study.

In the representative PET images in Figure 4.21, which was taken at the end of the study, tumours are visible, although the outlines are uncertain. This was a problem when calculating tumour volume using the Vivoquant software, as the software uses the relative tumour intensity compared to background intensity to calculate tumour volume. However, it is possible to visually evaluate the size difference, where the tumour in Figure 4.21A is distinctly larger than B, D and E, which correlates with calliper measurements used to calculate tumour volume, as shown in Figure 4.20. External calliper measurements, while unable to account for irregularities in tumour shapes, are currently the standard method for measuring tumour volume due to its simplicity, low cost and high throughput (Jensen *et al.*, 2008). Therefore, the results of the tumour monitoring can be confidently used to evaluate the action of γT3 in an *in vivo* study.

5.4 STUDY LIMITATIONS AND FURTHER WORK

There were several limitations in the study that may have directly contributed to the insignificant findings. This section will identify and discuss those factors.

5.4.1 Cell lines and Bcl-2

One limitation in this study was the cell lines used. SH-SY5Y and SK-N-BE(2) were chosen as wild-type and *MYCN* amplified neuroblastoma cell lines, respectively. However, other characteristics of cell lines that need to be taken into consideration were only identified after completing this study.

As previously discussed, neuroblastoma tumours are known to possess higher Bcl-2 expression than healthy tissues as well as other tumours (Goldsmith *et al.*, 2012). Neuroblastoma cell lines, such as SH-SY5Y were also considered to possess higher than normal Bcl-2 expression (Reed *et al.*, 1991). More recent research however, has shown that most neuroblastoma cell lines have significantly lower Bcl-2 expression than primary neuroblastoma tumours and therefore are not accurate disease models (Goldsmith *et al.*, 2012; Lamers *et al.*, 2012). The Bcl-2 expression most likely had a role in some of the more unexpected results.

13cRA had the same IC_{50} for both cell lines, unlike γT3, which has a lower IC_{50} in the SH-SY5Y cell line than SK-N-BE(2). This was unexpected because the SK-N-BE(2) cell line, as the high risk neuroblastoma model, should be more resistant to treatment.

On the other hand, when treated with 13cRA, the complex changes in apoptosis signalling and differentiation at lower doses that increase cell viability that were

previously discussed in *Section 5.1.1* (Waetzig *et al.*, 2019; Hadjidaniel & Reynolds, 2010) might also contribute to higher cell viability than predicted in SH-SY5Y cell line.

The effect of ABT-263 on cell viability, alone or combined with 13cRA, is not easily distinguishable between the two cell lines (Figures 4.3 and 4.6), unlike observations seen during the addition of γT3 to 13cRA (Figures 4.7 and 4.8). The calculated IC_{50} of ABT-263 was the same for both cell lines (40μM), and while the addition of ABT-263 to 13cRA treatment of both cell lines reduced the IC_{50} of 13cRA, it was not a significant reduction (Figure 4.9).

Resistance to ABT-263 was expected in the SK-N-BE(2) cell line because of its MYCN amplification, which is a known cause of treatment resistance (Park *et al.*, 2013). However, the SH-SY5Y cell line was expected to have a more prominent response to a Bcl-2 inhibitor because SH-SY5Y cell lines in particular are known to overexpress Bcl-2 (Reed *et al.*, 1991), in addition to neuroblastoma tumours having higher Bcl-2 expression compared to other healthy tissues (Goldsmith *et al.*, 2012). Therefore, using that logic to target Bcl-2 as a strategy to treat neuroblastoma, the theory was extrapolated to expect SH-SY5Y cell lines to be more sensitive to ABT-263 treatment than SK-N-BE(2) cell lines.

Unfortunately, our study shows that while SH-SY5Y cell lines might have a higher Bcl-2 expression compared to many other cancer cell lines and healthy cells, this Bcl-2 expression may not be sufficiently high enough, a fact that was not identified when initially planning this study.

Using Bcl-2 inhibiting drugs such as ABT-263 to treat neuroblastoma cell lines with high Bcl-2 protein expression caused apoptosis but did not have the same

effect in neuroblastoma cell lines with low Bcl-2 protein expression (Lamers *et al.*, 2012). In their study, a panel of 24 neuroblastoma cell lines and 88 neuroblastoma primary tumour samples were tested for Bcl-2 gene and protein expression. Results showed that while the majority of primary tumours have a high Bcl-2 protein expression, most neuroblastoma cell lines have comparatively lower Bcl-2 expression and out of the 24 cell lines studied here, including SH-SY5Y, only two cell lines (KCNR and SJNB12) matched the levels of Bcl-2 observed in the primary tumours.

A later study using ABT-199, a newer, more specific Bcl-2 inhibitor than ABT-263, showed that they could predict sensitivity to ABT-199 drug treatment based on Bcl-2 protein levels, as cell lines with lower levels of Bcl-2 were less sensitive to ABT-199. Bcl-2 protein expression of SH-SY5Y was significantly lower than in the CHP126 neuroblastoma line, which was reflected in the IC_{50} values of ABT-199: in the SH-SY5Y cell line, IC_{50} was 15.32μM compared to 0.01μM in the CHP126 cell line (Bate-Eya *et al.*, 2016).

ABT-263 alone was found to be ineffective in treating SH-SY5Y cell lines, and the hypothesis for this failure in treatment was due to another member of the Bcl-2 protein family, Mcl-1, which is also elevated to varying degrees in neuroblastoma cell lines and tumours. The researchers tested their theory by showing improved action (defined as induction of apoptosis and cell viability inhibition) of ABT-263 when paired with an norcantharidin, an anticancer drug linked to elevation of the endogenous Mcl-1 inhibitor, Noxa (Wang *et al.*, 2014). Another study that treated lymphoma *in vitro* and *in vivo* found that Mcl-1 overexpression cause resistance to ABT-737 (van Delft *et al.*, 2006).

SH-SY5Y cell lines also do express some degree of Mcl-1; the study mentioned earlier by Bate-Eya *et al.*, (2016) found relatively higher levels of Mcl-1 compared to Bcl-2 in SH-SY5Y cells, although this was not quantified. However, unlike SH-SY5Y, SK-N-BE(2) cell lines are considered Mcl-1 dependent (and also overexpress MYCN protein) (Nalluri *et al.*, 2015). Mcl-1 knockdown in neuroblastoma cell lines that are normally resistant to therapy by Bcl-2 inhibitor (ABT-737), as well as other conventional chemotherapy, overcame the treatment resistance conferred by Mcl-1 (Lestini *et al.*, 2009). So, the combined factors of treatment resistance, due to Mcl-1 dependence, in addition to overexpressed MYCN could account for the slightly lower effect of the Bcl-2 inhibitor ABT-263 to the IC_{50} of 13cRA when combined in the SK-N-BE(2) cell line compared to SH-SY5Y (17.5% reduction in IC_{50} vs 27.5%) (Figure 4.9), while lower sensitivity of SH-SY5Y than predicted to ABT-263 could be due to a combination of lower Bcl-2 expression than previously thought, combined with a possible resistance caused by some Mcl-1 expression.

Due to protein expression and *in silico* docking results which showed that γT3 binds to the hydrophobic groove of Bcl-2 to induce apoptosis via the intrinsic pathway (Tan *et al.*, 2016), ABT-263, a selective Bcl-2 inhibitor was chosen as a comparison for the Bcl-2 action of γT3. However, once again, the low Bcl-2 expression of this particular SH-SY5Y cell line, which was used to grow the xenografts in this mouse model, most likely contributed to the poor results of ABT-263. The results shown in Figure 4.20 reflect the observations documented by Lamers *et al.* (2012), as the final tumour volume from the ABT-263 combination group was only just slightly higher than the 13cRA only treatment group, and both were not significantly less compared to the vehicle control.

The importance of Bcl-2 expression to treatments in high risk neuroblastoma cannot be conclusively evaluated in this study due to the Bcl-2 levels in the chosen cell lines. Ideally, future work would use cell lines grown from primary tumours. An alternative plan would be to transfect SH-SY5Y with a Bcl-2 expression vector, in a similar manner as the low Bcl-xL-expressing SHEP-1 cell line in the study by Dole *et al.* (1995), which would then cause SH-SY5Y to express higher levels of Bcl-2. On the other hand, neuroblastoma cell lines that have Bcl-2 levels comparable to that of neuroblastoma tumours have been identified (Lamers *et al.*, 2012). Both SMS-KCNR and SJNB12 cell lines were shown to have comparable Bcl-2 expression to tumours, and SMS-KCNR has *MYCN* amplification (Beppu *et al.*, 2005), while SJNB12 does not have *MYCN* amplification (Shapiro *et al.*, 1993). The contrasting *MYCN* status of the cell lines is still important, as *MYCN* amplification is a commonly recognized classification factor for high risk neuroblastoma (Cohn *et al.*, 2009).

5.4.2 PET/CT imaging and tumours

Another part of this study that could be improved is the method of tumour growth monitoring in the *in vivo* experiment. While external callipers are the most convenient and affordable method to detect ectopic tumours, they are still less accurate and reproducible compared to PET imaging (Jensen *et al.*, 2008).

According to some published work, PET imaging has been successfully used to monitor tumour xenograft progression in small animals, including A431 epidermoid carcinoma and U251 glioblastoma cells in SCID mice (Fueger *et al.*, 2006), tumour metabolism in genetically engineered mouse lung cancer models (Wang *et al.*, 2015), and a combination of orthotopic SK-N-BE(2)c

neuroblastoma tumours with patient derived neuroblastoma tumour explants in mice (Braekeveldt *et al.*, 2015).

However, while the study by Braekeveldt *et al.* (2015) was able to successfully produce images of neuroblastoma tumours in mice, the tumour images in this study were much fainter than that of other tissues such as heart and other muscles (Figure 4.21 and Figure C1)). An important fact to consider is that the tumours used by Braekeveldt *et al.* (2015) were orthotopic. In a study that compared MDA-MB-231-H2N breast cancer tumours in mice that were either implanted subcutaneously (ectopic) or in the mammary fat pad (orthotopic), investigators found that orthotopic tumours grew faster and furthermore, possessed better vascular permeability compared to ectopic tumours. FITC-dextran, injected i.v., accumulated more in orthotopic tumours compared to similarly sized ectopic tumours, and immunostaining also showed better vascular density in orthotopic tumours (Ho *et al.*, 2012). As previously described, PET imaging utilises the higher glucose uptake of cancer cells compared to normal cells that results in accumulation of positron emissions (from 18-FDG) at the tumour, which can be detected by a PET scan (Koba, Jelicks & Fine, 2013). 18-FDG is injected (either i.v. or i.p.), and therefore a higher number of blood vessels would improve glucose uptake, as demonstrated by the FITC-dextran experiment (Ho *et al.*, 2012). A lower 18-FDG uptake, leading to lower positron emission by tumours in this study could therefore simply be explained by inadequate tumour vascularisation.

One potential way to overcome the vascularisation shortcoming would be to use bioluminescence imaging. This imaging technique was found to be superior to

both PET and ultrasound imaging when used to detect early tumour formation and growth in a rat liver carcinoma *in vivo* model (Hwang *et al.*, 2015) and . This method has been used successfully to monitor tumour growth in mouse models of a variety of cancers, using cell lines that were stably transfected with luciferase reporter gene: acute myeloid leukaemia (Konopleva *et al.*, 2006), pancreatic (Kunnumakkara *et al.*, 2010) and colorectal (Prasad *et al.*, 2016). Bioluminescence imaging also carries lower health and safety risks than PET imaging as it does not require use of radioactive substances such as 18-FDG, and is superior to external calliper measurements as this imaging method is suitable for use in both ectopic and orthotopic tumours (Koba *et al.*, 2011). Additionally, future experiments could also consider the use of orthotopic tumours instead of ectopic, as this would provide better clinical representation (Huynh *et al.*, 2011). We were unable to use orthotopic tumours for several reasons, including a lack of facilities and expertise to induce orthotopic tumours, as well as regulations by The University of Nottingham Animal Ethic Committee that require orthotopic studies to be preceded by ectopic studies.

5.4.3 Cell death assays

The cell death experiments, LDH assay and flow cytometry, could be better supported with expanded protein expression studies, or an additional apoptosis assay such as the TUNEL (terminal deoxynucleotidyl transferase-mediated dUTP nick-end labelling) assay. Due to higher sensitivity than other methods, it is considered the gold standard to detect apoptosis in situ, although drawbacks include false positives from necrosis and sample handling (Galluzzi *et al.*, 2009). It would work well as an additional assay as it is not recommended to rely on it as the sole apoptosis assay (Kepp *et al.*, 2011). Further evidence for presence or

absence of apoptosis can be collected with other methods, such as protein expression studies, i.e. Western blot. Due to factors such as human error, relying on just one or two methods may not be sufficient, resulting in statistically insignificant results and/or large error bars (Figures 4.10 to 4.13).

Protein expression studies here were not completely conclusive, and the scope of proteins studied requires expansion. One way to overcome this limitation would be to include Bax, in order to calculate a Bcl-2/Bax ratio, as a better representation of cell survival after γT3 treatments, as demonstrated in past research (Then *et al.*, 2009; Tan *et al.*, 2016). The complex relationship between Bcl-2 and Bax was also described Cory and Adams (2005), and how understanding the interaction and balance of both these proteins played a role in establishing Bcl-2 as a valid target in cancer therapy. In addition to different proteins assayed, transferring the protein from the gel to the membrane in wet conditions rather than semi-dry is considered more reliable (Yang & Mahmood, 2012), and could be the preferred future method. We also trialled a protein capillary assay called Jess (Appendix B), which is another potential method for protein assay.

For more efficient identification of caspase alterations, a caspase assay kit such as that used by Tan *et al.* (2016) could be used. However, for results that are more conclusive than those presented in this study, both the activate and inactive forms of caspase-3 should be studied, as the trigger for apoptosis is the activation of inactive procaspase-3 (Würstle et al., 2012). This approach was used in a study investigating effects of cytotoxic drug treatments against neuroblastoma cell lines, and the vehicle only control cells did not express cleaved caspases,

unlike the treated cell lines (Fang *et al.*, 2011). The incorrectly used caspases here was simply due to oversight when planning the experiment.

Apart from caspases, cytochrome c can also be studied as an indicator of initiation of apoptosis. Furthermore, as cytochrome c must be released from the mitochondria in order to continue the intrinsic apoptosis cascade, samples could be separated into cytoplasmic and organelle fractions in order to compare different treatment effects (Lamers *et al.*, 2012).

Other proteins from the Bcl-2 protein family could be included in a future study. Mcl-1 is also found to be overexpressed in various neuroblastoma cell lines, and was shown to be linked to some treatment resistance (van Delft *et al.*, 2006; Lestini *et al.*, 2009). It would be interesting to study not only the protein expression of Mcl-1 in neuroblastoma after treatment with γT3 but also to investigate possible affinity of γT3 for Mcl-1. As γT3 is known to have multiple targets (Kannappan *et al.*, 2012; Tham *et al.*, 2019), a future *in silico* docking study to investigate its binding affinity should be conducted with more proteins, such as Mcl-1 and Bcl-xL, both of which have similar actions as Bcl-2, and have already been studied together as therapeutic targets of the Bcl-2 antagonist, ABT-199 (Bate-Eya *et al.*, 2016).

In addition to traditional qualitative and quantitative methods of evaluating protein expression, a possible future experiment would be to study interactions between Bcl-2 pro-survival and BH3-only proteins to compare the effects of different treatments. The quantitative, high-throughput method uses fluorescent fusion proteins of the proteins of interest, and their interactions are viewed using confocal microscopy. According to the researchers, they were able to view the

movements of proteins in the cytoplasm and mitochondria, as well as quantify fluorescent intensity from each cell compartment (Wong *et al.*, 2012a).

Finally, future studies should consider the use of ABT-199 instead of ABT-263, as not only has it been shown to be the most selective of Bcl-2 compared to ABT-263 and ABT-737 (Souers *et al.*, 2013), it has recently been approved for use in several types of leukaemia, making it more relevant clinically (Bohl, Bullinger & Rücker, 2019; Wei *et al.*, 2019). ABT-199 was developed from ABT-263, and stocks of ABT-263 had already been purchased and *in vitro* studies began when publications that used ABT-199 became more prominent.

CHAPTER 6 CONCLUSION

At the beginning of this study, a list of aims and objectives was made that had to be fulfilled in order to investigate our hypothesis. This hypothesis was composed of several parts. First, we hypothesised that γT3 has significant anti-tumour effects on neuroblastoma, and that combining it with a current drug treatment for high risk neuroblastoma would have a synergistic effect. Finally, we hypothesised that γT3 binds to the hydrophobic groove of Bcl-2 in order to initiate the intrinsic apoptosis cascade, and that due to this binding, γT3 would show similar, although less significant anti-tumour effects when compared to the Bcl-2 inhibitor ABT-263.

The addition of γT3 to 13cRA adjuvant therapy in high risk neuroblastoma may be beneficial, based on the *in vitro* and *in vivo* results obtained in this study. *In vitro* results showed very significant improvements when treating both SH-SY5Y and SK-N-BE(2) cell lines with combined γT3 and 13cRA compared to individual treatments, as seen in raw MTS and LDH assay results. Additionally, combination index analysis proved that the combination of γT3 and 13cRA was clearly synergistic. Furthermore, the *in vivo* results showed that addition of γT3 was able to significantly reduce tumour volume compared to vehicle only and individual treatments, as well as compared to the Bcl-2 inhibitor, ABT-263.

While *in silico* docking evidence (Tan *et al.*, 2016) may have indicated that Bcl-2 alone was a clear lead towards determining the mode of action of γT3 in its anticancer properties for treating neuroblastoma, the evidence here is less clear. The investigation here focused on the intrinsic apoptosis pathway, due to evidence from past research. Flow cytometry with Annexin V-FITC/PI staining

showed that the combined γT3 and 13cRA treatments in both SH-SY5Y and SK-N-BE(2) cell lines increased the number of apoptotic cells slightly more than other treatment groups, but this increase was not statistically significant. When comparing single treatments against combination, combined γT3 and 13cRA in both cell lines caused a greater level of apoptosis than single agents, although once again, this was not statistically significant. Western blot of tumours obtained from the *in vivo* experiment also did not show conclusive results regarding caspase-9, caspase-3 or p53 protein expression after treatment with γT3. There were also no conclusive results for Bcl-2 and Bcl-xL protein expression for γT3 treatments in either *in vitro* or *in vivo* samples, although the combination γT3 treatment did significantly increase Bcl-2 expression compared to untreated control in the SK-N-BE(2) cell line. Overall, these results are indicative of γT3 possibly using apoptosis to kill neuroblastoma cells, as although flow cytometry analysis showed a visual increase in apoptotic cells, this was not statistically significant. And while protein expression results were inconclusive for all proteins studied, using the activated forms of caspase-9 and -3 could potentially give clearer results than what was obtained here.

Due to the importance of the role of overexpressed *MYCN* in high risk neuroblastoma, MYCN protein was investigated using Western blot in both *in vitro* and *in vivo* samples. There was a slight and statistically insignificant decrease in both single and combination γT3 treatment groups in the SH-SY5Y cell line but a statistically significant increase for the same groups in the SK-N-BE(2) cell line. Unfortunately, the *in vivo* samples did not yield results for analysis.

As a final conclusion, γT3 could potentially be used in combination with 13cRA, as part of the high risk neuroblastoma maintenance therapy, as it has shown significant anti-tumour effects on neuroblastoma, both *in vitro* and *in vivo*. This γT3 combination treatment had a synergistic effect and showed more significant anti-tumour effects on neuroblastoma cell lines and an *in vivo* tumour model than the selective Bcl-2 inhibitor ABT-263. However, based on the current evidence, it is not possible to conclusively identify the mechanism of action of γT3 as binding to the Bcl-2 protein in the intrinsic apoptosis pathway. Although these results were still indicative of apoptosis, further work is required to further investigate the exact proteins and processes involved in this method of cell death.

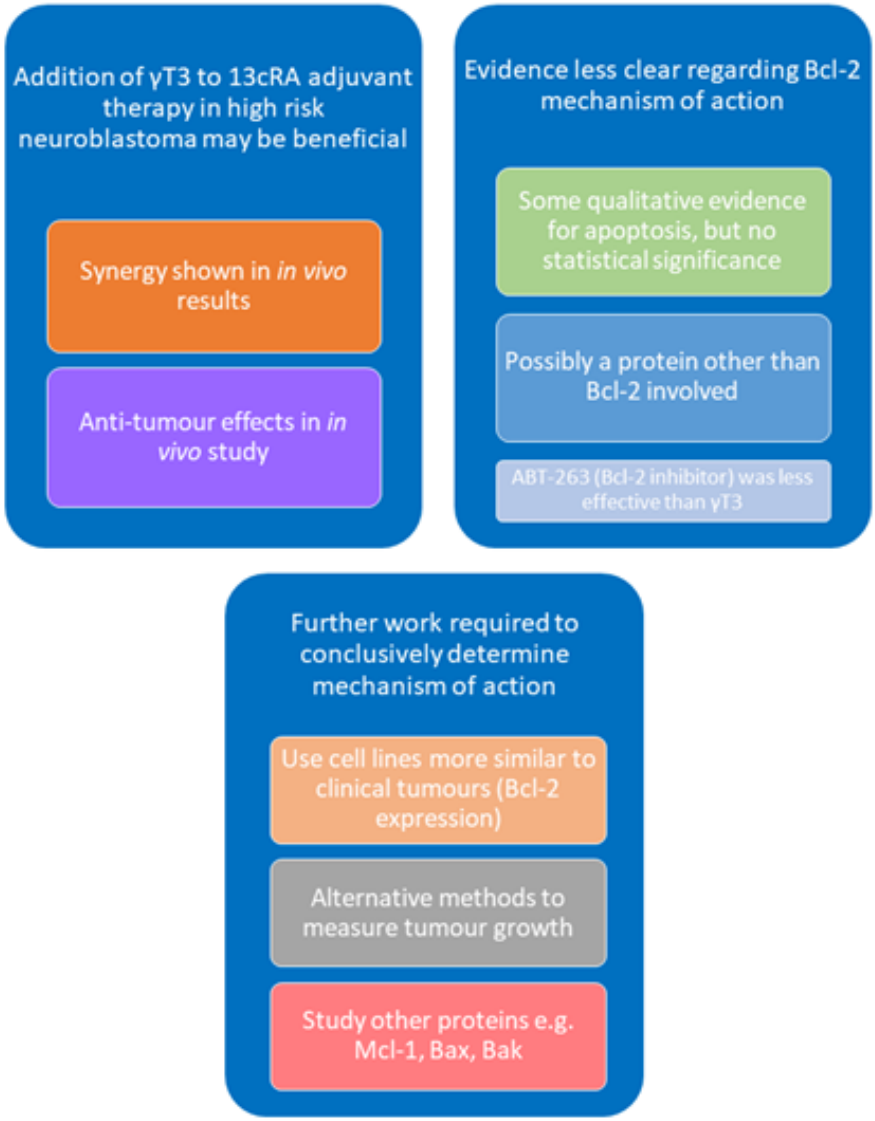

Figure 6.1: Summary of study findings: γT3 and 13cRA has anti-cancer effects *in vitro* and *in vivo*. However, the mechanism of action cannot yet be confirmed based on the results of this study and further work is needed

REFERENCES

Abdul Rahman, A., A Jamal, A.R., Harun, R., Mohd Mokhtar, N., et al. (2014) Gamma-tocotrienol and hydroxy-chavicol synergistically inhibits growth and induces apoptosis of human glioma cells. *BMC complementary and alternative medicine*. [Online] 14 (1), 213. Available from: doi:10.1186/1472-6882-14-213 [Accessed: 1 November 2014].

Abubakar, I.B., Lim, K.H., Kam, T.S. & Loh, H.S. (2017) Enhancement of apoptotic activities on brain cancer cells via the combination of γ-tocotrienol and jerantinine A. *Phytomedicine*. [Online] 30, 74–84. Available from: doi:10.1016/j.phymed.2017.03.004.

Ackler, S., Mitten, M.J., Chen, J., Clarin, J., et al. (2012) Navitoclax (ABT-263) and bendamustine ± rituximab induce enhanced killing of non-Hodgkin's lymphoma tumours in vivo. *British journal of pharmacology*. [Online] 167 (4), 881–891. Available from: doi:10.1111/j.1476-5381.2012.02048.x [Accessed: 10 November 2014].

Adams, J.M. & Cory, S. (2007) The Bcl-2 apoptotic switch in cancer development and therapy. *Oncogene*. [Online] 26 (9), 1324–1337. Available from: doi:10.1038/sj.onc.1210220 [Accessed: 12 August 2014].

Aggarwal, B.B., Sundaram, C., Prasad, S. & Kannappan, R. (2010) Tocotrienols, the vitamin E of the 21st century: its potential against cancer and other chronic diseases. *Biochemical pharmacology*. [Online] 80 (11), 1613–1631. Available from: doi:10.1016/j.bcp.2010.07.043 [Accessed: 13 September 2014].

Aggarwal, V., Kashyap, D., Sak, K., Tuli, H.S., et al. (2019) Molecular Mechanisms of Action of Tocotrienols in Cancer: Recent Trends and Advancements. *International journal of molecular sciences*. [Online] 20 (3). Available from: doi:10.3390/ijms20030656.

Ahmed, R.A., Alawin, O.A. & Sylvester, P.W. (2016) γ-Tocotrienol reversal of epithelial-to-mesenchymal transition in human breast cancer cells is associated with inhibition of canonical Wnt signalling. *Cell Proliferation*. [Online] 49 (4), 460–470. Available from: doi:10.1111/cpr.12270.

Ahsan, H., Ahad, A., Iqbal, J. & Siddiqui, W. a (2014) Pharmacological potential of tocotrienols: a review. *Nutrition & metabolism*. [Online] 11 (1), 52. Available from: doi:10.1186/1743-7075-11-52 [Accessed: 11 February 2015].

Animal Care and Use Committee (2015) *Equivalent Surface Area Dosage Conversion Factors*. [Online]. Available from: https://ncifrederick.cancer.gov/lasp/acuc/frederick/Media/Documents/ACUC42.pdf.

Ashkenazi, A., Fairbrother, W.J., Leverson, J.D. & Souers, A.J. (2017) From

basic apoptosis discoveries to advanced selective BCL-2 family inhibitors. *Nature Reviews Drug Discovery*. [Online] 16 (4), 273–284. Available from: doi:10.1038/nrd.2016.253.

Aubrey, B.J., Kelly, G.L., Janic, A., Herold, M.J., et al. (2018) How does p53 induce apoptosis and how does this relate to p53-mediated tumour suppression? *Cell death and differentiation*. [Online] 25 (1), 104–113. Available from: doi:10.1038/cdd.2017.169.

Avery-Kiejda, K.A., Bowden, N.A., Croft, A.J., Scurr, L.L., et al. (2011) P53 in human melanoma fails to regulate target genes associated with apoptosis and the cell cycle and may contribute to proliferation. *BMC Cancer*. [Online] 11. Available from: doi:10.1186/1471-2407-11-203.

Baj, G. & Tongiorgi, E. (2009) BDNF splice variants from the second promoter cluster support cell survival of differentiated neuroblastoma upon cytotoxic stress. *Journal of cell science*. [Online] 122 (Pt 1), 36–43. Available from: doi:10.1242/jcs.03506.

Bate-Eya, L.T., den Hartog, I.J.M., van der Ploeg, I., Schild, L., et al. (2016) High efficacy of the BCL-2 inhibitor ABT199 (venetoclax) in BCL-2 high-expressing neuroblastoma cell lines and xenografts and rational for combination with MCL-1 inhibition. *Oncotarget*. [Online] 7 (19), 27946–27958. Available from: doi:10.18632/oncotarget.8547.

Baumans, V., Brain, P.F., Brugére, H., Clausing, P., et al. (1994) Pain and distress in laboratory rodents and lagomorphs: Report of the Federation of European Laboratory Animal Science Associations (FELASA) Working Group on Pain and Distress accepted by the FELASA Board of Management November 1992. *Laboratory Animals*. [Online] 28 (2), 97–112. Available from: doi:10.1258/002367794780745308.

Beppu, K., Nakamura, K., Linehan, W.M., Rapisarda, A., et al. (2005) Topotecan blocks hypoxia-inducible factor-1α and vascular endothelial growth factor expression induced by insulin-like growth factor-1 in neuroblastoma cells. *Cancer Research*. [Online] 65 (11), 4775–4781. Available from: doi:10.1158/0008-5472.CAN-04-3332.

Bohl, S.R., Bullinger, L. & Rücker, F.G. (2019) New targeted agents in acute myeloid leukemia: New hope on the rise. *International Journal of Molecular Sciences*. [Online] 20 (8). Available from: doi:10.3390/ijms20081983.

Bommer, G.T., Gerin, I., Feng, Y., Kaczorowski, A.J., et al. (2007) p53-Mediated Activation of miRNA34 Candidate Tumor-Suppressor Genes. *Current Biology*. [Online] 17 (15), 1298–1307. Available from: doi:10.1016/j.cub.2007.06.068.

Braekeveldt, N., Wigerup, C., Gisselsson, D., Mohlin, S., et al. (2015) Neuroblastoma patient-derived orthotopic xenografts retain metastatic patterns and geno- and phenotypes of patient tumours. *International*

journal of cancer. Journal international du cancer. [Online] 136 (5), E252-61. Available from: doi:10.1002/ijc.29217.

Brodeur, G.M. (2003) Neuroblastoma: biological insights into a clinical enigma. *Nature reviews. Cancer*. [Online] 3 (3), 203–216. Available from: doi:10.1038/nrc1014 [Accessed: 5 November 2014].

Brodeur, G.M. & Bagatell, R. (2014) Mechanisms of neuroblastoma regression. *Nature reviews. Clinical oncology*. [Online] 11 (12), 704–713. Available from: doi:10.1038/nrclinonc.2014.168.

Canete, A., Gerrard, M., Rubie, H., Castel, V., et al. (2009) Poor survival for infants with MYCN-amplified metastatic neuroblastoma despite intensified treatment: the International Society of Paediatric Oncology European Neuroblastoma Experience. *Journal of clinical oncology : official journal of the American Society of Clinical Oncology*. [Online] 27 (7), 1014–1019. Available from: doi:10.1200/JCO.2007.14.5839 [Accessed: 26 February 2015].

Cardenas, E. & Ghosh, R. (2013) Vitamin E: a dark horse at the crossroad of cancer management. *Biochemical pharmacology*. [Online] 86 (7), 845–852. Available from: doi:10.1016/j.bcp.2013.07.018 [Accessed: 18 October 2014].

Casara, P., Davidson, J., Claperon, A., Le Toumelin-Braizat, G., et al. (2018) S55746 is a novel orally active BCL-2 selective and potent inhibitor that impairs hematological tumor growth. *Oncotarget*. [Online] 9 (28), 20075–20088. Available from: doi:https://dx.doi.org/10.18632/oncotarget.24744.

Chen, L., Iraci, N., Gherardi, S., Gamble, L.D., et al. (2010) p53 is a direct transcriptional target of MYCN in neuroblastoma. *Cancer Research*. [Online] 70, 1377–1388. Available from: doi:10.1158/0008-5472.CAN-09-2598.

Cheung, N.-K. V & Dyer, M. a (2013) Neuroblastoma: developmental biology, cancer genomics and immunotherapy. *Nature reviews. Cancer*. [Online] 13, 397–411. Available from: doi:10.1038/nrc3526.

Chou, T.-C. (2010) Drug Combination Studies and Their Synergy Quantification Using the Chou-Talalay Method. *Cancer Research*. [Online] 70 (2), 440–446. Available from: doi:10.1158/0008-5472.CAN-09-1947.

Chou, T.-C. (2006) Theoretical Basis, Experimental Design, and Computerized Simulation of Synergism and Antagonism in Drug Combination Studies. *Pharmacological Reviews*. [Online] 58 (3), 621–681. Available from: doi:10.1124/pr.58.3.10.

Cohn, S.L., Pearson, A.D.J., London, W.B., Monclair, T., et al. (2009) The International Neuroblastoma Risk Group (INRG) classification system: an INRG Task Force report. *Journal of clinical oncology : official journal of the American Society of Clinical Oncology*. [Online] 27 (2), 289–297.

Available from: doi:10.1200/JCO.2008.16.6785 [Accessed: 18 July 2014].

Cole, K.A. & Maris, J.M. (2012) New strategies in refractory and recurrent neuroblastoma: Translational opportunities to impact patient outcome. *Clinical Cancer Research*. [Online] 18 (9), 2423–2428. Available from: doi:10.1158/1078-0432.CCR-11-1409.

Cory, S. & Adams, J.M. (2005) Killing cancer cells by flipping the Bcl-2/Bax switch. *Cancer cell*. [Online] 8 (1), 5–6. Available from: doi:10.1016/j.ccr.2005.06.012 [Accessed: 23 September 2014].

Czabotar, P.E., Lessene, G., Strasser, A. & Adams, J.M. (2014) Control of apoptosis by the BCL-2 protein family: implications for physiology and therapy. *Nature reviews. Molecular cell biology*. [Online] 15 (1), 49–63. Available from: doi:10.1038/nrm3722 [Accessed: 11 July 2014].

Delbridge, A.R.D., Grabow, S., Bouillet, P., Adams, J.M., et al. (2015) Functional antagonism between pro-apoptotic BIM and anti-apoptotic BCL-XL in MYC-induced lymphomagenesis. *Oncogene*. [Online] 34 (14), 1872–1876. Available from: doi:10.1038/onc.2014.132.

Delbridge, A.R.D., Grabow, S., Strasser, A. & Vaux, D.L. (2016) Thirty years of BCL-2: translating cell death discoveries into novel cancer therapies. *Nature Reviews Cancer*. [Online] 16 (2), 99–109. Available from: doi:10.1038/nrc.2015.17.

van Delft, M.F., Wei, A.H., Mason, K.D., Vandenberg, C.J., et al. (2006) The BH3 mimetic ABT-737 targets selective Bcl-2 proteins and efficiently induces apoptosis via Bak/Bax if Mcl-1 is neutralized. *Cancer Cell*. [Online] 10 (5), 389–399. Available from: doi:10.1016/j.ccr.2006.08.027.

Devarajan, E., Sahin, A.A., Chen, J.S., Krishnamurthy, R.R., et al. (2002) Down-regulation of caspase 3 in breast cancer: A possible mechanism for chemoresistance. *Oncogene*. [Online] 21 (57), 8843–8851. Available from: doi:10.1038/sj.onc.1206044.

Doerflinger, M., Glab, J. a. & Puthalakath, H. (2015) BH3-only proteins: a 20-year stock-take. *FEBS Journal*. [Online] 282, 1006–1016. Available from: doi:10.1111/febs.13190.

Dole, M., Nuñez, G., Merchant, A.K., Maybaum, J., et al. (1994) Bcl-2 inhibits chemotherapy-induced apoptosis in neuroblastoma. *Cancer Research*. [Online] 54, 3253–3259. Available from: http://www.ncbi.nlm.nih.gov/pubmed/8205548.

Dole, M.G., Jasty, R., Cooper, M.J., Thompson, C.B., et al. (1995) Bcl-xL Is Expressed in Neuroblastoma Cells and Modulates Chemotherapy-induced Apoptosis. *Cancer Research*. 55 (12), 2576–2582.

Dwane, S., Durack, E. & Kiely, P. a (2013) Optimising parameters for the differentiation of SH-SY5Y cells to study cell adhesion and cell migration. *BMC research notes*. [Online] 6 (1), 366. Available from:

doi:10.1186/1756-0500-6-366.

Encinas, M., Iglesias, M., Liu, Y., Wang, H., et al. (2000) Sequential treatment of SH-SY5Y cells with retinoic acid and brain-derived neurotrophic factor gives rise to fully differentiated, neurotrophic factor-dependent, human neuron-like cells. *Journal of Neurochemistry*. [Online] 75 (3), 991–1003. Available from: doi:10.1046/j.1471-4159.2000.0750991.x.

Esiashvili, N., Goodman, M., Ward, K., Marcus, R.B., et al. (2007) Neuroblastoma in adults: Incidence and survival analysis based on SEER data. *Pediatric blood & cancer*. [Online] 49 (1), 41–46. Available from: doi:10.1002/pbc.20859.

Evans, H.M. & Bishop, K.S. (1922) On the existence of a hitherto unrecognized dietary factor essential for reproduction. *Science*. [Online] 56 (1458), 650 LP – 651. Available from: doi:10.1126/science.56.1458.650.

Fairus, S., Nor, R.M., Cheng, H.M. & Sundram, K. (2012) Alpha-tocotrienol is the most abundant tocotrienol isomer circulated in plasma and lipoproteins after postprandial tocotrienol-rich vitamin E supplementation. *Nutrition Journal*. [Online] 11 (1), 5. Available from: doi:10.1186/1475-2891-11-5.

Fang, H., Harned, T.M., Kalous, O., Maldonado, V., et al. (2011) Synergistic activity of fenretinide and the Bcl-2 family protein inhibitor ABT-737 against human neuroblastoma. *Clinical Cancer Research*. [Online] 17 (22), 7093–7104. Available from: doi:10.1158/1078-0432.CCR-11-0578.

Fesik, S.W. (2005) Promoting apoptosis as a strategy for cancer drug discovery. *Nature reviews. Cancer*. [Online] 5 (11), 876–885. Available from: doi:10.1038/nrc1736 [Accessed: 28 November 2014].

Fletcher, S. & Prochownik, E. V. (2015) Small-molecule inhibitors of the Myc oncoprotein. *Biochimica et Biophysica Acta (BBA) - Gene Regulatory Mechanisms*. [Online] 1849 (5), 525–543. Available from: doi:10.1016/j.bbagrm.2014.03.005.

Fong, P.Y., Xue, W.C., Ngan, H.Y.S., Chiu, P.M., et al. (2006) Caspase activity is downregulated in choriocarcinoma: A cDNA array differential expression study. *Journal of Clinical Pathology*. [Online] 59 (2), 179–183. Available from: doi:10.1136/jcp.2005.028027.

Fotakis, G. & Timbrell, J.A. (2006) In vitro cytotoxicity assays: Comparison of LDH, neutral red, MTT and protein assay in hepatoma cell lines following exposure to cadmium chloride. *Toxicology Letters*. [Online] 160 (2), 171–177. Available from: doi:10.1016/j.toxlet.2005.07.001.

Fu, J.-Y., Che, H.-L., Tan, D.M.-Y. & Teng, K.-T. (2014) Bioavailability of tocotrienols: evidence in human studies. *Nutrition & metabolism*. [Online] 11 (1), 5. Available from: doi:10.1186/1743-7075-11-5.

Fueger, B.J., Czernin, J., Hildebrandt, I., Tran, C., et al. (2006) Impact of animal handling on the results of 18F-FDG PET studies in mice. *J Nucl Med*. [Online] 47 (6), 999–1006. Available from: doi:47/6/999 [pii].

Fulda, S., Los, M., Friesen, C. & Debatin, K.M. (1998) Chemosensitivity of solid tumor cells in vitro is related to activation of the CD95 system. *International Journal of Cancer*. [Online] 76 (1), 105–114. Available from: doi:10.1002/(SICI)1097-0215(19980330)76:1<105::AID-IJC17>3.0.CO;2-B.

Galluzzi, L., Aaronson, S.A., Abrams, J., Alnemri, E.S., et al. (2009) Guidelines for the use and interpretation of assays for monitoring cell death in higher eukaryotes. *Cell Death and Differentiation*. [Online] 16 (8), 1093–1107. Available from: doi:10.1038/cdd.2009.44.

Gargiulo, S., Greco, A., Gramanzini, M., Esposito, S., et al. (2012) Mice anesthesia, analgesia, and care, Part I: anesthetic considerations in preclinical research. *ILAR journal / National Research Council, Institute of Laboratory Animal Resources*. [Online] 53 (1), E55-69. Available from: doi:10.1093/ilar.53.1.55 [Accessed: 22 October 2014].

Gatta, G., Botta, L., Rossi, S., Aareleid, T., et al. (2014) Childhood cancer survival in Europe 1999-2007: Results of EUROCARE-5-a population-based study. *The Lancet Oncology*. [Online] 15 (1), 35–47. Available from: doi:10.1016/S1470-2045(13)70548-5.

Ghosh, S.P., Kulkarni, S., Hieber, K., Toles, R., et al. (2009) Gamma-tocotrienol, a tocol antioxidant as a potent radioprotector. *International journal of radiation biology*. [Online] 85 (7), 598–606. Available from: doi:10.1080/09553000902985128 [Accessed: 13 January 2015].

Van Goethem, A., Yigit, N., Moreno-Smith, M., Vasudevan, S.A., et al. (2017) Dual targeting of MDM2 and BCL2 as a therapeutic strategy in neuroblastoma. *Oncotarget*. [Online] 8 (34), 57047–57057. Available from: doi:10.18632/oncotarget.18982.

Goldsmith, K.C., Gross, M., Peirce, S., Luyindula, D., et al. (2012) Mitochondrial Bcl-2 Family Dynamics Define Therapy Response and Resistance in Neuroblastoma. *Cancer Research*. [Online] 72 (10), 2565–2577. Available from: doi:10.1158/0008-5472.CAN-11-3603.

Goldsmith, K.C., Lestini, B.J., Gross, M., Ip, L., et al. (2010) BH3 response profiles from neuroblastoma mitochondria predict activity of small molecule Bcl-2 family antagonists. *Cell death and differentiation*. [Online] 17, 872–882. Available from: doi:10.1038/cdd.2009.171.

Goolsby, C., Paniagua, M., Tallman, M. & Gartenhaus, R.B. (2005) Bcl-2 regulatory pathway is functional in chronic lymphocytic leukemia. *Cytometry Part B - Clinical Cytometry*. [Online] 63 (1), 36–46. Available from: doi:10.1002/cyto.b.20034.

Gopalan, Y., Shuaib, I.L., Magosso, E., Ansari, M.A., et al. (2014) Clinical

investigation of the protective effects of palm vitamin E tocotrienols on brain white matter. *Stroke; a journal of cerebral circulation*. [Online] 45 (5), 1422–1428. Available from: doi:10.1161/STROKEAHA.113.004449 [Accessed: 19 January 2015].

Guo, C., White, P.S., Weiss, M.J., Hogarty, M.D., et al. (1999) Allelic deletion at 11q23 is common in MYCN single copy neuroblastomas. *Oncogene*. [Online] 18 (35), 4948–4957. Available from: doi:10.1038/sj.onc.1202887.

Guthrie, N., Gapor, A., Chambers, A.F. & Carroll, K.K. (1997) Inhibition of proliferation of estrogen receptor-negative MDA-MB-435 and -positive MCF-7 human breast cancer cells by palm oil tocotrienols and tamoxifen, alone and in combination. *The Journal of nutrition*. [Online] 127 (3), 544S-548S. Available from: doi:10.1093/jn/127.3.544S.

Hadjidaniel, M.D. & Reynolds, C.P. (2010) Antagonism of cytotoxic chemotherapy in neuroblastoma cell lines by 13-cis-retinoic acid is mediated by the antiapoptotic Bcl-2 family proteins. *Molecular cancer therapeutics*. [Online] 9 (12), 3164–3174. Available from: doi:10.1158/1535-7163.MCT-10-0078.

Ham, J., Costa, C., Sano, R., Lochmann, T.L., et al. (2016) Exploitation of the Apoptosis-Primed State of MYCN-Amplified Neuroblastoma to Develop a Potent and Specific Targeted Therapy Combination. *Cancer Cell*. [Online] 29 (2), 159–172. Available from: doi:10.1016/j.ccell.2016.01.002.

Han, K., Jeng, E.E., Hess, G.T., Morgens, D.W., et al. (2017) Synergistic drug combinations for cancer identified in a CRISPR screen for pairwise genetic interactions. *Nature Biotechnology*. [Online] 35 (5), 463–474. Available from: doi:10.1038/nbt.3834.

Hata, A.N., Engelman, J.A. & Faber, A.C. (2015) The BCL2 family: Key mediators of the apoptotic response to targeted anticancer therapeutics. *Cancer Discovery*. [Online] 5 (5), 475–487. Available from: doi:10.1158/2159-8290.CD-15-0011.

Hixson, E.J., Burdeshaw, J.A., Denine, E.P. & Harrison, S.D. (1979) Comparative subchronic toxicity of all-trans- and 13-cis-retinoic acid in Sprague-Dawley rats. *Toxicology and Applied Pharmacology*. [Online] 47 (2), 359–365. Available from: doi:10.1016/0041-008X(79)90331-4.

Ho, K.S., Poon, P.C., Owen, S.C. & Shoichet, M.S. (2012) Blood vessel hyperpermeability and pathophysiology in human tumour xenograft models of breast cancer: A comparison of ectopic and orthotopic tumours. *BMC Cancer*. [Online] 12 (1), 1. Available from: doi:10.1186/1471-2407-12-579.

Huynh, A.S., Abrahams, D.F., Torres, M.S., Baldwin, M.K., et al. (2011) Development of an orthotopic human pancreatic cancer xenograft model

using ultrasound guided injection of cells. *PLoS ONE*. [Online] 6 (5), 1–9. Available from: doi:10.1371/journal.pone.0020330.

Hwang, G.L., van den Bosch, M. a, Kim, Y.I., Katzenberg, R., et al. (2015) Development of a High-Throughput Molecular Imaging-Based Orthotopic Hepatocellular Carcinoma Model. *Cureus*. [Online] 7 (6). Available from: doi:10.7759/cureus.281.

International Society of Paediatric Oncology Europe Neuroblastoma (2014) *High-Risk Neuroblastoma Study*. [Online]. 2014. Available from: http://www.siopen.org/siopen-studies/current/high-risk-study [Accessed: 11 November 2014].

Jämsä, A., Hasslund, K., Cowburn, R.F., Bäckström, A., et al. (2004) The retinoic acid and brain-derived neurotrophic factor differentiated SH-SY5Y cell line as a model for Alzheimer's disease-like tau phosphorylation. *Biochemical and Biophysical Research Communications*. [Online] 319 (3), 993–1000. Available from: doi:10.1016/j.bbrc.2004.05.075.

Jensen, M.M., Jørgensen, J.T., Binderup, T. & Kjaer, A. (2008) Tumor volume in subcutaneous mouse xenografts measured by microCT is more accurate and reproducible than determined by 18F-FDG-microPET or external caliper. *BMC medical imaging*. [Online] 8 (1), 16. Available from: doi:10.1186/1471-2342-8-16.

Jiang, Q., Rao, X., Kim, C.Y., Freiser, H., et al. (2012) Gamma-tocotrienol induces apoptosis and autophagy in prostate cancer cells by increasing intracellular dihydrosphingosine and dihydroceramide. *International journal of cancer. Journal international du cancer*. [Online] 130 (3), 685–693. Available from: doi:10.1002/ijc.26054 [Accessed: 29 October 2014].

Ju, J., Picinich, S.C., Yang, Z., Zhao, Y., et al. (2010) Cancer-preventive activities of tocopherols and tocotrienols. *Carcinogenesis*. [Online] 31 (4), 533–542. Available from: doi:10.1093/carcin/bgp205 [Accessed: 29 September 2014].

Kannappan, R., Gupta, S.C., Kim, J.H. & Aggarwal, B.B. (2012) Tocotrienols fight cancer by targeting multiple cell signaling pathways. *Genes & nutrition*. [Online] 7 (1), 43–52. Available from: doi:10.1007/s12263-011-0220-3 [Accessed: 29 September 2014].

Karmakar, S., Choudhury, S.R., Banik, N.L. & Ray, S.K. (2011) Induction of Mitochondrial Pathways and Endoplasmic Reticulum Stress for Increasing Apoptosis in Ectopic and Orthotopic Neuroblastoma Xenografts. *Journal of cancer therapy*. [Online] 2 (2), 77–90. Available from: doi:10.4236/jct.2011.22009 [Accessed: 15 October 2014].

Kelly, P.N. & Strasser, a (2011) The role of Bcl-2 and its pro-survival relatives in tumourigenesis and cancer therapy. *Cell death and differentiation*. [Online] 18 (9), 1414–1424. Available from: doi:10.1038/cdd.2011.17.

Kepp, O., Galluzzi, L., Lipinski, M., Yuan, J., et al. (2011) Cell death assays for drug discovery. *Nature Reviews Drug Discovery*. [Online] 10 (3), 221–237. Available from: doi:10.1038/nrd3373.

Khanna, S., Patel, V., Rink, C., Roy, S., et al. (2005) Delivery of orally supplemented α-tocotrienol to vital organs of rats and tocopherol-transport protein deficient mice. *Free Radical Biology and Medicine*. [Online] 39 (10), 1310–1319. Available from: doi:10.1016/j.freeradbiomed.2005.06.013.

Klein, E.A., Thompson, I.M., Tangen, C.M., Crowley, J.J., et al. (2011) Vitamin E and the risk of prostate cancer: the Selenium and Vitamin E Cancer Prevention Trial (SELECT). *JAMA*. [Online] 306 (14), 1549–1556. Available from: doi:10.1001/jama.2011.1437 [Accessed: 25 November 2014].

Koba, W., Jelicks, L. a & Fine, E.J. (2013) MicroPET/SPECT/CT imaging of small animal models of disease. *The American journal of pathology*. [Online] 182 (2), 319–324. Available from: doi:10.1016/j.ajpath.2012.09.025.

Koba, W., Kim, K., Lipton, M.L., Jelicks, L., et al. (2011) Imaging devices for use in small animals. *Seminars in Nuclear Medicine*. [Online] 41 (3), 151–165. Available from: doi:10.1053/j.semnuclmed.2010.12.003.

Konopleva, M., Contractor, R., Tsao, T., Samudio, I., et al. (2006) Mechanisms of apoptosis sensitivity and resistance to the BH3 mimetic ABT-737 in acute myeloid leukemia. *Cancer Cell*. [Online] 10 (5), 375–388. Available from: doi:10.1016/j.ccr.2006.10.006.

Koopman, G., Reutelingsperger, C.P., Kuijten, G.A., Keehnen, R.M., et al. (1994) Annexin V for flow cytometric detection of phosphatidylserine expression on B cells undergoing apoptosis. *Blood*. [Online] 84 (5), 1415–1420. Available from: http://www.ncbi.nlm.nih.gov/pubmed/8068938.

Kuida, K. (2000) Caspase-9. *The international journal of biochemistry & cell biology*. [Online] 32 (2), 121–124. Available from: doi:10.1016/s1357-2725(99)00024-2.

Kulkarni, S.S., Cary, L.H., Gambles, K., Hauer-Jensen, M., et al. (2012) Gamma-tocotrienol, a radiation prophylaxis agent, induces high levels of granulocyte colony-stimulating factor. *International immunopharmacology*. [Online] 14 (4), 495–503. Available from: doi:10.1016/j.intimp.2012.09.001 [Accessed: 12 October 2014].

Kunnumakkara, A.B., Sung, B., Ravindran, J., Diagaradjane, P., et al. (2010) {Gamma}-tocotrienol inhibits pancreatic tumors and sensitizes them to gemcitabine treatment by modulating the inflammatory microenvironment. *Cancer research*. [Online] 70 (21), 8695–8705. Available from: doi:10.1158/0008-5472.CAN-10-2318 [Accessed: 29 October 2014].

Laezza, C., D'Alessandro, A., Paladino, S., Maria Malfitano, A., et al. (2012) Anandamide inhibits the Wnt/β-catenin signalling pathway in human breast cancer MDA MB 231 cells. *European Journal of Cancer*. [Online] 48 (16), 3112–3122. Available from: doi:10.1016/j.ejca.2012.02.062.

Lamers, F., Schild, L., den Hartog, I.J.M., Ebus, M.E., et al. (2012) Targeted BCL2 inhibition effectively inhibits neuroblastoma tumour growth. *European journal of cancer (Oxford, England : 1990)*. [Online] 48 (16), 3093–3103. Available from: doi:10.1016/j.ejca.2012.01.037 [Accessed: 23 September 2014].

Lasorella, A., Iavarone, A. & Israel, M.A. (1995) Differentiation of neuroblastoma enhances Bcl-2 expression and induces alterations of apoptosis and drug resistance. *Cancer Research*. 55 (20), 4711–4716.

Lee, I., Cook, N.R., Gaziano, J.M., Gordon, D., et al. (2005) Vitamin E in the primary prevention of cardiovascular disease and cancer: the Women's Health Study: a randomized controlled trial. *JAMA*. [Online] 294 (1), 56–65. Available from: doi:10.1001/jama.294.1.56 [Accessed: 14 February 2015].

Lestini, B.J., Goldsmith, K.C., Fluchel, M.N., Liu, X., et al. (2009) Mcl1 downregulation sensitizes neuroblastoma to cytotoxic chemotherapy and small molecule Bcl2-family antagonists. *Cancer biology & therapy*. [Online] 8 (16), 1587–1595. Available from: doi:10.1097/OPX.0b013e3182540562.The.

Lim, G.C.C. (2002) Overview of cancer in Malaysia. *Japanese journal of clinical oncology*. [Online] 32 Suppl (Supplement 1), S37-42. Available from: doi:10.1093/jjco/hye132 [Accessed: 11 November 2014].

Lim, S.-W., Loh, H.-S., Ting, K.-N., Bradshaw, T.D., et al. (2014) Cytotoxicity and apoptotic activities of alpha-, gamma- and delta-tocotrienol isomers on human cancer cells. *BMC complementary and alternative medicine*. [Online] 14, 469. Available from: doi:10.1186/1472-6882-14-469.

Lim, Y. & Traber, M.G. (2010) Alpha-Tocopherol Transfer Protein (α-TTP): Insights from Alpha-Tocopherol Transfer Protein Knockout Mice. *Nutrition Research and Practice*. [Online] 1 (4), 247. Available from: doi:10.4162/nrp.2007.1.4.247.

Ling, M.T., Luk, S.U., Al-Ejeh, F. & Khanna, K.K. (2012) Tocotrienol as a potential anticancer agent. *Carcinogenesis*. [Online] 33 (2), 233–239. Available from: doi:10.1093/carcin/bgr261 [Accessed: 23 October 2014].

Lopes, R.B., Gangeswaran, R., McNeish, I.A., Wang, Y., et al. (2007) Expression of the IAP protein family is dysregulated in pancreatic cancer cells and is important for resistance to chemotherapy. *International Journal of Cancer*. [Online] 120 (11), 2344–2352. Available from: doi:10.1002/ijc.22554.

Louis, C.U. & Shohet, J.M. (2015) Neuroblastoma: molecular pathogenesis

and therapy. *Annual review of medicine*. [Online] 66 (Figure 1), 49–63. Available from: doi:10.1146/annurev-med-011514-023121.

Lu, J.J., Pan, W., Hu, Y.J. & Wang, Y.T. (2012) Multi-target drugs: The trend of drug research and development. *PLoS ONE*. [Online] 7 (6). Available from: doi:10.1371/journal.pone.0040262.

Lück, C., Haitjema, C. & Heger, C. (2021) Simple Western: Bringing the Western Blot into the Twenty-First Century. *Methods in Molecular Biology*. [Online] 2261, 481–488. Available from: doi:10.1007/978-1-0716-1186-9_30.

Van Maerken, T., Vandesompele, J., Rihani, A., De Paepe, A., et al. (2009) Escape from p53-mediated tumor surveillance in neuroblastoma: Switching off the p14ARF-MDM2-p53 axis. *Cell Death and Differentiation*. [Online] 16 (12), 1563–1572. Available from: doi:10.1038/cdd.2009.138.

Maguire, L.H., Thomas, A.R. & Goldstein, A.M. (2015) Tumors of the neural crest: Common themes in development and cancer. *Developmental Dynamics*. [Online] 244 (3), 311–322. Available from: doi:10.1002/dvdy.24226.

Manu, K. a, Shanmugam, M.K., Ramachandran, L., Li, F., et al. (2012) First evidence that γ-tocotrienol inhibits the growth of human gastric cancer and chemosensitizes it to capecitabine in a xenograft mouse model through the modulation of NF-κB pathway. *Clinical cancer research : an official journal of the American Association for Cancer Research*. [Online] 18 (8), 2220–2229. Available from: doi:10.1158/1078-0432.CCR-11-2470 [Accessed: 15 October 2014].

Matthay, K.K. (2013) Targeted isotretinoin in neuroblastoma: kinetics, genetics, or absorption. *Clinical cancer research : an official journal of the American Association for Cancer Research*. [Online] 19 (2), 311–313. Available from: doi:10.1158/1078-0432.CCR-12-3313 [Accessed: 19 November 2014].

Matthay, K.K., Reynolds, C.P., Seeger, R.C., Shimada, H., et al. (2009) Long-term results for children with high-risk neuroblastoma treated on a randomized trial of myeloablative therapy followed by 13-cis-retinoic acid: a children's oncology group study. *Journal of clinical oncology : official journal of the American Society of Clinical Oncology*. [Online] 27 (7), 1007–1013. Available from: doi:10.1200/JCO.2007.13.8925 [Accessed: 29 October 2014].

Matthay, K.K., Villablanca, J.G., Seeger, R.C., Stram, D.O., et al. (1999) Treatment of high-risk neuroblastoma with intensive chemotherapy, radiotherapy, autologous bone marrow transplantation, and 13-cis-retinoic acid. Children's Cancer Group. *The New England journal of medicine*. [Online] 341 (16), 1165–1173. Available from: doi:10.1056/NEJM199910143411601 [Accessed: 25 February 2015].

Mazlan, M., Sue Mian, T., Mat Top, G. & Wan Ngah, W.Z. (2006) Comparative effects of alpha-tocopherol and gamma-tocotrienol against hydrogen peroxide induced apoptosis on primary-cultured astrocytes. *Journal of the neurological sciences*. [Online] 243 (1–2), 5–12. Available from: doi:10.1016/j.jns.2005.10.006 [Accessed: 23 September 2014].

Meganathan, P. & Fu, J.Y. (2016) Biological properties of tocotrienols: Evidence in human studies. *International Journal of Molecular Sciences*. [Online] 17 (11). Available from: doi:10.3390/ijms17111682.

Mérino, D., Khaw, S.L., Glaser, S.P., Anderson, D.J., et al. (2012) Bcl-2, Bcl-x L, and Bcl-w are not equivalent targets of ABT-737 and navitoclax (ABT-263) in lymphoid and leukemic cells. *Blood*. [Online] 119 (24), 5807–5816. Available from: doi:10.1182/blood-2011-12-400929 [Accessed: 23 September 2014].

Milanovic, D., Sticht, C., Röhrich, M., Maier, P., et al. (2015) Inhibition of 13-cis retinoic acid-induced gene expression of reactive-resistance genes by thalidomide in glioblastoma tumours in vivo. *Oncotarget*. [Online] 6 (30), 28938–28948. Available from: doi:10.18632/oncotarget.4727.

Miquel, C., Borrini, F., Grandjouan, S., Aupérin, A., et al. (2005) Role of bax mutations in apoptosis in colorectal cancers with microsatellite instability. *American Journal of Clinical Pathology*. [Online] 123 (4), 562–570. Available from: doi:10.1309/JQ2X3RV3L8F9TGYW.

Monni, O., Joensuu, H., Franssila, K., Klefstrom, J., et al. (1997) BCL2 overexpression associated with chromosomal amplification in diffuse large B-cell lymphoma. *Blood*. 90 (3), 1168–1174.

Müller, M., Wilder, S., Bannasch, D., Israeli, D., et al. (1998) p53 activates the CD95 (APO-1/Fas) gene in response to DNA damage by anticancer drugs. *Journal of Experimental Medicine*. [Online] 188 (11), 2033–2045. Available from: doi:10.1084/jem.188.11.2033.

Nakagawara, A., Li, Y., Izumi, H., Muramori, K., et al. (2018) Neuroblastoma. *Japanese Journal of Clinical Oncology*. [Online] 48 (3), 214–241. Available from: doi:10.1093/jjco/hyx176.

Nalluri, S., Peirce, S.K., Tanos, R., Abdella, H.A., et al. (2015) EGFR signaling defines Mcl - 1 survival dependency in neuroblastoma. *Cancer Biology and Therapy*. [Online] 16 (2), 276–286. Available from: doi:10.1080/15384047.2014.1002333.

National Cancer Institute (2014) *Neuroblastoma Treatment (PDQ ®) Health Professional Version Treatment Option Overview for Neuroblastoma*. [Online]. 2014. Available from: http://www.cancer.gov/cancertopics/pdq/treatment/neuroblastoma/HealthProfessional/page4 [Accessed: 11 November 2014].

Nesaretnam, K. (2008) Multitargeted therapy of cancer by tocotrienols. *Cancer letters*. [Online] 269 (2), 388–395. Available from:

doi:10.1016/j.canlet.2008.03.063 [Accessed: 29 September 2014].

Nesaretnam, K., Ambra, R., Selvaduray, K.R., Radhakrishnan, A., et al. (2004) Tocotrienol-rich fraction from palm oil affects gene expression in tumors resulting from MCF-7 cell inoculation in athymic mice. *Lipids*. [Online] 39 (5), 459–467. Available from: doi:10.1007/s11745-004-1251-1.

Nesaretnam, K., Meganathan, P., Veerasenan, S.D. & Selvaduray, K.R. (2012) Tocotrienols and breast cancer: the evidence to date. *Genes & nutrition*. [Online] 7 (1), 3–9. Available from: doi:10.1007/s12263-011-0224-z [Accessed: 17 December 2014].

Nesaretnam, K., Selvaduray, K.R., Abdul Razak, G., Veerasenan, S.D., et al. (2010) Effectiveness of tocotrienol-rich fraction combined with tamoxifen in the management of women with early breast cancer: A pilot clinical trial. *Breast Cancer Research*. [Online] 12 (5). Available from: doi:10.1186/bcr2726.

Ng, S.M., Abdullah, W.A., Lin, H.P. & Chan, L.L. (1999) Presenting features and treatment outcome of 78 Malaysian children with neuroblastoma. *The Southeast Asian journal of tropical medicine and public health*. [Online] 30 (1), 149–153. Available from: http://www.ncbi.nlm.nih.gov/pubmed/10695803 [Accessed: 30 January 2015].

Niizuma, H., Nakamura, Y., Ozaki, T., Nakanishi, H., et al. (2006) Bcl-2 is a key regulator for the retinoic acid-induced apoptotic cell death in neuroblastoma. *Oncogene*. [Online] 25 (36), 5046–5055. Available from: doi:10.1038/sj.onc.1209515.

Olejniczak, E.T., Van Sant, C., Anderson, M.G., Wang, G., et al. (2007) Integrative genomic analysis of small-cell lung carcinoma reveals correlates of sensitivity to Bcl-2 antagonists and uncovers novel chromosomal gains. *Molecular Cancer Research*. [Online] 5 (4), 331–339. Available from: doi:10.1158/1541-7786.MCR-06-0367.

Oltersdorf, T., Elmore, S.W., Shoemaker, A.R., Armstrong, R.C., et al. (2005) An inhibitor of Bcl-2 family proteins induces regression of solid tumours. *Nature*. [Online] 435 (7042), 677–681. Available from: doi:10.1038/nature03579 [Accessed: 10 July 2014].

Otsuka, K., Sasada, M., Iyoda, T., Nohara, Y., et al. (2019) Combining peptide TNIIIA2 with all-trans retinoic acid accelerates N-Myc protein degradation and neuronal differentiation in MYCN-amplified neuroblastoma cells. *American journal of cancer research*. [Online] 9 (2), 434–448. Available from: http://www.ncbi.nlm.nih.gov/pubmed/30906641%0Ahttp://www.pubmedcentral.nih.gov/articlerender.fcgi?artid=PMC6405964.

Paediatric Formulary Committee (2014) *BNF for Children (BNFC) [online]*. 2014th–2015th edition. [Online]. 2014. Available from:

https://www.medicinescomplete.com/mc/bnfc/current/index.htm [Accessed: 15 April 2015].

Parajuli, P., Tiwari, R. V. & Sylvester, P.W. (2015) Anti-proliferative effects of γ-tocotrienol are associated with suppression of c-Myc expression in mammary tumour cells. *Cell Proliferation*. [Online] 48 (4), 421–435. Available from: doi:10.1111/cpr.12196.

Park, J.R., Bagatell, R., London, W.B., Maris, J.M., et al. (2013) Children's Oncology Group's 2013 blueprint for research: neuroblastoma. *Pediatric blood & cancer*. [Online] 60 (October 2012), 985–993. Available from: doi:10.1002/pbc.

Peinemann, F., van Dalen, E.C., Enk, H. & Berthold, F. (2017) Retinoic acid postconsolidation therapy for high-risk neuroblastoma patients treated with autologous haematopoietic stem cell transplantation. *The Cochrane database of systematic reviews*. [Online] 8 (8), CD010685. Available from: doi:10.1002/14651858.CD010685.pub3.

Peinemann, F., van Dalen, E.C., Tushabe, D.A. & Berthold, F. (2015) Retinoic acid post consolidation therapy for high-risk neuroblastoma patients treated with autologous hematopoietic stem cell transplantation. *Cochrane Database of Systematic Reviews 2015*. [Online] CD010685 (1). Available from: doi:10.1002/14651858.CD003983.pub2.

PerkinElmer Informatics (2019) *ChemDraw Professional 16.0*.

Pinto, N.R., Applebaum, M.A., Volchenboum, S.L., Matthay, K.K., et al. (2015) Advances in risk classification and treatment strategies for neuroblastoma. *Journal of Clinical Oncology*. [Online] 33 (27), 3008–3017. Available from: doi:10.1200/JCO.2014.59.4648.

Prasad, S., Gupta, S.C., Tyagi, A.K. & Aggarwal, B.B. (2016) γ-Tocotrienol suppresses growth and sensitises human colorectal tumours to capecitabine in a nude mouse xenograft model by down-regulating multiple molecules. *British journal of cancer*. [Online] 115 (7), 814–824. Available from: doi:10.1038/bjc.2016.257.

Promega (2012) *CellTiter 96® Aqueous One Solution Cell Proliferation Assay Protocol, Instruction for use of products G3580, G3581 and G3582. [Online document]. 12.2012 [zuletzt aufgerufen am 05.09.2017]. Verfügbar unter: https://www.promega.de/-/media/files/resources/pr*. [Online]. Available from: https://www.promega.de/-/media/files/resources/protocols/technical-bulletins/0/celltiter-96-aqueous-one-solution-cell-proliferation-assay-system-protocol.pdf.

Ramsay, R.R., Popovic-Nikolic, M.R., Nikolic, K., Uliassi, E., et al. (2018) A perspective on multi-target drug discovery and design for complex diseases. *Clinical and Translational Medicine*. [Online] 7 (1). Available from: doi:10.1186/s40169-017-0181-2.

Reagan-Shaw, S., Nihal, M. & Ahmad, N. (2008) Dose translation from animal

to human studies revisited. *The FASEB journal : official publication of the Federation of American Societies for Experimental Biology*. [Online] 22 (3), 659–661. Available from: doi:10.1096/fj.07-9574LSF.

Reed, J.C., Meister, L., Tanaka, S., Cuddy, M., et al. (1991) Differential Expression of bcl2 Protooncogene in Neuroblastoma and Other Human Tumor Cell Lines of Neural Origin. *Cancer Research*. 51 (24), 6529–6538.

Reesink-Peters, N., Hougardy, B.M.T., Van Den Heuvel, F.A.J., Ten Hoor, K.A., et al. (2005) Death receptors and ligands in cervical carcinogenesis: An immunohistochemical study. *Gynecologic Oncology*. [Online] 96 (3), 705–713. Available from: doi:10.1016/j.ygyno.2004.10.046.

Reynolds, C.P., Matthay, K.K., Villablanca, J.G. & Maurer, B.J. (2003) Retinoid therapy of high-risk neuroblastoma. *Cancer Letters*. [Online] 197 (1–2), 185–192. Available from: doi:10.1016/S0304-3835(03)00108-3 [Accessed: 29 October 2014].

Reynolds, C.P., Schindler, P.F., Jones, D.M., Gentile, J.L., et al. (1994) Comparison of 13-cis-retinoic acid to trans-retinoic acid using human neuroblastoma cell lines. *Progress in clinical and biological research*. [Online] 385, 237–244. Available from: http://www.ncbi.nlm.nih.gov/pubmed/7972215.

Riccardi, C. & Nicoletti, I. (2006) Analysis of apoptosis by propidium iodide staining and flow cytometry. *Nature Protocols*. [Online] 1 (3), 1458–1461. Available from: doi:10.1038/nprot.2006.238.

Sailo, B.L., Banik, K., Padmavathi, G., Javadi, M., et al. (2018) Tocotrienols: The promising analogues of vitamin E for cancer therapeutics. *Pharmacological research*. [Online] 130, 259–272. Available from: doi:10.1016/j.phrs.2018.02.017.

Schleiermacher, G., Janoueix-Lerosey, I. & Delattre, O. (2014) Recent insights into the biology of neuroblastoma. *International journal of cancer. Journal international du cancer*. [Online] 135 (10), 2249–2261. Available from: doi:10.1002/ijc.29077 [Accessed: 28 November 2014].

Schott, A.F., Apel, I.J., Nuñez, G. & Clarke, M.F. (1995) Bcl-XL protects cancer cells from p53-mediated apoptosis. *Oncogene*. [Online] 11 (7), 1389–1394. Available from: http://www.ncbi.nlm.nih.gov/pubmed/7478561.

Seeger, R.C., Brodeur, G.M., Sather, H., Dalton, A., et al. (1985) Association of multiple copies of the N-myc oncogene with rapid progression of neuroblastomas. *The New England journal of medicine*. [Online] 313 (18), 1111–1116. Available from: doi:10.1056/NEJM198510313131802 [Accessed: 23 February 2015].

Sen, C.K., Khanna, S. & Roy, S. (2006) Tocotrienols: Vitamin E beyond tocopherols. *Life sciences*. [Online] 78 (18), 2088–2098. Available from:

doi:10.1016/j.lfs.2005.12.001 [Accessed: 15 December 2014].

Shapiro, D.N., Valentine, M.B., Rowe, S.T., Sinclair, A.E., et al. (1993) Detection of N-myc gene amplification by fluorescence in situ hybridization: Diagnostic utility for neuroblastoma. *American Journal of Pathology*. 142 (5), 1339–1346.

Shelake, S., Eslin, D., Sutphin, R.M., Sankpal, U.T., et al. (2015) Combination of 13 cis-retinoic acid and tolfenamic acid induces apoptosis and effectively inhibits high-risk neuroblastoma cell proliferation. *International Journal of Developmental Neuroscience*. [Online] 46, 92–99. Available from: doi:10.1016/j.ijdevneu.2015.07.012.

Shen, X.G., Wang, C., Li, Y., Wang, L., et al. (2010) Downregulation of caspase-9 is a frequent event in patients with stage II colorectal cancer and correlates with poor clinical outcome. *Colorectal Disease*. [Online] 12 (12), 1213–1218. Available from: doi:10.1111/j.1463-1318.2009.02009.x.

Shoemaker, A.R., Mitten, M.J., Adickes, J., Ackler, S., et al. (2008) Activity of the Bcl-2 family inhibitor ABT-263 in a panel of small cell lung cancer xenograft models. *Clinical cancer research : an official journal of the American Association for Cancer Research*. [Online] 14 (11), 3268–3277. Available from: doi:10.1158/1078-0432.CCR-07-4622 [Accessed: 15 October 2014].

Shuangshoti, S., Shuangshoti, S., Nuchprayoon, I., Kanjanapongkul, S., et al. (2012) Natural course of low risk neuroblastoma. *Pediatric blood & cancer*. [Online] 58 (5), 690–694. Available from: doi:10.1002/pbc.23325 [Accessed: 30 January 2015].

Singh, V.K., Beattie, L. a & Seed, T.M. (2013) Vitamin E: tocopherols and tocotrienols as potential radiation countermeasures. *Journal of radiation research*. [Online] 54 (6), 973–988. Available from: doi:10.1093/jrr/rrt048 [Accessed: 23 October 2014].

Slatter, T.L., Hung, N., Campbell, H., Rubio, C., et al. (2011) Hyperproliferation, cancer, and inflammation in mice expressing a Δ133p53-like isoform. *Blood*. [Online] 117 (19), 5166–5177. Available from: doi:10.1182/blood-2010-11-321851.

Small, S., Keerthivasan, G., Huang, Z., Gurbuxani, S., et al. (2010) Overexpression of survivin initiates hematologic malignancies in vivo. *Leukemia*. [Online] 24 (11), 1920–1926. Available from: doi:10.1038/leu.2010.198.

Smith, S.M., Wunder, M.B., Norris, D.A. & Shellman, Y.G. (2011) A simple protocol for using a LDH-Based cytotoxicity assay to assess the effects of death and growth inhibition at the same time. *PLoS ONE*. [Online] 6 (11). Available from: doi:10.1371/journal.pone.0026908.

Smith, V. & Foster, J. (2018) High-Risk Neuroblastoma Treatment Review. *Children*. [Online] 5 (9), 114. Available from:

doi:10.3390/children5090114.

Sokol, E. & Desai, A. (2019) The Evolution of Risk Classification for Neuroblastoma. *Children*. [Online] 6 (2), 27. Available from: doi:10.3390/children6020027.

Souers, A.J., Leverson, J.D., Boghaert, E.R., Ackler, S.L., et al. (2013) ABT-199, a potent and selective BCL-2 inhibitor, achieves antitumor activity while sparing platelets. *Nature Medicine*. [Online] 19 (2), 202–208. Available from: doi:10.1038/nm.3048.

Sylvester, P.W. (2012) Synergistic anticancer effects of combined γ-tocotrienol with statin or receptor tyrosine kinase inhibitor treatment. *Genes & Nutrition*. [Online] 7 (1), 63–74. Available from: doi:10.1007/s12263-011-0225-y.

Tan, A.M. & Ha, C. (2005) *First Report of the Singapore Childhood Cancer Registry (1997-2005)*. [Online]. Available from: https://www.nrdo.gov.sg/uploadedFiles/NRDO/Publications/Spore Childhood Cancer.Registry Report.pdf.

Tan, J.-K., Then, S.-M., Mazlan, M., Raja Abdul Rahman, R.N.Z., et al. (2016) Gamma-tocotrienol acts as a BH3 mimetic to induce apoptosis in neuroblastoma SH-SY5Y cells. *The Journal of Nutritional Biochemistry*. [Online] 31, 28–37. Available from: doi:10.1016/j.jnutbio.2015.12.019.

Tang, X.X., Zhao, H., Kung, B., Kim, D.Y., et al. (2006) The MYCN enigma: significance of MYCN expression in neuroblastoma. *Cancer research*. [Online] 66 (5), 2826–2833. Available from: doi:10.1158/0008-5472.CAN-05-0854 [Accessed: 13 February 2015].

Tanos, R., Karmali, D., Nalluri, S. & Goldsmith, K.C. (2016) Select Bcl-2 antagonism restores chemotherapy sensitivity in high-risk neuroblastoma. *BMC Cancer*. [Online] 16 (1), 1–9. Available from: doi:10.1186/s12885-016-2129-0s.

Teijido, O. & Dejean, L. (2010) Upregulation of Bcl2 inhibits apoptosis-driven BAX insertion but favors BAX relocalization in mitochondria. *FEBS letters*. [Online] 584 (15), 3305–3310. Available from: doi:10.1016/j.febslet.2010.07.002 [Accessed: 23 September 2014].

Teitz, T., Stanke, J.J., Federico, S., Bradley, C.L., et al. (2011) Preclinical models for neuroblastoma: establishing a baseline for treatment. *PloS one*. [Online] 6 (4), e19133. Available from: doi:10.1371/journal.pone.0019133 [Accessed: 20 October 2014].

Tham, S.Y., Loh, H.S., Mai, C.W. & Fu, J.Y. (2019) Tocotrienols modulate a life or death decision in cancers. *International Journal of Molecular Sciences*. [Online] 20 (2). Available from: doi:10.3390/ijms20020372.

Then, S.-M., Sanfeliu, C., Top, G.M., Wan Ngah, W.Z., et al. (2012) γ-Tocotrienol does not substantially protect DS neurons from hydrogen

peroxide-induced oxidative injury. *Nutrition & metabolism*. [Online] 9, 1. Available from: doi:10.1186/1743-7075-9-1 [Accessed: 23 September 2014].

Then, S.M., Mazlan, M., Mat Top, G. & Wan Ngah, W.Z. (2009) Is vitamin E toxic to neuron cells? *Cellular and molecular neurobiology*. [Online] 29 (4), 485–496. Available from: doi:10.1007/s10571-008-9340-8 [Accessed: 23 September 2014].

Theriault, A., Chao, J., Wang, Q., Gapor, A., et al. (1999) Tocotrienol: a review of its therapeutic potential. *Clinical Biochemistry*. [Online] 32 (5), 309–319. Available from: doi:10.1016/S0009-9120(99)00027-2 [Accessed: 1 November 2014].

Thornborrow, E.C., Patel, S., Mastropietro, A.E., Schwartzfarb, E.M., et al. (2002) A conserved intronic response element mediates direct p53-dependent transcriptional activation of both the human and murine bax genes. *Oncogene*. [Online] 21 (7), 990–999. Available from: doi:10.1038/sj.onc.1205069.

Toma, S., Isnardi, L., Raffo, P., Dastoli, G., et al. (1997) Effects of all-trans-retinoic acid and 13-cis-retinoic acid on breast-cancer cell lines: Growth inhibition and apoptosis induction. *International Journal of Cancer*. [Online] 70 (5), 619–627. Available from: doi:10.1002/(SICI)1097-0215(19970304)70:5<619::AID-IJC21>3.0.CO;2-6.

Tse, C., Shoemaker, A.R., Adickes, J., Anderson, M.G., et al. (2008) ABT-263: a potent and orally bioavailable Bcl-2 family inhibitor. *Cancer research*. [Online] 68 (9), 3421–3428. Available from: doi:10.1158/0008-5472.CAN-07-5836 [Accessed: 15 October 2014].

Vandenberg, C.J. & Cory, S. (2013) ABT-199, a new Bcl-2-specific BH3 mimetic, has in vivo efficacy against aggressive Myc-driven mouse lymphomas without provoking thrombocytopenia. *Blood*. [Online] 121 (12), 2285–2288. Available from: doi:10.1182/blood-2013-01-475855.

Veal, G.J., Errington, J., Rowbotham, S.E., Illingworth, N. a, et al. (2013) Adaptive dosing approaches to the individualization of 13-cis-retinoic acid (isotretinoin) treatment for children with high-risk neuroblastoma. *Clinical cancer research : an official journal of the American Association for Cancer Research*. [Online] 19 (2), 469–479. Available from: doi:10.1158/1078-0432.CCR-12-2225 [Accessed: 18 November 2014].

Vikhanskaya, F., Lee, M.K., Mazzoletti, M., Broggini, M., et al. (2007) Cancer-derived p53 mutants suppress p53-target gene expression - Potential mechanism for gain of function of mutant p53. *Nucleic Acids Research*. [Online] 35 (6), 2093–2104. Available from: doi:10.1093/nar/gkm099.

Waetzig, V., Haeusgen, W., Andres, C., Frehse, S., et al. (2019) Retinoic acid-induced survival effects in SH-SY5Y neuroblastoma cells. *Journal of*

cellular biochemistry. [Online] 120 (4), 5974–5986. Available from: doi:10.1002/jcb.27885.

Wagner, A.D., Syn, N.L.X., Moehler, M., Grothe, W., et al. (2017) Chemotherapy for advanced gastric cancer. *Cochrane Database of Systematic Reviews*. [Online] 2017 (8). Available from: doi:10.1002/14651858.CD004064.pub4.

Walensky, L.D. (2006) BCL-2 in the crosshairs: Tipping the balance of life and death. *Cell Death and Differentiation*. [Online] 13 (8), 1339–1350. Available from: doi:10.1038/sj.cdd.4401992.

Wali, V.B. & Sylvester, P.W. (2007) Synergistic antiproliferative effects of γ-tocotrienol and statin treatment on mammary tumor cells. *Lipids*. [Online] 42 (12), 1113–1123. Available from: doi:10.1007/s11745-007-3102-0.

Wang, X., Gu, Z., Li, G., Zhang, S., et al. (2014) Norcantharidin enhances ABT-263-mediated anticancer activity in neuroblastoma cells by upregulation of Noxa. *Oncology Reports*. [Online] 32 (2), 716–722. Available from: doi:10.3892/or.2014.3228.

Wang, Y., Tseng, J.-C., Sun, Y., Beck, A.H., et al. (2015) Noninvasive Imaging of Tumor Burden and Molecular Pathways in Mouse Models of Cancer. *Cold Spring Harbor Protocols*. [Online] 2015 (2), 135–144. Available from: doi:10.1101/pdb.top069930.

Ward, E., DeSantis, C., Robbins, A., Kohler, B., et al. (2014) Childhood and adolescent cancer statistics, 2014. *CA: a cancer journal for clinicians*. [Online] 64 (2), 83–103. Available from: doi:10.3322/caac.21219 [Accessed: 24 October 2014].

Wei, A.H., Strickland, S.A., Hou, J.Z., Fiedler, W., et al. (2019) Venetoclax combined with low-dose cytarabine for previously untreated patients with acute myeloid leukemia: Results from a phase Ib/II study. *Journal of Clinical Oncology*. [Online] 37 (15), 1277–1284. Available from: doi:10.1200/JCO.18.01600.

Wilkins, R.C., Kutzner, B.C., Truong, M., Sanchez-Dardon, J., et al. (2002) Analysis of radiation-induced apoptosis in human lymphocytes: Flow cytometry using Annexin V and propidium iodide versus the neutral comet assay. *Cytometry*. [Online] 48 (1), 14–19. Available from: doi:10.1002/cyto.10098.

Wong, C., Anderson, D.J., Lee, E.F., Fairlie, W.D., et al. (2012a) Direct visualization of Bcl-2 family protein interactions using live cell fluorescent protein redistribution assays. *Cell death & disease*. [Online] 3 (3), e288. Available from: doi:10.1038/cddis.2012.28 [Accessed: 15 October 2014].

Wong, R.S.Y. & Radhakrishnan, A.K. (2012) Tocotrienol research: past into present. *Nutrition reviews*. [Online] 70 (9), 483–490. Available from: doi:10.1111/j.1753-4887.2012.00512.x [Accessed: 29 September 2014].

Wong, W.Y., Poudyal, H., Ward, L.C. & Brown, L. (2012b) Tocotrienols reverse cardiovascular, metabolic and liver changes in high carbohydrate, high fat diet-fed rats. *Nutrients*. [Online] 4 (10), 1527–1541. Available from: doi:10.3390/nu4101527.

Workman, P., Aboagye, E.O., Balkwill, F., Balmain, a, et al. (2010) Guidelines for the welfare and use of animals in cancer research. *British journal of cancer*. [Online] 102 (11), 1555–1577. Available from: doi:10.1038/sj.bjc.6605642 [Accessed: 21 September 2014].

Würstle, M.L., Laussmann, M.A. & Rehm, M. (2012) The central role of initiator caspase-9 in apoptosis signal transduction and the regulation of its activation and activity on the apoptosome. *Experimental Cell Research*. [Online] 318 (11), 1213–1220. Available from: doi:10.1016/j.yexcr.2012.02.013.

Yalçin, B., Kremer, L., Caron, H. & van Dalen, E. (2013) High-dose chemotherapy and autologous haematopoietic stem cell rescue for children with high-risk neuroblastoma (Review). *Cochrane Database of Systematic Reviews 2013*. [Online] (8). Available from: doi:10.1002/14651858.CD006301.pub3.

Yang, P.-C. & Mahmood, T. (2012) Western blot: Technique, theory, and trouble shooting. *North American Journal of Medical Sciences*. [Online] 4 (9), 429. Available from: doi:10.4103/1947-2714.100998.

Yap, W.N., Chang, P.N., Han, H.Y., Lee, D.T.W., et al. (2008) Gamma-tocotrienol suppresses prostate cancer cell proliferation and invasion through multiple-signalling pathways. *British journal of cancer*. [Online] 99 (11), 1832–1841. Available from: doi:10.1038/sj.bjc.6604763 [Accessed: 29 September 2014].

Yusof, K., Makpol, S., Jamal, R., Harun, R., et al. (2015) γ-Tocotrienol and 6-Gingerol in Combination Synergistically Induce Cytotoxicity and Apoptosis in HT-29 and SW837 Human Colorectal Cancer Cells. *Molecules*. [Online] 20 (6), 10280–10297. Available from: doi:10.3390/molecules200610280.

Zhang, S., Kuang, G., Zhao, G., Wu, X., et al. (2013) Involvement of the mitochondrial p53 pathway in PBDE-47-induced SH-SY5Y cells apoptosis and its underlying activation mechanism. *Food and Chemical Toxicology*. [Online] 62, 699–706. Available from: doi:10.1016/j.fct.2013.10.008.

Zingg, J.-M. (2007) Vitamin E: an overview of major research directions. *Molecular aspects of medicine*. [Online] 28 (5–6), 400–422. Available from: doi:10.1016/j.mam.2007.05.004 [Accessed: 17 December 2014].

APPENDIX A

Table A1: Signs of pain and distress in laboratory rodents and lagomorphs (Baumans *et al.*, 1994) and additional note from The University of Nottingham Animal Ethic Committee.

Mild	**Moderate**	**Substantial**
Reduced weight gain or weight loss of up to 10%	Weight loss of up to 20%	Weight loss greater than 25%
Food and water consumption 40-70% of normal for 72hrs	Food and water consumption <40% of normal for 72hrs	Food and water consumption less than 40% for 7 days
Partial piloerection	Staring coat and marked piloerection	Anorexia (total inappetence) for 72 hrs
Subdued but responsive, animal shows normal provoked patterns of behaviour	Subdued animal shows subdued behaviour patterns even when provoked	Staring coat –marked piloerection with other signs of dehydration such as skin tenting
Interacts with peers	Little peer interaction	Unresponsive to extraneous activity and provocation
Transiently hunched especially after dosing	Hunched intermittently	Hunched persistently (frozen)
Transient vocalisation	Intermittent vocalisation when provoked	Distressed - vocalisation unprovoked

Continued…

…continued

Oculo-nasal discharge transient (typical signs of chromorhinodacryorrhoea in rodents)	Oculo-nasal discharge persistent	Oculo-nasal discharge –persistent and copious
Normal respiration	Intermittent abnormal breathing patterns	Laboured respiration
Transient tremors	Intermittent tremors	Persistent tremors
No convulsions	Intermittent convulsions	Persistent convulsions
No prostration	Transient prostration (<1hr)	Prolonged prostration (>1hr)
	No self-mutilation	Self-mutilation.

Note: Action required at the University of Nottingham:

The clinical signs listed represent the upper limit of severity in each category.

Observation of a combination of signs of moderate severity should result in immediate action such as cessation of dosing, amelioration of the signs by treatment, euthanasia. The Named Persons or their nominees should be informed.

Observation of a single clinical sign from the substantial severity limit should result in immediate action (usually euthanasia). The Named Persons or their nominees should be informed.

APPENDIX B

JESS PROTEIN ASSAY

Jess protein analysis is an automated western blotting process that uses a capillary based system to reduce time and reagents compared to traditional western blot. Furthermore, the automation reduces many steps that may cause errors, as well as reduces the amount of protein sample required (Lück, Haitjema & Heger, 2021).

The western blot results from the tissue samples were not very conclusive (Figure 4.22). However, we still had a small amount of protein from the tumour tissues. Additionally, we wanted to attempt using activated caspases instead of the procaspases. Due to the limited time and tissue samples, we chose to consult a professional service (Biomed Global) that would carry out the Jess assay for us. This assay was carried out in order to both assess the usefulness of the Jess system in our lab, as well as to add to the current data we obtained from traditional western blot.

Method

Protein samples from ectopic tumours were extracted and protein concentration determined as described in *Sections 3.3.8.2 and 3.3.8.3*, respectively. All five treatment groups from the *in vivo* study were assessed: no vehicle control, 13cRA only, γT3 only, γT3 and 13cRA, and ABT-263 and 13cRA (*Section 3.3*).

The following polyclonal antibodies were used:

Table B1: Details of primary antibodies used in Jess Protein Assay

Antibody	Cat. No.	Manufacturer	Dilution Factor	MW
Caspase-9	E-AB-63242	Elabscience	1:10	37kDa/47kDa
Cleaved-CASP3 p17	E-AB-30004	Elabscience	1:10	20-32kDa
p53	E-AB-32469	Elabscience	1:10	43-44 kDa
MYCN	E-AB-62132	Elabscience	1:10	45-49 kDa

The amount of protein required for each sample was 3µg, and each sample was diluted in 0.1X sample buffer and then denatured at 95°C for 5 minutes, and then vortexed and spun down. and the ProteinSimple Jess system (Bio-Techne, USA) was loaded according to the microplate layout in *Figure B1*, as provided by Biomed Global.

Figure B1: Layout of Jess automated system microplate. The microplate was laid out with wells from A1 to F25, with reagents and/or samples transferred to each well as per the manufacturer's protocol. Samples, each containing 3µg of protein each were added to wells in row A2-21. Rows 22 to 25 were no lysate controls for each antibody. Protein normalization reagent was added to row B for automatic normalisation when the software analyses the bands. Row C contained antibody diluent (10µL/well). Four antibodies were used at a 1:10 dilution (row D), while secondary anti-rabbit antibodies provided in the kit) were added to row E. Row F contained the luminol. Finally, A1 contained 5µL of the biotinylated ladder (12-230kDa) and E1 had 10µL Streptavidin-NIR, a fluorescence biotin binding protein.

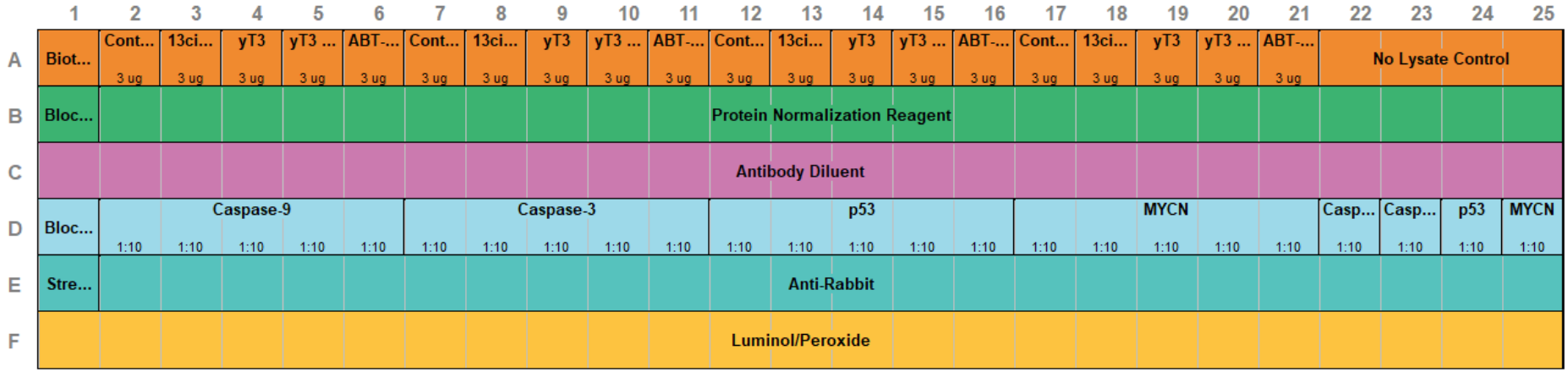

After the microplate was filled as per *Figure B1*, the plate was centrifuged for 5 minutes at 1000xg at room temperature before being placed into the Jess automated system. The microplate was read using the fluorescence immunoassay setting with Compass Software (Bio-Techne, USA) and after the run was complete, image analysis was also performed using Compass Software. Protein normalisation is automatically calculated by the software. Biomed Global analysed the images and provided a full report.

Results

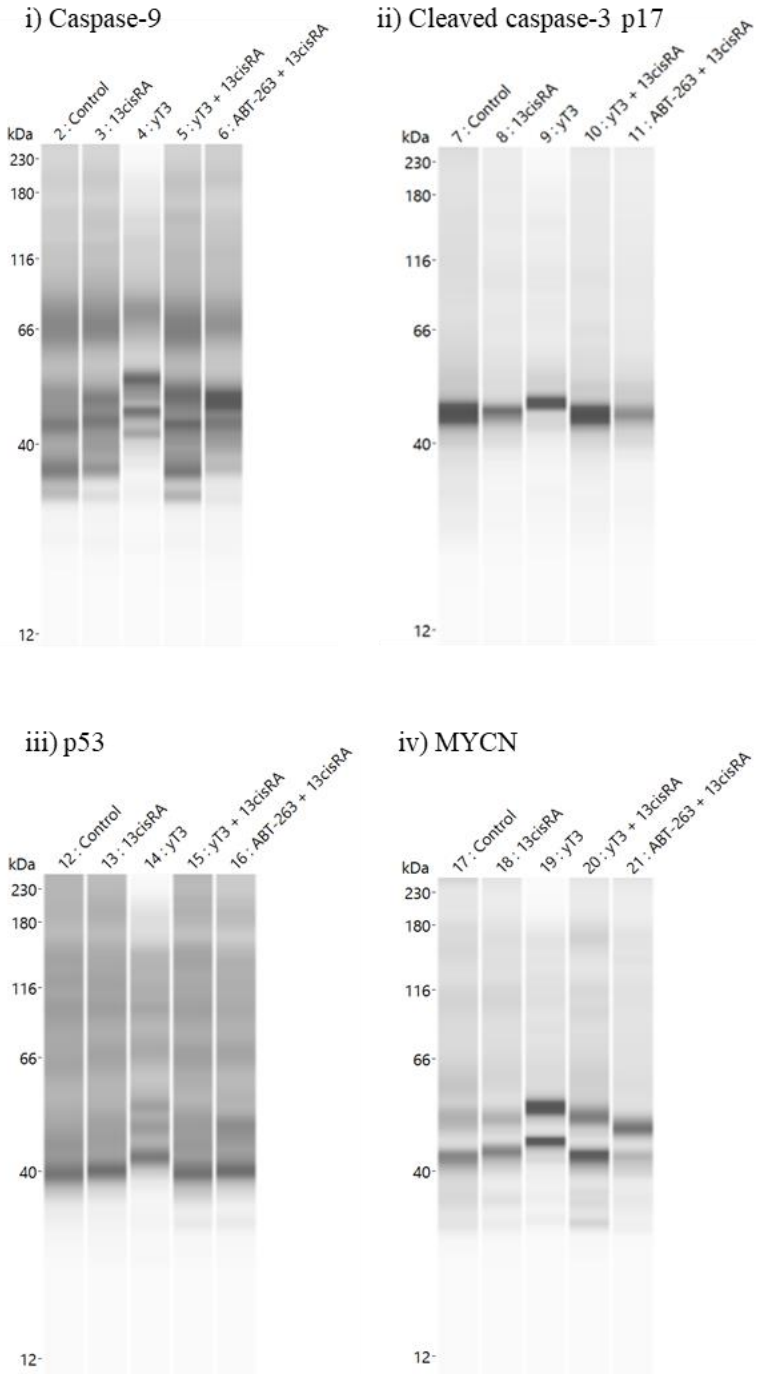

Figure B2: Effect of 13cRA and γT3, alone and in combination, and ABT-263 in combination with 13cRA, compared to vehicle only control on protein expression of (i) caspase-9, (ii)cleaved caspase-3 p-17, (iii) p53 and (iv) MYCN, in ectopic tumours grown in nude mice from an SH-SY5Y neuroblastoma cell line. Bands were obtained from Jess protein assay. No statistical test performed as n=1.

Table B2: Summary of relative density values, obtained from Jess protein assay. Samples were obtained from ectopic mouse tumours (grown from SH-SY5Y cell lines) and subjected to 5 treatment groups, including untreated control. No statistical test performed as n=1.

	Density (relative units)				
	Control	**13cisRA**	**yT3**	**yT3 + 13cisRA**	**ABT-263 + 13cisRA**
caspase-9 (37kDa)	1.00	1.28	1.39	1.09	1.53
caspase-9 (47kDa)	1.00	1.03	0.98	0.88	1.00
caspase-3	1.00	0.73	1.26	0.80	0.71
p53	1.00	0.87	1.50	0.82	1.09
MYCN	1.00	1.00	1.95	1.12	0.95

APPENDIX C

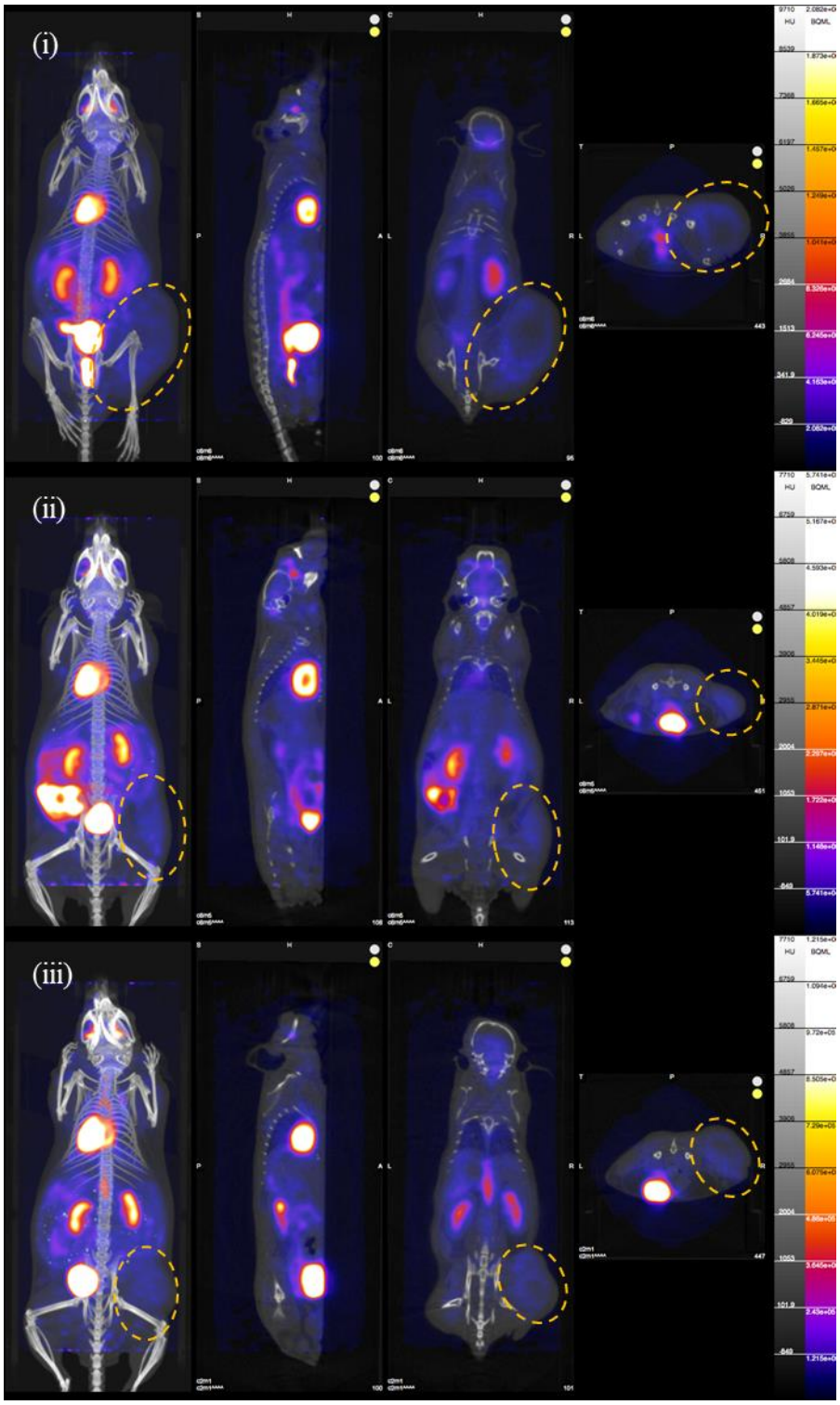

(Continued)

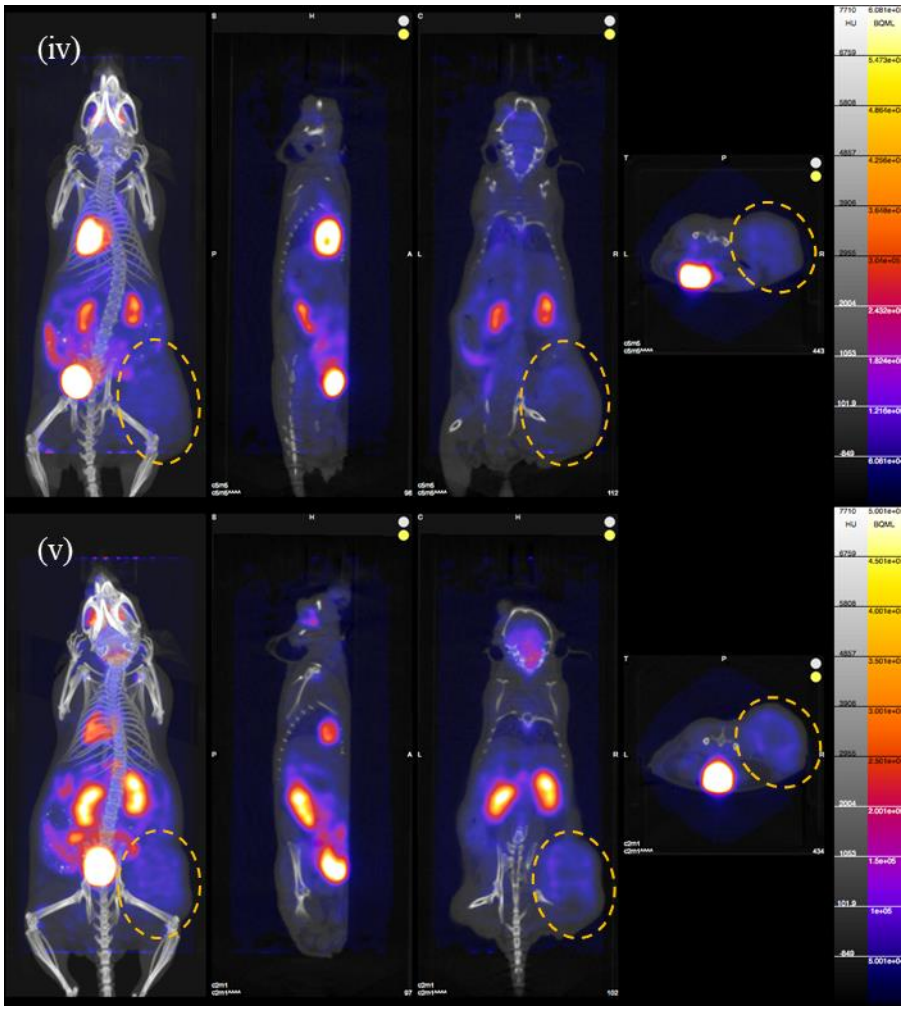

Figure C1: Representative images obtained from PET/CT scan and processed by Vivoquant software to show signal intensity. From left to right: whole mouse (viewed from above), then sagittal, coronal and transversal slices. Tumour is indicated by yellow dashes. The colour bars on the right show intensity of 18-FDG: blue indicates no signal while yellow/white show high signal intensity. Treatment group: (i) vehicle only control; (ii) 13cRA (53mg/kg); (iii) γT3 (80mg/kg); (iv) γT3 (80mg/kg) and 13cRA (53mg/kg); and (v) ABT-263 (100mg/kg) and 13cRA (53mg/kg).

APPENDIX D

List of conferences attended:

Qin Ting Ch'ng, Wan Zurinah Wan Ngah, Musalmah Mazlan, Kang-Nee Ting, Hwei-San Loh, Suresh K Mohankumar, Sue-Mian Then. 2015.
Investigating gamma-tocotrienol (γT3) as a potential anti-tumour agent to treat neuroblastoma. Oral presentation at *1st Biomedical Sciences Postgraduate Research Symposium*, University of Nottingham Malaysia, 24 July.

Qin Ting Ch'ng, Wan Zurinah Wan Ngah, Musalmah Mazlan, Kang-Nee Ting, Hwei-San Loh, Suresh K Mohankumar, Sue-Mian Then. 2016.
A synergistic combination of gamma-tocotrienol and 13-cis retinoic acid to treat neuroblastoma cell lines. Poster presentation at *2nd Biomedical Sciences Postgraduate Research Symposium*, University of Nottingham Malaysia, 22 July.

Qin Ting Ch'ng, Wan Zurinah Wan Ngah, Musalmah Mazlan, Kang-Nee Ting, Hwei-San Loh, Suresh K Mohankumar, Sue-Mian Then. 2016.
The combination of gamma-tocotrienol and 13-cis retinoic acid to treat neuroblastoma cell lines is synergistic. Oral presentation at *30th Scientific Meeting of Malaysian Society of Pharmacology and Physiology*, Shangri-La Hotel, Putrajaya, 15-16 August.

Qin Ting Ch'ng, Wan Zurinah Wan Ngah, Musalmah Mazlan, Kang-Nee Ting, Hwei-San Loh, Suresh K Mohankumar, Sue-Mian Then. 2017.
Comparison of combination treatment of 13-cis retinoic acid with either gamma-tocotrienol or ABT-263 on neuroblastoma cell lines. Oral presentation at *3rd Biomedical Sciences Postgraduate Research Symposium*, University of Nottingham Malaysia, 21 July.

Qin Ting Ch'ng, Wan Zurinah Wan Ngah, Musalmah Mazlan, Hanafi Damanhuri, Kang-Nee Ting, Hwei-San Loh, Suresh K Mohankumar, Sue-Mian Then. 2018.
The combination of γ-tocotrienol and 13-cis-retinoic acid: effects on neuroblastoma cell lines and tumours in a mouse model. Poster presentation at *2nd Faculty of Science Postgraduate Research Showcase*, University of Nottingham Malaysia, 20 June.

Qin Ting Ch'ng, Wan Zurinah Wan Ngah, Musalmah Mazlan, Hanafi Damanhuri, Kang-Nee Ting, Hwei-San Loh, Suresh K Mohankumar, Sue-Mian Then. 2018.
In vivo neuroblastoma tumour volume reduction and in vitro synergy of gamma-tocotrienol and 13-cis retinoic acid. Oral presentation at *International Conference on Biochemistry, Molecular Biology and Biotechnology*, Four Points by Sheraton, Puchong, 15-16 August.